OPTIMIZATION OF CONCRETE PAVEMENT DESIGN TO TRUCK PLATOON LOADING

by

MOHSEN TALEBSAFA

DISSERTATION

Submitted in partial fulfillment of the requirements
for the degree of Doctor of Philosophy in Civil Engineering at
The University of Texas at Arlington
December, 2021

Arlington, Texas

Supervising Committee:

Dr. Stefan Romanoschi, Supervising Professor
Dr. Xinbao Yu,
Dr. Suyun Ham,
Dr. Stefan Dancila.

Acknowledgments

First and foremost, I would like to express my sincere gratitude and appreciation to my advisor Professor Stefan A. Romanoschi for his kind guidance, encouragement, and endless support throughout the course of this research and during my time working under his supervision as his student. This research would not have been possible without his supervision and support.

I would also like to acknowledge my committee members, Dr. Xianbao Yu, Dr. Suyun Ham, and Dr. Stefan Dancila for providing valuable comments and reviewing this dissertation.

Last but not least, I would like to express my appreciation to my beloved wife, Nadia Arabkhazaeli, for her love, encouragement, patience, and emotional support in all my endeavors. Also, I would like to extend my deepest gratitude to my parents for their love, care, and support during all stages of my life.

December, 2021

Abstract

OPTIMIZATION OF CONCRETE PAVEMENT DESIGN TO TRUCK PLATOON LOADING

Mohsen Talebsafa, Ph.D.

The University of Texas at Arlington, 2021

Supervising Professor: Stefan A. Romanoschi

Transportation is the major contributor toward economic growth and development. In the United States, more than 90% of commodities are transported through the roadway system. Due to the high demand for transportation of goods, there is a high demand in the road freight industry for innovative solutions, and new technologies to improve the sustainability and efficiency of transportation. Truck platooning is one of the most recent technologies with great potential to make road freight safer, cleaner, and more efficient. This technology uses connectivity technologies and automated driving systems to interconnect two or more trucks in a convoy. These automation technologies provide unique characteristics to truck platooning traffic which leads to a different impact on pavement structures compared to normal traffic. The lateral position of trucks in real traffic is random, but it is generally assumed that this position is normally distributed across the lane. This variation in lateral position is called wheel wander which has a positive impact on the service life of pavements. However, platooning technology removes wheel wander and keeps the trucks at a fixed distance from the edge of the lane. This channelized traffic leads to a higher accumulation of fatigue damage in the wheel path of the platoon. It cancels the positive effect of wheel wander on pavement life and significantly reduces the service life of the pavement.

This study aims to investigate several solutions to improve the performance of rigid pavements and extend their longevity to withstand against truck platooning traffic. To do so,

Three-Dimensional Finite Element (3-D FE) modeling was implemented to model JPCP and CRCP structures and analyze pavement responses under truck platooning loading. Fatigue analysis was conducted to investigate possible performance improvement of various design considerations including increasing the thickness of the PCC layer, thickened PCC layer under the wheel path, increasing the size of dowel bars/rebars, and implementing larger diameter dowel bars/rebars within the wheel path. In addition, normal traffic with wheel wander was simulated to investigate the performance of each design alternative under traffic with wheel wander. The results indicate that increasing the thickness of concrete slab significantly improves the fatigue performance of pavements under channelized traffic and traffic with normal wander. Although using larger size dowel bars/rebars under the wheel path slightly improves the fatigue performance of pavements under truck platooning traffic, the effectiveness of this measure reduces as the thickness of the slab increases. Also, it was observed that the relative improvement in fatigue performance is highly dependent on fatigue models used in the calculations. In addition, to determine the optimal design alternative to withstand truck platooning a cost analysis based on the cost of materials was performed. It was found that increasing the size of dowel bars in JPCP is the most cost-effective measure since by 3% increase in the cost of construction, improves the fatigue performance by 44%. In CRCP structures, however, increasing the thickness of slab under the wheel path by 2.0 inches was found to be an optimal measure as it provides a 41% improvement of fatigue life only with a 6% increase in the cost of materials.

Table of Contents

List of Figures

List of Tables

CHAPTER 1: INTRODUCTION

1.1. Background

Transportation has always played an important role in economic growth and development. Due to the increase in population and ever-increasing demand for transportation, it is imperative to use new technologies for transporting commodities and provide infrastructure systems allowing the optimum use of these technologies to enhance their benefits. However, only some parts of this demand can be met by building new roads (EL Bouchihati, 2020). This draws attention to the importance of having more efficient and sustainable alternatives for road freight transport to increase its efficiency and safety, and to reduce the environmental effect. One of the most recent innovations in this matter is truck platooning.

Truck platooning is a technology involving a series of remotely connected trucks in a convoy that follow a leading truck using state-of-the-art vehicle-to-vehicle (V2V) connectivity technology and automated driving support systems to communicate. In this technology, the leading truck is the controlling truck and the vehicles behind automatically react and adapt to the changes in the leader truck's movements with no action from the drivers (ACEA, 2016). Owing to this automation, the trucks in a platoon are capable of maintaining close distance between each other. Truck platooning offers three benefits for road transportation. It provides safer, cleaner, and more efficient transportation. Thus, it is expected to be extensively used in the future. However, because of the unique characteristics of truck platooning traffic such as channelized load application, it will have an impact on pavement performance and longevity (Gungor & Al-Qadi, 2020).

Rigid pavements are one of the three major types of pavements widely used for roads and highways in the United States. The structure of a rigid pavement is comprised of a Portland cement

concrete (PCC) surface layer resting on a base or a subbase layer which is placed on top of the existing subgrade soil. Rigid pavements are categorized into three major types depending on the construction type and jointing system used to control crack development including Jointed Plain Concrete Pavement (JPCP), Jointed Reinforced Concrete Pavement (JRCP), and Continuously Reinforced Concrete Pavement (CRCP). JPCP is the most widely used rigid pavement and is designed as individual concrete slabs separated by joints to eliminate the development of transverse shrinkage cracks. These slabs have lengths of 15 to 20 ft. and widths of 12 to 14 ft. To reduce joint deflection, slabs are connected to each other using short steel bars called dowel bars which provide a mechanical connection between slabs without restricting horizontal movement. The dowel bars allow adjacent slabs to expand and contract independent of one another. CRCP, however, is constructed free of joints. Transverse cracks are allowed to form, but they are held tight using longitudinal reinforcement steel bars located in the mid-depth of the concrete slab. The steel constitutes typically 0.6% to 0.8% of the cross-section area (ACPA, 2009). The transverse cracks typically occur 3 to 6 ft. apart from each other (AASHTO, 2008). JRCP contains both dowel bars and reinforcement steel. Although this type of pavement was widely used in the past, it is less common today especially in state highways because of its performance issues (Delatte, 2014). It was observed that the embedded steel cannot hold mid-panel cracks together which leads to erosion and faulting in mid-panel cracks (ACPA, 2009).

The failure mechanism of pavement depends on the type of pavement, loading, and environmental condition. Fatigue cracking is the major failure in PCC pavements which is induced by repeated stresses due to traffic loading, temperature gradient, moisture gradient, or the combination of all three (Roesler, 1998). Repeated load applications on pavement surface create micro-cracks in concrete slabs which eventually propagate to the surface leading to transverse

cracks (cracks perpendicular to the pavement centerline), longitudinal cracks (cracks parallel to the pavement centerline) in PCC slabs, and punchouts (a localized area of the slab broken into pieces) in CRCP. For fatigue damage analysis in PCC pavements, the maximum induced tensile stress at the bottom of the PCC layer near the midway of the longitudinal edge is used (Gillespie et al, 1993). However, this critical location may change when temperature and moisture gradients are considered (Hiller, 2007). Another major distress type occurring in concrete pavements is transverse joint faulting which is defined as the difference in elevation across a transverse joint. Joint faulting occurs due to the application of repeated heavy traffic loads along with insufficient load transfer between the slabs at the joint.

Trucks are the major contributors toward pavement failure and the induced stresses are highly dependent on magnitude, location of traffic loads, and configuration of the axles (Sargand & Abdalla, 2006). Therefore, it is necessary to evaluate how and to what extent they affect pavement structural response and performance. This knowledge contributes to designing new pavements with longer service life, as well as implementing better remedial measures to existing pavements. It also allows state DOTs and local agencies a proper estimation of damage caused by truck axle loads and configurations since the fees and penalties allocated to commercial truck operators are based on the damage induced by trucks to pavements (Zaghloul & White, 1994).

1.2. Problem Statement

Truck platooning is reshaping the future of mobility and transport. Despite the advancement in platooning technology, the first step toward the commercial viability of this technology is to provide, construct, and upgrade the road infrastructure allowing platooning. Thereby, in order to obtain all the benefits offered by truck platooning, it is imperative to assess the impacts of platooning on pavement structures. Typically, drivers tend to control their vehicles

in the center of the road lanes as the vehicle travels along the lane. If the vehicle deviates from this lateral position, the driver tries to steer the vehicle toward the center of the lane. Various measurements conducted through video processing and road sensor instrumentation proved that vehicles seldom pass in the same lateral position on the pavement surface and their lateral position is uncertain (Buiter & Litzka, 1989; Blab et al., 1995; Lennie & Bunker, 2003; Stempihar et al., 2005; Timm & Priest, 2005). This lateral distribution of vehicle position over a pavement section is known as wheel wander. Several factors such as driver's habit, weather condition, traffic condition, time of travel, and road and vehicle characteristics affect the vehicle wheel wander (Buiter & Litzka al., 1989; Luo & Wang, 2013). Traffic wheel wander distributes the wheel loads across the lane, so it has a positive impact on increasing the design life of pavement structures (Erlingsson, 2012). The existing pavement design technique in AASHTO Pavement ME considers the effect of wheel wander on pavement structure design which results in the distribution of pavement damage across the width of the lane and allows more load repetitions on pavement. However, this is not the case for truck platooning since trucks in a platoon follow the leading truck and their wheels pass over the same lateral position over pavement surface. Therefore, wheel loads concentrate only over a certain portion of the pavement surface and apply channelized traffic to the pavement. This channelized traffic cancels the positive effect of wheel wander on pavement life which leads to a higher accumulation of fatigue damage in the wheel path of the platoon. This significantly reduces the service life of pavement due to fatigue damage.

Since truck platooning technology is relatively new and has not been yet implemented in real-world situations, the available data on their impact on pavement structures is extremely limited. Therefore, it is essential to understand how and to what extent a truck platoon affects the pavement response and performance. This would help in designing new pavements as well as

implementing remedial measures to make existing pavements perform better under truck platooning and have longer service lives. Although such a study can be conducted using field tests, they are extremely expensive as they require extensive pavement construction and instrumentation of pavement sections with stress and strain sensors. Therefore, the preferred alternative is to evaluate the response and performance of pavement structures using analytical models. Three-Dimensional Finite Element (3-D FE) modeling is a robust and widely accepted numerical technique that can be used to investigate the effect of truck axle loads on stress induced in rigid pavements.

1.3. Objectives of the study

The primary objective of this study is to investigate what would be the potential solutions to improve the performance and longevity of JPCP and CRCP pavements to withstand against truck platooning traffic through evaluating the impact of truck platooning on the structural response of these pavement. These objectives will be accomplished by employing three-dimensional finite element modeling of both pavement types subjected to a truck platooning including a multi-axle truck (Class 9 according to FHWA truck classification). Several design considerations for JPCP and CRCP structures will be examined to mitigate the negative impact of channelized traffic on pavement performance and enhance the expected service life of these pavements under truck platooning. The design considerations studied in this research include:

1) Increasing the thickness of the PCC layer on stress reduction in JPCP and CRCP.
2) Thickened PCC layer under the trucks' wheel path on reduction of induced stress in JPCP and CRCP.
3) Employing dowel bars with a larger diameter in the wheel path of the platoon on induced stress in JPCP.

4) Implementing larger diameter dowel bars in JPCP and rebars in CRCP in the wheel path of platoon on the pavements' performance.

The efficiency of these design considerations will be evaluated, and the most optimized design consideration will be selected. Such knowledge will help to fill the knowledge gap on the commercial application of truck platooning technology. It also helps highway engineers in the optimization of rigid pavement design and maintenance activities in a manner that eliminates reduction in service life due to fatigue damage by minimizing the magnitude of induced stresses in the PCC layer.

1.4. Dissertation Outline

This dissertation is divided into seven chapters. Chapter 1 presents introductory remarks of this study which includes a brief background on truck platooning, rigid pavement structure, and their failure mechanism along with the problem statement and the objectives of the study.

Chapter 2 provides an introduction to truck platooning technology. The concept of truck platooning will be explained, and its characteristics, applications, benefits, and recent advancements are described, and a literature review on the previous studies on truck platooning will be covered. In addition, the published literature related to damages and failure mechanisms of JPCP and CRCP caused by heavy vehicles and the strategies used by other researchers in topics related to truck damage evaluation will be addressed and previous studies based on finite element modeling of rigid pavement structures will be summarized.

Chapter 3 provides a comprehensive description of the development of finite element models (FEMs) of JPCP and CRCP pavement structures including types of interfaces and interaction between pavement layers, the interaction between concrete slabs, and dowel bars in

JPCP, concrete slabs and steel reinforcements interaction in CRCP, material modeling, truck loads modeling, boundary conditions, and meshing strategies. Also, the position of trucks in which the maximum stress in JPCP slabs occurs will be determined.

Chapter 4 discusses the effect of different design considerations on improving the performance of JPCP and CRCP. The design considerations include increasing the thickness of the PCC layer, thickened PCC layer under the wheel path, using dowel bars with a larger diameter, implementing larger diameter dowel bars and rebars within the wheel path in JPCP and CRCP respectively. Furthermore, the performance of these design considerations under channelized traffic and normal traffic with wheel wander will be evaluated.

Chapter 5 provides a discussion on the cost analysis of the proposed pavement structures to determine the most cost-effective design consideration for JPCP and CRCP to withstand against truck platooning traffic.

Lastly, the finding and conclusions of the study are presented in Chapter 6. In addition, the recommendations for future studies will be presented.

CHAPTER 2: LITERATURE REVIEW

2.1. Introduction

Transportation is the major contributor toward economic growth and development. As the population will continue to grow and the economy will expand, it is expected that the demand for freight transportation increases significantly. International Transport Forum (ITF) predicted that the surface freight transport (road and rail) in Organization for Economic Co-operation and Development (OECD) countries increases between 40 to 125% by 2050 compared to the level observed in 2010. However, this increase can be up to 400% for developing countries (Alam et al, 2015). Even though some part of this increase will be handled by rail freight transportation, the escalation in road freight transportation will be significant, especially in the United States in which more than 90% of commodities are transported by roadways (Zhou et al., 2019). Expanding the transportation infrastructure system is one of the ways for quenching this ever-increasing demand. However, expanding the roadway network has a limited effect on meeting the demand and requires more effort in maintaining and managing this network (El Bouchihati, 2020). According to the U.S. Department of Transportation (U.S. DOT), trucks carry more than 70% of the total daily freight by weight, which is equivalent to 38.2 million tons on more than 4 million miles of public roads. Also, the trucking industry contributes over 84% of the revenue in the U.S. commercial transportation sector (U.S. DOT, 2020). These statistics show the importance of the truck freight industry in the transportation system. However, there are some critical issues in the trucking industry which include the following:

1) *Safety:* The high contribution of trucks in total freight is associated with a higher risk of accidents. According to Federal Motor Carrier Safety Administration (FMCSA), 4,862 people died in truck-involved crashes in 2018 alone, which constitute 13.8 % of the total

number of all highway fatalities. Also, truck-involved crashes accounted for 112,000 injuries in 2018 (FMCSA, 2021).

2) *High fuel consumption:* American Transportation Research Institute (ATRI) reported that trucks constitute only 5% of total vehicles, but they consume 20% of total transportation fuel (ATRI, 2020).
3) *Driver shortage:* According to the "Truck Driver Shortage Analysis" report by American Trucking Association (ATA), the United States was facing a serious shortage of commercial truck drivers. This shortage is reported around 60,000 drivers for 2019, and it is expected that this number will increase to 160,000 truck drivers in 2028 (ATA, 2019).
4) *Drivers' condition:* According to surveys conducted by ATA, the average driver age in the truck industry is 46 and 55% of drivers are older than 45. This increases the risk of accidents. Statistics revealed that they were involved in 57% of total truck crashes (ATA, 2019).
5) *Congestion:* The impact of trucks increases traffic congestion. Trucks impact the traffic flow and car drivers' behavior. It has been observed that car drivers increase the space gap, decelerate, and change the lane when they confront a truck. Also, trucks occupy more space in a lane in comparison to cars. Therefore, a higher percentage of trucks decreases the total number of vehicles (Kong et al., 2016). Congestion increase causes economic productivity loss and waste of fuel. According to ATRI, the cost of congestion in the trucking industry in 2018 was $74.5 billion which is equivalent to the annual productivity of 425,000 truck drivers (U.S. DOT, 2020).

These issues draw attention to the need for developing more efficient, safer, and more sustainable alternatives for road freight transportation. One of the most recent innovations in this matter is truck platooning.

2.2. Truck Platooning Concept

Truck platooning is a technology involving a series of remotely connected trucks in a convoy following a leading truck using state-of-the-art vehicle-to-vehicle (V2V) dedicated short-range communication (DSRC) technology and automated driving support systems to communicate. In this technology, the leading truck is the controlling truck and the vehicles behind react automatically and adapt to changes in the leader truck's movements with no action from the drivers (ACEA, 2016). Figure 1 illustrates an operation of truck platooning. The trucks in the platoon are capable of maintaining a set close distance between each other in the longitudinal direction. The truck which runs at the head of the platoon is called the leading truck, while the following trucks are trailing trucks. If the leading truck brakes, the electronic communication technology ensures that all the trailing trucks in the platoon brake as well. The distance between consecutive trucks can be as low as 0.3 seconds, which is about 22 ft. at speed of 50 mph (Janssen, 2015). Several technologies including Adaptive Cruise Control (ACC), Cooperative Adaptive Cruise Control (CACC), and truck automation work together to offer this level of interaction between the trucks. ACC system allows the driver to set the traveling speed and activates automated brakes and acceleration to maintain a safe distance from the leading vehicle. This system alone cannot be used to operate a platoon since it lacks the coordination and control mechanism required for maintaining a safe short distance between the vehicles. However, CACC through including V2V communication technology provides important information such as speed

and location of the leading truck which allows a quick speed adjustment, smoother acceleration and deceleration, and shorter gap for the following trucks (Greer et al., 2018).

Figure 2-1. Truck Platooning in operation.

To maximize the benefits of truck platooning different coordination strategies, such as global, local, or ad-hoc, can be implemented to form a platoon. According to the report by California Partners for Advanced Transportation Technology (PATH) program, truck platooning consists of four primary stages (Nowakowski, 2015):

1) *Forming:* in this stage, platoon operators should identify their potential partners based on their characteristics such as their current location, destination, type of truck, etc.
2) *Steady-State Cruising:* This stage pertains to the platoon in operation which constitutes the largest period of time. After the formation of a platoon, drivers operate their trucks according to the level of automation in the vehicle.

3) *Departing or Splitting:* This stage accounts for the case when a truck needs to depart from the platoon to reach its destination. After the departure of the truck, the following trucks close the gap made by the departed trucks to re-form the platoon by the set distance.
4) *Abnormal Conditions:* This stage considers any other situations not included in the previous stages, such as potential errors in the system or unexpected operation conditions in which the truck platooning system should be able to address them.

2.3. Automation levels

Truck platooning system comprised of sensors, localization services, V2V communication system, software, hardware, and human interface. Truck platooning relies on a combination of various short- and long-range sensors such as light detection and ranging (LIDAR), radar, and cameras working together to detect other trucks in the platoon and evaluate other objects in the surrounding environment. In order to determine the location of the vehicle, Global positioning systems (GPS) and inertial navigation systems (INS) are utilized to feed the necessary information to the vehicle for navigation of the system. A redundancy in sensors and localization services is needed so that the system can safely operate in case any of them fails. In addition, the V2V communication system transmits vehicle performance information, such as speed and location between vehicles, with low latency allowing the CACC system to synchronize to the movement of the leading truck. However, the CACC system requires software for processing the information received from sensors, localization services, and the V2V communication system. The essential part of platooning is the hardware components performing the required adjustment commanded by CACC in vehicle speed, steering, braking, etc. Finally, the human interface informs the driver about the change made by the system (Greer, 2015).

A stepwise approach for implementing truck platooning in public roads is to consider different levels for platooning (Vissers, 2018). According to the Society of Automotive Engineers (SAE), five different levels of automation are envisioned for truck platooning (Greer et. al, 2018; Gungor et. al, 2020). They are summarized in Table 1.

Table 2-1. Truck platooning levels

Level	**Description**
I. Driver Assistance	The driver mostly controls the vehicle, and the automated driving system is only assisting the driver.
II. Partial Automation	The majority of vehicle functions such as acceleration and steering are controlled by an automated driving system, but the presence of the driver is necessary for monitoring the environment and intervening to take the control of the truck.
III. Conditional Automation	The automated driving system monitors the traveling environment, and the driver only takes full control of the vehicle in situations such as certain traffic and weather conditions and requests to intervene by other vehicles.
IV. High Automation	The automated system performs all driving functions under certain conditions, and the presence of the driver is in the leading truck necessary.
V. Full Automation	There is no designated driver, and the automated system performs all driving functions such as cruising and merging in all conditions.

Currently, platooning technology with trucks equipped with the platooning system from a single brand is available - up to Level 2 of automation - which is called mono-brand platooning. However, multi-brand platooning is still under research and development and its feasibility depends on its ability to form a platoon between different platooning brands (Neubauer et al, 2019). According to SAE, multi-brand platoons should be possible by 2023 across Europe (ACEA, 2016).

2.4. Benefits of Truck Platooning

Truck platooning provides safer, cleaner, and more efficient freight transportation. Truck platooning facilitates safe road freight transportation. In 2018 alone, 4,862 people died in truck-involved crashes (FMCSA, 2021). Typically, 90% of all accidents occur by human error, and platooning technology prevents human-induced accidents (Janssen, 2015). Automatic and immediate braking enhances safety and reduces the chance of possible accidents and fatalities with nearly-zero reaction time compared to human braking. Without truck platooning technology, drivers require to maintain a safe following distance to have enough time to react to potentially dangerous situations. According to FMCSA, the safe following distance should be one second for every ten feet of vehicle length, and an extra second for speeds over 40 mph (FMCSA, 2002). This distance for trucks is about 550 ft. The safe following distance can be broken into different categories as illustrated in Figure 2-2(a). The first category pertains to the driver's perception. This is the distance that the truck travels until the driver perceives he/she needs to brake. The second category considers reaction time, which is between 1 to 1.5 seconds. The attention buffer reflects the driver's attentive state to the driving task (Tawari et. al, 2014). The last two categories account for the time lag in the braking system of trucks and the braking capability of different trucks (Peloton, 2019). The implementation of the platooning technology dramatically reduces the time associated with most of these categories. This technology is capable of reacting within 30 milliseconds. Thus, the time associated with perception, reaction, and attention buffer goes down to zero as shown in Figure 2-2(b). However, the distance can be reduced even further by synchronizing the braking system (Figure 2-2(c)). The connectivity technology used in truck platooning keeps each truck at a safe distance and is able to adapt and react to any change in the

movement of the leading truck in about one-fifth of the time that a driver would react. Deploying trucks closer to each other provides many benefits in road freight transportation.

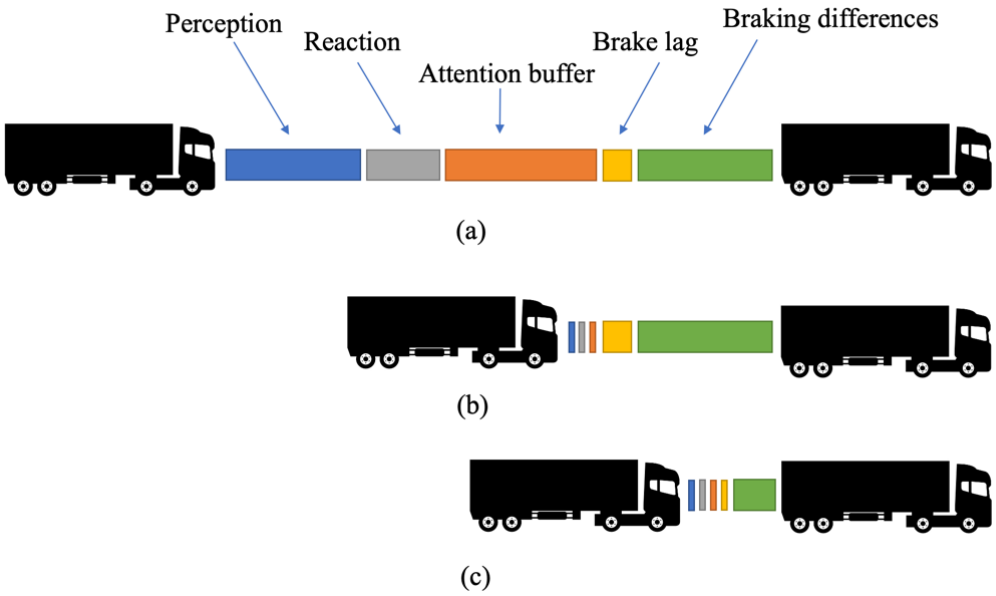

Figure 2-2. Following distance components (Peloton, 2019).

Shorter spacing of the trucks in a platoon significantly reduces aerodynamic drag (ACEA, 2016; Jensen, 2019). Aerodynamic drag is a significant source of energy loss in trucks, especially at high speeds, and it is responsible for up to 20% of energy loss (Vohra et. al, 2018). Thereby, the aerodynamic effect of closely spaced vehicles in truck platooning alleviates the effect of aerodynamic drag leading to reduced energy loss, fuel consumption, and CO_2 emission. Aerodynamic drag in trucks is generated by the pressure difference between the front (high-pressure field) and rear (low-pressure field) of the vehicle. Deploying a truck platooning changes the pressure difference created between the vehicles present in the platoon (Patten et al., 2012). The small gap between the trucks increases the pressure between the trucks. Therefore, the leading truck benefits from increased pressure in its rear which results in reduced pressure differential and lower aerodynamic drag. In addition, the leading truck acts as a shield for the trailing trucks against

the high-speed air, so it decreases the high-pressure field in front of the trailing truck resulting in a reduction in pressure differential and aerodynamic drag. Figure 2-3 represents the pressure field result from the simulation of a two-vehicle platoon with 16, 33, and 66 ft. spacing gaps. As it can be observed, the pressure in front of the trailing truck significantly reduces when the following distance reduces. In addition, the leading truck benefits from the shorter gap distance because the closer proximity of the trailing truck leads to enhancing the pressure generated behind the leading truck. Thus, the overall aerodynamic drag result from pressure difference decreases (Alam et al., 2015).

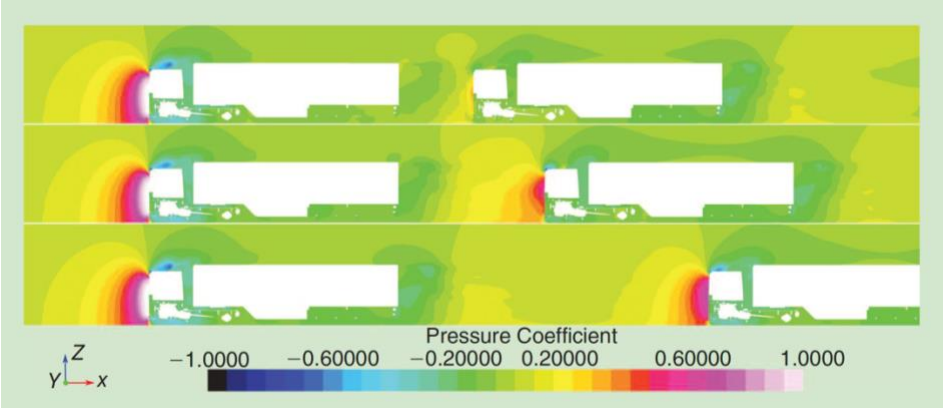

Figure 2-3. Pressure fields in a truck platooning at spacing of a) 16 ft., b) 33 ft., and c) 66 ft. (Alam et al., 2015).

Moreover, in a truck platooning consisting of three trucks, the trailing trucks in the middle of the platoon benefit from both changes in pressure fields in both its front and rear, so it will experience the lowest pressure differential, aerodynamic drag, and fuel consumption (McAuliffe et al., 2017). Several studies have proven that truck platooning reduces fuel consumption in a range of 4% to 8% for the leading truck and 10% to 12% for the trailing trucks. Also, for a platoon consisting of three trucks, the average fuel saving is close to 10%. Although this saving is mostly due to reduction in aerodynamic drag, some portion of it is derived from more consistent

acceleration and deceleration of the platooning system in comparison to those for driver-controlled trucks (Cambridge Systematics, 2017). However, many other factors such as geometrical characteristics and spacing of trucks, ambient wind, and traffic conditions also impact aerodynamic drag reduction (Tadakuma et al, 2016). It should be noted that the aerodynamic advantage from platooning applies at high speeds; fuel savings significantly decrease at low speeds. Janssen et al. (2015) performed a business case study for three logistics service providers in the Netherlands and compared the benefits of using truck platooning instead of conventional cruise control. It was found that the savings offered by platooning are sizable for the providers and savings from fuel alone offset the costs for the technology, additional periodic testing, and training of drivers (Janssen, 2015).

The environmental benefit of truck platooning is directly related to the reduction in fuel consumption. According to Pandazis et al. (2015), platooning lowers the CO_2 emission by up to 8% from the leading vehicle and by up to 16% from the trailing vehicles. A liter of diesel produces 2.6 kg of emitted CO_2 so this range of fuel reduction can result in considerable environmental benefits (Janssen, 2015).

Truck platooning optimizes road transport by using the roads more effectively and offering faster transporting commodities. Compared to regular traffic, a closer following distance in a platoon causes that roads can be exploited more efficiently, and the number of vehicles that can operate on highway lane segment at high-speed increases accordingly (ACEA, 2016). Deploying two human-driven trucks with a length of 62 ft. and a 2 seconds gap at speed of 50 mph occupies 270 ft. of the road. However, deploying a truck platooning using similar vehicles with 0.3 second gap would decrease the lane usage to 145 ft., which represents a 46% reduction (Jenssen, 2015). In addition, this reduction in congestion results in more fuel saving and reduction in CO_2 emission.

Auburn University conducted a study sponsored by FHWA on the impact of truck platooning on travel time-saving. Traffic simulation of driver-assistive truck platooning (DATP) conducted using the CORSIM software showed a significant travel time reduction ranging from 7.69 to 13.26 seconds in a five-mile section of I-85 Alabama (Gordon, 2015).

Another benefit of truck platooning pertains to driver operations. Truck platooning in higher levels of automation can reduce the number of truck drivers so it can address the truck driver shortage issue. It can reduce the cost of operation, as well. For example, a three-truck platoon with only one driver in the leading truck and autonomous following trucks decreases the driver cost by 67%. Another alternative can be having a spare driver in the leading truck to reduce the time of long-hauls trips while abiding by the FMCSA Hours of Service regulations (Cambridge Systematics, 2017).

2.5. Truck platooning studies

Texas Transportation Institute (TTI) performed a study sponsored by TxDOT to investigate the feasibility of truck platooning in a specific corridor in Texas. In this project, regulations that could impede the implementation of truck platooning in fleet operation were investigated. A two-truck platoon with Level 2 automation was tested in a closed track and simulated for fuel consumption and emission. It was observed that trucks were able to maintain close following distance and navigate with no deviation at tight turns. The simulation of the platoon in a mixed traffic condition using the Vissim microscopic simulation showed that it can reduce fuel consumption by up to 12%. Also, these fuel savings as high as 20% for the leading truck and 40% for the trailing truck were estimated (Kuhn et al, 2017).

In 2017, the University of California (Berkeley) Partners for Advanced Transportation Technology (PATH) under the U.S. Federal Highway Administration (FHWA) exploratory advanced research program, in collaboration with Volvo trucks, developed and tested truck platooning technology in closed-track testing at a facility near Montreal, Canada, and also along I-580 highway between Dublin and Tracy in California. The main purpose of this study was to carry out high-speed testing of a 3-truck platoon, determine its maneuverability such as entering and leaving the platoon and evaluate the impacts on fuel consumption (Shladover et. al, 2019). The study revealed that platooning with three standard trucks can save 5% energy on average; the last truck saves the most and the leading truck saves the least energy. In addition, using aerodynamic trucks can enhance energy saving by 12-14% in comparison to standard trucks. The evaluation of the effect of spacing between trucks on energy saving showed that changing the time gap between trucks from 0.6 to 1.5 seconds (equal to 57 ft to 143 ft gap at 65mph) decreases aerodynamic drag energy saving from 6% to 5% for the second truck. These values drop from 11% to 9% for the third truck. Therefore, it was concluded that aerodynamic drag energy saving is not significant when the time gap increases from 0.6 to 1.5 seconds. Moreover, it was observed that the automated driving system was able to properly and safely respond to cut-in vehicles and increase the gap to accommodate them (Shladover et. al, 2018).

UC Berkeley PATH also conducted another study consisting of a three-truck platoon with 20 ft. spacing at speed of 53 mph in the SR722 Nevada corridor. The objective of this study was to perform high-speed testing of the platoon, examine platoon splitting and joining, investigate fuel saving, and fault detection. It was observed that line-of-sight is necessary for V2V communication and the middle truck showed a 1.5 ft. lateral offset. Moreover, fuel saving of

4.54%, 11.91%, and 18.4% was attained for leading and following trucks respectively (Cambridge Systematics, 2017).

In a European collaborative project called the SARTRE Project with the participation of 7 entities from 4 countries, the aerodynamic benefits of platooning and resultant fuel savings were investigated at the IDIADA high-speed test track in Spain. The platoon tested in this experiment consisted of two trucks with spacing as low as 16 ft. The finding showed that at the following distance of 16 ft. (5 m) fuel saving for the leading and following trucks are 8% and 13% respectively. However, these values at the following distance of 82 ft. (25m) decrease to 1.5% and 7.5% (Dávila and Nombela, 2011)

In a research project funded by the U.S. Department of Energy (DOE), the fuel consumption reduction of two truck platoon was investigated. In this project, class 8 tractor-trailers were deployed at the Continental Tire Proving Grounds in Uvalde, Texas, on an 8.5-mile asphalt track, and fuel consumption at different travel speeds ranging from 55 to 75 mph and following distances ranging from 20 to 70 ft. The results showed that the average fuel consumption of the leading truck reduces in a range of 2.7% to 5.3% as the following distance decreased. This fuel saving for the trailing trucks was higher ranging from 2.8% to 9.7%. Also, the overall fuel saving of the platoon was between 3.7% to 6.4% with the best result at speed of 55 mph and 30 ft. following distance (Lammert, 2014). A similar study conducted by Alam et al (2010) on a truck platoon with two identical European cab-over trucks at speed of 70 mph and the fuel saving of 4.7% to 7.7% was observed depending on following distances. Tsugawa et al. (2016) performed a study of a three-truck platoon in a test track at speed of 50 mph and investigated fuel consumption reduction of the platoon at various spacing. Figure 2-4 represents the results obtained by this study. It was observed that the entire platoon with the spacing of 66 ft. improves fuel saving by 9%. The

saving increases to 16% as the spacing decreases to 15 ft. Also, as expected, the leading truck experiences the least and the middle truck experiences the highest fuel saving improvement.

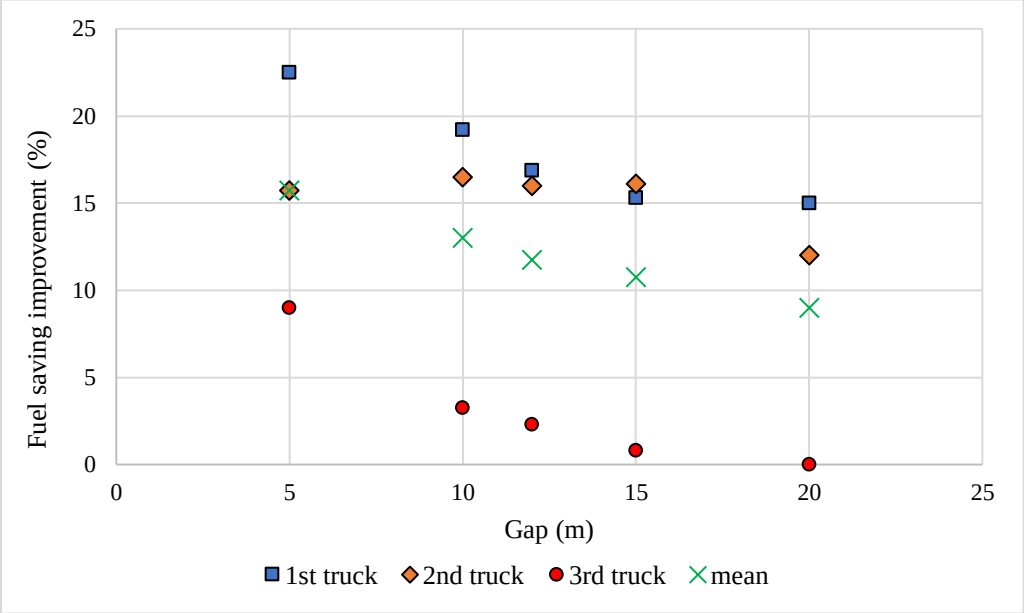

Figure 2-4. Fuel saving reduction at different truck spacings (Tsugawa et al. 2016).

A similar study was conducted by the New Energy and Industrial Technology Development Organization (NEDO) in Japan, and an average of 15% improvement in fuel consumption was observed for cab-over trucks at speed of 50 mph (Ashley, 2013). Furthermore, The UC PATH program estimated a potential fuel saving of 20% to 25% through modeling the impact of wind resistance and shorter following distance as low as 10 ft. However, this short distance requires a dedicated lane for platooning due to safety issues because such a short distance restricts the ability of other vehicles to change lanes across the platoon, and the truck drivers would not have enough time to safely react in emergency situations (Nowakowski, 2015).

2.6. Impact of truck platooning on pavement performance and design

The major difference between automated-driven trucks in truck platooning technology and driver-controlled trucks is how they run along the lane. Drivers, typically, tend to control their

vehicles in the center of the road lanes as the vehicle travels along the lane. However, their lateral position in the lane changes from time to time they deviate from the center of the lane and steer to bring the vehicle back in the center of the lane. This lateral distribution of the vehicles along the lane is called wheel wander and it has a positive impact on the pavement response and damage accumulation. It distributes the damage across the lane and consequently, it allows more load repetitions on the pavement before failure than for the case of the channelized traffic (Erlingsson, 2012).

Past studies have indicated that wheel wander can be represented by a normal distribution with a mean of zero (relative to the centerline of the lane) and a standard deviation of 10.0 inches (MEPDG, 2004). The AASHTO Pavement ME considers the effect of wheel wander on pavement structure design which results in the distribution of pavement damage and allows more load repetitions on the pavement. Since automated-driven trucks are equipped with advanced positioning technologies (such as lane detection sensors and GPS) to position the vehicles in the middle of the lane more accurately (Zhou et al., 2019), the lack of wheel wander of truck platoons traffic induces more damages to the pavement structure including fatigue cracking and also rutting in flexible pavements.

The impact of channelized traffic on the reduction of pavement performance has been verified by several experimental studies. Harvey et al. (2000) implemented a heavy-vehicle simulator to assess the impact of channelized traffic on flexible pavement performance. The comparison between sections under channelized traffic and sections subjected to traffic with a normal distribution revealed that the channelized traffic results in 25% to 45% greater rutting. Monismith et al. (2000) conducted a study on the impact of wheel wander on the WesTrack project. The results showed that channelized traffic increases fatigue cracking failure by at least three folds.

Later, Wu and Harvey (2008) studied the effect of wheel wander on rutting development in a flexible pavement using the Heavy Vehicle Simulator at the University of California's Pavement Research Center. Two identical pavement sections were subjected to channelized and non-channelized traffic at speed of 6 mph. After application of 3,000 load repetitions, they found that wheel wander reduces permanent deformation by 25%. Also, it was observed that the shape of the rutting profile changes as the location of maximum rutting shifts from the edge of the tire to the center of the tires.

Noorvand et al. (2017) evaluated the impact of autonomous trucks on flexible pavement performance. They implemented mechanistic-empirical models to predict pavement performance under various combinations of autonomous and non-autonomous trucks and determined the pavement thickness to support these traffic combinations. The results indicated that the equivalency factor for rutting for autonomous trucks (no wheel wander) was in the range of 2.1 to 2.3 of the number of passes for non-autonomous trucks. This equivalency factor for fatigue cracking was observed to be in the range of 1.15 to 1.27. Also, as expected, the presence of autonomous trucks led to a reduction in the overall performance of pavement, thus, the required pavement thickness increases. Zhou et al (2019) studied the impact of channelized traffic by automated vehicles (AV) on hydroplaning potential and longevity of flexible pavement and found that channelized traffic increases the rut depth by 30% and reduces fatigue life by 20%. Al-Qadi et. al (2021) evaluated the impact of truck platooning on flexible pavement performance using finite element modeling. The effects of the rest period and lateral position of trucks were studied on pavement performance. It was found that strain accumulation in the flexible pavement structure is negligible for truck spacing greater than 10 ft. It was also observed that channelized traffic

increases the fatigue damage and the rutting potential by 60% and 25%, respectively, compared to normal traffic.

Figure 2-5 schematically represents the difference in induced damage caused by normal traffic and channelized traffic. Figure 2-5(a) shows the damage created by three normal traffic in which trucks have similar axle loads passing with different wheel wanders. As can be seen, all three trucks create damage with the same magnitudes but distribute it in different lateral positions. Figure 2-5(b) shows the damage created by the same trucks in a platoon. As can be seen, due to lack of wheel wander, all three trucks create damages in the same lateral location, so the induced damage accumulates in the wheel path of the platoon leading to higher magnitudes of damage in comparison to normal traffic which significantly reduces the service life of the pavement. Also, the location of maximum damage in channelized traffic will be in the wheel path while this location changes depending on lateral locations of trucks in normal traffic. The decrease in the service life of the pavement due to channelized traffic increases the frequency and cost of maintenance and rehabilitation activities. Therefore, new measures should be considered in the design of pavement structures to address all the impacts of truck platooning traffic on pavement performance.

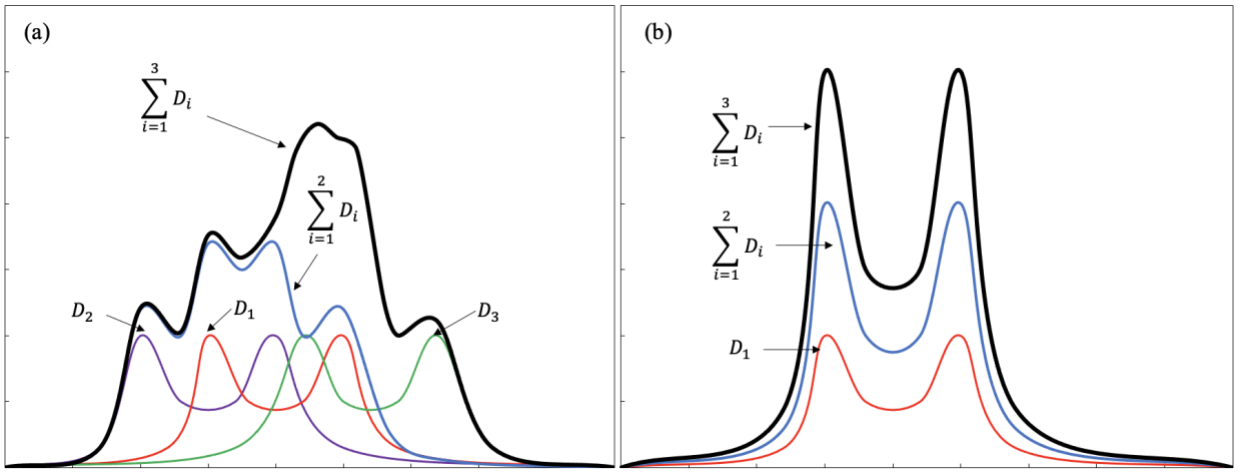

Figure 2-5. Damage accumulation caused by (a) normal traffic vs (b) channelized traffic.

2.7. Rigid Pavements

The most widely used rigid pavements include jointed plain concrete pavement (JPCP) and continuous reinforced concrete pavement (CRCP). Generally, JPCP is designed with short joint spacing to control the location of natural cracks. Transverse joints constructed between slabs to control stress and strain in the slabs caused by environmental loads such as changes in temperature and moisture. JPCP does not contain any reinforcement steel, but it uses dowel bars at transverse joints and tie bars at longitudinal joint as load transfer devices. Dowel bars installed at transverse joints transfer traffic load across the joint (primarily by shear mechanism) to reduce the relative deflection at the joint face. Figure 2-6 shows the configuration of dowel bars and tie bars in JPCP.

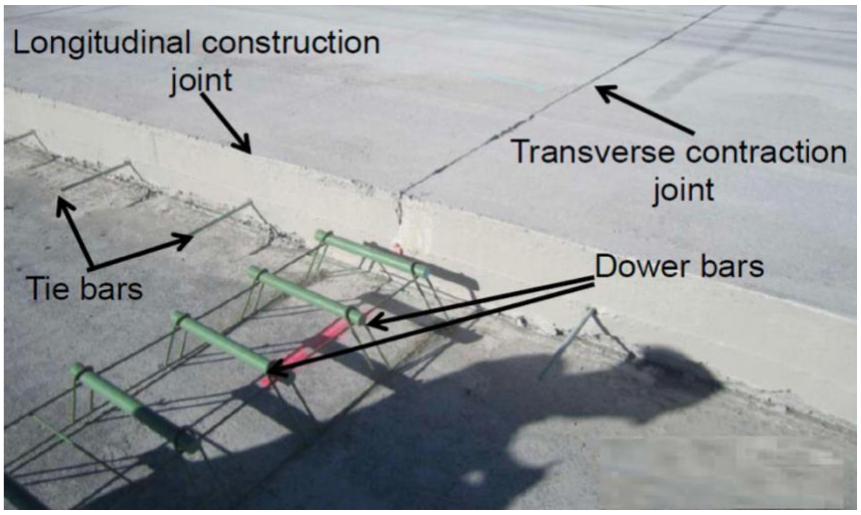

Figure 2-6. Components of jointed plain concrete pavement.

Although JPCP showed a good performance with reasonable construction cost, the high maintenance cost of damages created near the joints resulted in the use of CRCP (Kim et al, 2020). CRCP is another concrete pavement type in which concrete is placed after arranging continuous longitudinal steel bars, and it is constructed without any transverse joint. CRCP structure is designed to allow cracks to occur, but they are held together tightly by continuously placed steel

bars, so the pavement acts as a continuous system. Figure 2-7 illustrates the arrangement of continuous reinforcement steel in CRCP. Since there is no transverse joint in CRCP, joint distresses that occur in JPCP do not occur in CRCP. Although the initial cost of construction of CRCP is higher than other concrete pavement types because of the use of a high quantity of steel bars, it requires less repair and maintenance and consequently, its life cycle cost is less than that of JPCP (ACPA, 2009; Kim et al, 2020).

Figure 2-7. reinforcement steels in continuous reinforced concrete pavement.

2.8. Failure mechanisms of concrete pavements

The failure mechanism of pavement depends on pavement materials characteristics, traffic loading, and environmental conditions. Varieties of distresses exist in concrete pavements including spalling, faulting, cracking, joint seal damage, longitudinal cracks, transverse fatigue cracks, D-cracking, popouts, pumping, settlement, etc. However, in this study only the load-related distresses of rigid pavements are discussed.

Fatigue cracking is a major failure in concrete pavement. It is due to repetitive induced stresses in concrete pavements caused by traffic loading, temperature gradients, moisture gradients, or a combination of all three that may not exceed the flexural strength of concrete

(Roesler, 1998). However, repetition of these loadings yields to micro-cracks accumulation and propagation in the concrete slab which eventually appear to the surface of the slab in form of transverse cracks, longitudinal cracks, corner breaks, or punchouts in CRCP (see Figure 2-8). Transverse cracking is the major deterioration mechanism in concrete pavements which may occur in two modes of bottom-up and top-down cracks depending on the temperature and moisture gradients. Bottom-up cracks initiate from the bottom of slabs when temperature and moisture gradients are positive, while top-down cracks develop from the surface of slabs when they are subjected to negative temperature and moisture gradients.

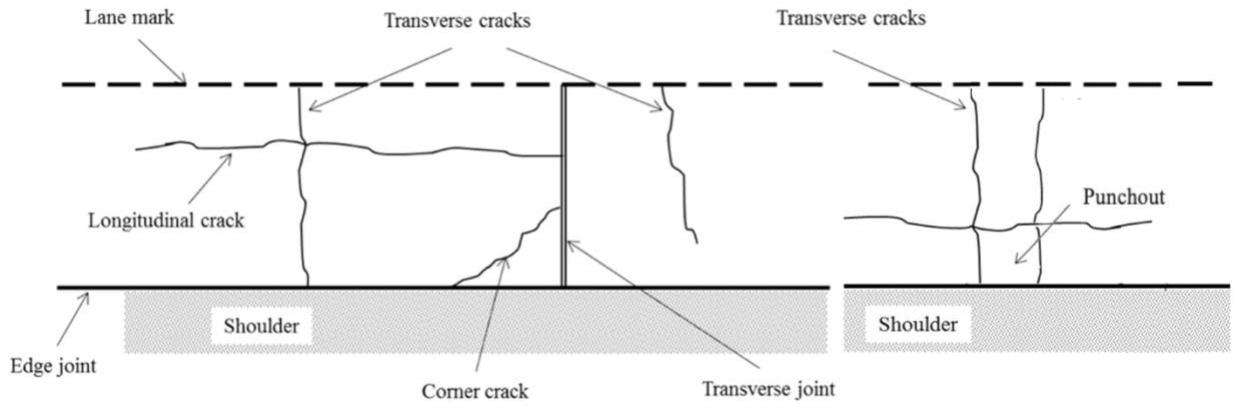

Figure 2-8. Types of fatigue cracking in concrete pavements

Faulting is another major distress in JPCP manifested as a difference in elevation across joints or cracks (Figure 2-9). Faulting mainly occurs in pavement structures subjected to repeated heavy loading insufficient load transfer between adjacent slabs, erodible foundation, and excess moisture. Insufficient load transfer increases the difference in vertical deflection of leave and approach slabs subjected to heavy loading. This high deflection under high-speed loading creates a pumping effect at the joint which ejects excess water along with fine materials from erodible base/subbase leading to the creation of a void under the slab. Significant faulting can create a corner crack in the slabs.

Figure 2-9. Joint faulting

Punch-out is a type of load-related distress created between closely spaced transverse cracks in CRCP. It is defined as a block of concrete that is bounded by two consecutive transverse cracks, a longitudinal crack on one side and the pavement edge on the other. Figure 2-10 depicts typical punch-out distress in CRCP. The occurrence of punch-out is associated with erosion of the underlying layers between two closely spaced transverse cracks. Reduction in aggregate interlock at the transverse cracks increases the induced tensile stress on the top of the slab which results in the formation of longitudinal crack typically 2 to 5 ft. away from the pavement edge. Progression of punch-out distress continues with repetitive traffic loading and results in severe faulting (Roesler et al, 2016).

Figure 2-10. A typical CRCP punch-out distress

2.9. Concrete Pavement Design

There are varieties of factors that impact the structural responses of concrete pavements. They include the thickness of the concrete slab, concrete properties, load transfer devices, distance between joints, subgrade characteristics, environmental effects, magnitude, and location of traffic loads (Mallick & El-Korchi, 2013). In the early stages of concrete pavement design, the thickness pavement was chosen based on experience. Although the pavement design method has gradually developed, empiricism yet plays a critical role. Since the flexural stress of concrete has long been considered as a crucial or even the only, factor in the design of concrete pavements, the development of design methods was not as significant as that of flexible pavements (Huang, 2003). Empirical pavement design was considering the ability of pavement to withstand against traffic during a certain period of time by the Present Serviceability Index (PSI) as a criterion for designing pavements. This concept was introduced by the American Association of State Highway Officials (AASHO) Road Test as a rating factor for pavement performance showing the ride quality. PSI ranges from 0 to 5 where PSI of 5 represents a pavement with excellent performance (Huang, 2003). Typically, a PSI of 1.5 is considered as a minimum tolerance for end of service life (AASHTO 1993). Later, empirical design equations were developed for rigid and flexible pavements using the historical data from AASHO Road Test. However, these equations were developed for a specific pavement structure, climate, and design condition and may not suit other regions or conditions. In addition, the empirical method for designing CRCP was to modify the performance equations of JPCP developed in the AASHO test or determine the required thickness for JPCP and use less thickness for CRCP. This reduction was determined based on local experiences. The reason for choosing reduced thickness was a better load transfer mechanism in

CRCP compared to JPCP (Won, 1989). Extensive field studies on performance of CRCP in Texas showed different performance despite employed similar design and construction techniques.

To overcome the limitations of empirical equations, the Mechanistic-Empirical (M-E) pavement design method was developed in the 1970s. This method utilizes mechanical modeling and performance observations throughout the pavement life for the design of pavement. The a mechanical model determines pavement responses under combinations of loading conditions, while the empirical part uses the calculated responses by mechanical model to predict the life of pavement based on site-specific field performance (Timm and Barret, 2005). Figure 2-11 depicts the design procedure according to the Mechanistic-Empirical Design Guide (MEPDG).

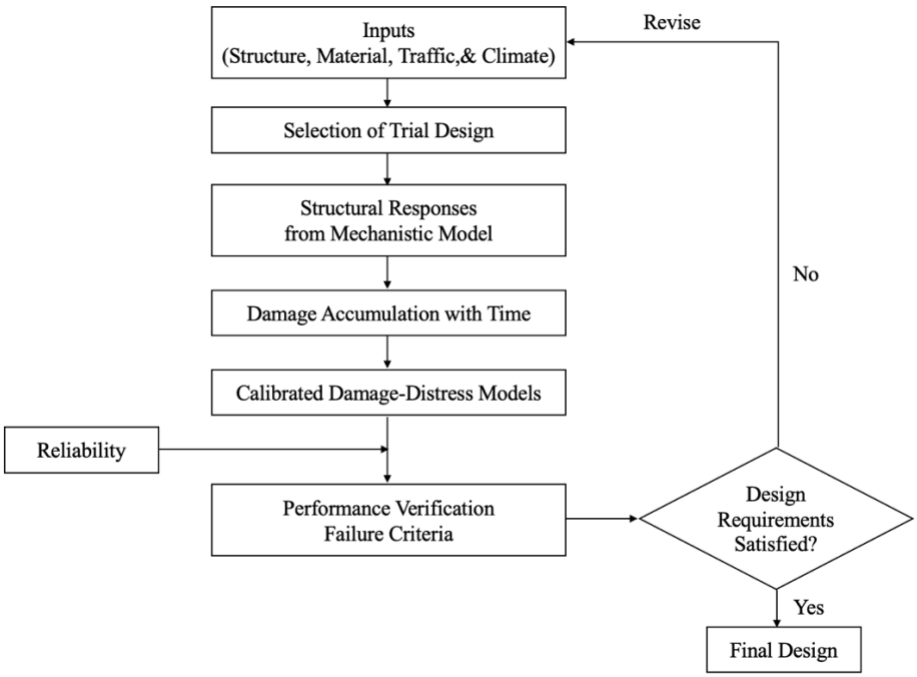

Figure 2-11. Pavement design procedure based on MEPDG.

2.10. Concrete Pavement Response Models

The response of concrete pavements under traffic loads is highly affected by various factors including size of slabs, presence of discontinuities (e.g., joints and cracks), load transfer

mechanisms (e.g., aggregate interlocks, dowel bars), environmental factors (e.g., temperature warping and moisture curling). These factors make the analysis of concrete pavements complicated and more challenging compared to the flexible pavement (Kim, 2017). concrete pavements should be evaluated under various load cases at different load locations. Although field studies can be conducted to analyze these factors, these studies are very expensive as it requires extensive pavement construction and instrumentation (McCracken, 2006; Chatti et al., 2009). Considering the important factor in rigid pavement responses, various response models with different levels of simplifications have been developed.

2.10.1. Westergaard Analytical Response Model

In earliest attempts, Westergaard (1926) presented a closed-form analytical solution for calculating concrete pavement responses under traffic loading and environmental effects based upon elasticity theory. This analytical solution was developed considering the following assumptions:

i) The concrete slab is considered as a homogeneous, isotropic, and elastic thin plate in equilibrium.

ii) Slabs are considered to be semi-finite in the horizontal direction and the effect of discontinues is ignored.

iii) The transverse shear stresses are ignored.

iv) The reaction of the subgrade is proportional to the deflection of the slab and acts only in the vertical direction.

v) The subgrade layer is considered as a dense liquid (Winkler) foundation and modeled as a set of springs with a constant of k which is represented by the modulus of subgrade reaction (k-value), and it is independent of the deflection of the slab.

vi) The concrete slab has a uniform thickness.

vii) The concrete slab is only subjected to one wheel load with uniform load distribution over a circular area.

Westergaard considered three load cases including interior loading, corner, and edge loading as shown in Figure 2-12.

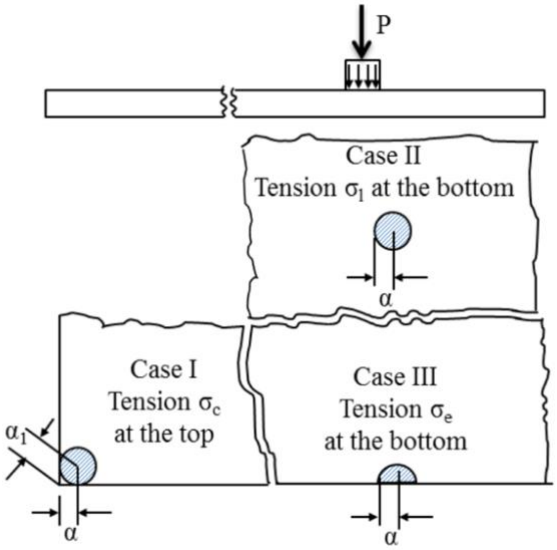

Figure 2-12. Three loading conditions in Westergaard model.

Westergaard defined the term of the radius of relative stiffness (ℓ) which quantifies the stiffness of the slab relative to the stiffness of the subgrade. The relative stiffness can be computed using the following equation:

$$\ell = \sqrt[4]{\frac{Eh^3}{12k(1-\nu^2)}} \quad (2\text{-}1)$$

in which, h is the thickness of slab (m), and E and ν are Elastic modulus (MPa) and the Poisson ratio of concrete, and k is modulus of subgrade reaction (MPa/m). The following equations

represent Westergaard's equations for calculating stresses (σ) and deflections (Δ) of rigid pavement for the three loading conditions:

1) Wheel load close to the corner of slab

$$\sigma = \frac{3P}{h^2}\left[1 - \left(\frac{\alpha\sqrt{2}}{\ell}\right)^{0.6}\right] \quad (2\text{-}2)$$

$$\Delta = \frac{P}{k\ell^2}\left[1.1 - 0.88\left(\frac{\alpha\sqrt{2}}{\ell}\right)\right] \quad (2\text{-}3)$$

Where, α is contact radius (m), and P is concentrated loading (N)

2) Wheel load at interior of a slab

$$\sigma = \frac{3P(1+\nu)}{2\pi h^2}\left(ln\frac{\ell}{b} + 0.6159\right) \quad (2\text{-}4)$$

$$\Delta = \frac{P}{8k\ell^2}\left\{1 + \frac{1}{2\pi}\left[ln\left(\frac{a}{2\ell}\right) - 0.673\right]\left(\frac{a}{\ell}\right)^2\right\} \quad (2\text{-}5)$$

Where,

$b = a$, when $a \geq 1.724h$

$b = \sqrt{1.6a^2 + h^2} - 0.675h$, when $a \leq 1.724h$

3) Wheel load at the edge of slab

$$\sigma = \frac{3P(1+\nu)}{\pi(3+\nu)h^2}\left[ln\left(\frac{Eh^3}{100ka^4} + 1.84 - \frac{4\nu}{3} + \frac{1-\nu}{2} + \frac{1.18(1+2\nu)a}{\ell}\right)\right] \quad (2\text{-}6)$$

$$\Delta = \frac{\sqrt{2+1.2\nu P}}{\sqrt{Eh^3k}}\left[1 - \frac{(0.76+0.4\nu)a}{\ell}\right] \quad (2\text{-}7)$$

Although these equations calculate the stress and deflection under traffic loading and curling, the calculated values do not reflect the actual rigid pavement behaviors due to

simplification considered in assumptions. All pavement layers underneath the slab should be represented by an equivalent modulus of subgrade reaction which leads to a decrease in accuracy. In addition, this model is not capable of considering discontinuities nor computing pavement responses under multiple wheel loads (Williams, 2003).

Many attempts have been made to improve Westergaard's model. Picket and Ray (1951) improved Westergaard's equations by considering multiple wheel loads and developed influence charts for deflection, moment, and reactive pressure under the interior, edge, and center loadings. Later, the Newton-Raphson iteration method was used to convert multiple loadings including dual, tandem, and tridem axles to an equivalent single load producing the same bending stress Salsilli et al. (1993). Despite many improvements, assumptions associated with these analytical models result in too many limitations making the analysis complicated.

Empirical methods have been derived from experiences in several states. In the current design procedures, the design method for continuous reinforced concrete pavements was developed through modifying the equations of jointed concrete pavements developed in the AASHO Road Test.

2.10.2. Finite Element Models

To overcome the limitations of analytical models, Finite Element Method (FEM) as a powerful numerical technique has become a widely used technique for solving problems with complicated geometry, loading, and material properties since the early 1970s. Several two-dimensional (2-D) finite element models have been developed for analyzing rigid pavements incorporating curling stresses.

JPCP Finite Element Models

Cheung and Zienkiewicz (1965) established the very first algorithm for analyzing concrete slabs on both a semi-infinite elastic continuum and a Winkler foundation. Later, Huang and Wang (1973) used this algorithm to develop a finite element procedure to compute the response of thin plates with Winkler foundations. Chou (1984) improved the Huang and Wang model to take the multi-layer system into the calculation and developed a 2-D FE program called WESLIQID which was able to analyze a two-layered pavement system under multiple wheel loads. Tabatabaie (1978) developed the first 2-D FE program for concrete pavement analysis known as ILLISLAB. In this program, pavement layers were considered as medium-thick elements on a Winkler foundation. ILLISLAB was able to consider the effect of bonded or un-bonded base layers under the concrete slab subjected to multiple wheel loads. Also, it was capable of evaluating the effect of different load transfer mechanisms. However, this program could only consider the thermal loads with a linear temperature gradient in-depth for one slab. Tayabji and Colley (1986) implemented the formulation of ILLISLAB and developed the JSLAB program which was able to evaluate the effect of warping due to moisture and thermal gradient and calculate principal stresses. JSLAB was further improved to consider different axle configurations and subgrade types (spring, Winkler, Boussinesq, Vlasov, Kerr, ZSS foundations) for two-layer jointed concrete pavements up to nine slabs. To improve the accuracy and capability of ILLISLAB, it was further modified by different researchers (Ioannides, 1984; Korovesis, 1990; and Khazanovich and Ioannides, 1993). In 2000, Khazanovich et al., at the ERES Division of Applied Research Associates, developed an enhanced version of ILLISLAB program called ISLAB2000. This program can model a multi-layer pavement system which leads to more accurate analysis. Also, it has the capability of considering multiple slabs, mismatched joints, multiple loads, temperature curling, and evaluating

the effects of subgrade deformation under slab edges. This program was integrated into the new MEPDG as the response model for rigid pavement.

Despite significant improvements brought by 2-D FE programs on pavement analysis, they still cannot correctly model the behavior of components of concrete pavements. For instance, the interaction between dowel bar and concrete slab and horizontal frictional behavior of pavement layers cannot be accurately modeled. Some of these deficiencies can be addressed by employing three-dimensional (3-D) finite element programs. Owing to rapid advances in computer processing capabilities and memory capacity, 3-D FE programs were adopted by researchers to develop more realistic models considering multi-wheel loads, non-uniform load distribution, pavement cracks, and nonlinear dynamic analysis, etc., and better understand different modes of failures in rigid pavements.

In one of the earliest 3-D FE studies, Ioannides and Donnelly (1988) performed a study to provide guidance for the effective utilization of 3-D FE modeling for rigid pavements. GEOSYS program was employed to model a single concrete slab on a subgrade. The impact of mesh refinement and boundary conditions on pavement response were analyzed. Zaghloul et al. (1994) developed a nonlinear and dynamic finite element model of JPCP using the general-purpose finite element program ABAQUS. The subbase and subgrade were modeled by 3-D eight-node brick elements, and Mohr-Coulomb friction was applied between base and subbase layers. Joints were modeled using gap elements, and dowel bars were modeled by bar elements at the mid-depth of the slab. An 18-kips single axle load at the speed of 2.8 km/h was applied to the slabs and a parametric study was performed. The results showed that dowel bars significantly improve the load transfer efficiency and consequently decrease vertical deflections of slabs. In addition, it was found that decreasing the spacing of dowel bars increases load transfer efficiency. Beegle and

Sargand (1995) developed a 3-D FEM for JPCP to study the impact of varying material properties on pavement response under static truck loading and thermal gradient. 20-node solid brick elements were used to model slab, base, and subgrade, and beam element was used for dowel bars and tie bars. The results indicated that the presence of thermal gradient, increasing modulus of concrete slab leads to higher deflection. In addition, it was observed that decreasing subgrade increases the contact area between the curled slab and base layer. Uddin et al. (1995) evaluated the impact of rigid pavement discontinuities on the surface deflection of JPCP subjected to a falling weight deflectometer (FWD) load using finite element modeling. Pavement layers were modeled by 3-D eight-node brick elements, and dowel bars were modeled using beam elements. Also, gap elements were utilized to model cracks and transverse joints. The moduli of pavement layers were evaluated using backcalculated for uncracked pavement, cracked concrete slab, and base layer. Masad et al. (1996) conducted a FE study on the impact of temperature variation on concrete slabs using ABAQUS program considering the loss of contact between slab and foundation. Their results indicated a reasonable agreement with those obtained by KENSLABS, ILLI-SLAB, and JSLAB programs. In addition, they found that a nonlinear temperature gradient creates higher tensile stress compared to the linear gradient. Davids et al. (1998) developed a 3-D FE program called EverFE for simulating JPCP under static traffic load and environmental effects. In this program, slabs and base layer are modeled using 20-node quadratic brick elements, while the subbase layer is modeled by 8-node planar quadratic elements. The subgrade is simulated as a dense liquid foundation. This program permits modeling of temperature gradient (Up to 4 points of temperature changes), aggregate interlock, contact of dowels and ties with concrete, dowel looseness, and loss of contact between slab and base. Studies showed a good agreement between the pavement response calculated by EverFE and experimental results.

CRCP Finite Element Models

McCullough et al. (1975) under a project sponsored by the National Cooperative Highway Research Program (NCHRP) developed the first computer program for the mechanistic design of CRCP which was known as CRCP-1. This program was able to evaluate CRCP under traffic and environmental loads. The validity of the program was verified with extensive field studies. Later, CRCP-4 was developed based upon the improvement of CRCP-1, which had the capability of predicting transverse crack spacing and width, and steel stress in CRCP pavements (Won et al., 1991). Further improvement of this program led to the development of CRCP-5 which included fatigue failure models. CRCP-7 program was developed in 1992, as an enhanced CRCP model which adopted a one-dimensional FE model and included calibrated fatigue failure prediction models (Suh et al., 1992). However, simplified assumptions associated with the one-dimensional FE method were imposing many limitations in the analysis. In 1996, Texas Department of Transportation (TxDOT) initiated a research project to improve the mechanistic model for CRCP by considering the effect of temperature variations and moisture changes through the depth of the concrete (Kim et al., 1997 and 1998). TxDOT extended this research project aimed at the development of a new mechanistic model of CRCP called CRCP-9 in which 2-D and 3-D FE models were adopted to predict the crack spacing using the Monte Carlo simulation method. Also, a failure prediction model was developed using probability theories (Kim et al., 2000). The comparison of the results obtained from 2-D and 3-D FEM showed that 2-D models can approximate the result obtained from 3-D models except in the regions near the edge (Kim et al., 2000). CRCP-9 program could consider curling and warping of the slab due to temperature change and drying shrinkage through the depth. However, CRCP-9 implemented Westergaard equations to calculate the induced stresses by wheel loads instead of FE approach. To address this issue,

Won and McCullough (2001) developed CRCP-10 program and considered the effect of moving dynamic tandem axle loads. In CRCP-9 and CRCP 10 programs, the concrete layer and reinforcing steel bars are modeled using 3-D brick elements and beam elements respectively. The underlying layers, however, are considered as a Winkler foundation. The frictional interaction between the slab and underlying layer was modeled using horizontal springs and a bond stress-slip was considered between concrete and reinforcement steel and modeled using horizontal spring.

TxDOT's current design procedure for CRCP implements mechanistic-empirical (M-E) design principles to determine the required pavement thickness which includes mechanical modeling from CRCP-9 and CRCP-10 programs along with performance observations. This design procedure was developed by Ha et al. (2011 and 2012) and presented in a form of an Excel spreadsheet called TxCRCP-ME which evaluates the performance of CRCP in terms of punch-outs per mile. For the development of TxCRCP-ME, an FE-based mechanistic model was used. In this model, three-dimensional solid elements were used to model concrete and reinforcement steel, and the interaction between them was modeled as an 8-node plane quadrilateral interface element. A composite modulus of subgrade reaction (composite k-value) was considered to simulate the supporting layer. To determine this value, the supporting layers were modeled using ABAQUS 6.7 program in which the base layer was simulated by elastic solid elements, while the subgrade was considered as Winkler foundation modeled by a set of springs. A Static load was applied on the surface of the base layer, and the composite k-value was calculated by measuring the vertical deflection. To account for various types of supporting layers, a series of static analysis was conducted using different combinations of the layer properties, and a regression analysis was performed. However, studies showed that the material properties and thickness of each supporting layer, especially the base layer, significantly impact the response of the concrete layer, and

considering a composite k-value may not be a proper method for modeling the supporting layers (Aguirre, 2020).

Al-Qadi and Elseifi (2006) developed a 3-D FE model to study the mechanisms leading to transverse cracking in CRCP pavement and predict the crack spacing. To do so, a CRCP pavement structure at the Virginia Smart Road was simulated using ABAQUS program. Concrete slab and pavement layers were modeled using eight-node solid brick elements. The reinforcement steel was also modeled using three-dimensional continuum elements. The contact between concrete and steel bars was considered to be fully bonded. A linear temperature gradient was applied to the model. To verify the applicability of the 3-D FE model to predict crack spacing, the results were compared to the field performance of the pavement section. The FE model results showed a good agreement with the observed cracking pattern in the field. Kim et al. (2018) developed a 3-D finite element model to evaluate the cracking potential in CRCP under the combined effects of thermal and axle loads. In this model, the concrete slab, base, and subgrade layers were modeled using eight-node solid brick elements, while reinforcement steels were modeled by beam elements. A parametric analysis was performed to determine the impacts of loading location, concrete properties, and spacing of reinforcement steels on cracking potential. The results showed that the critical location of load is at the corner of the slab in the presence of a positive temperature gradient. Also, it was observed that the critical tensile stress in concrete decreases by increasing base modulus, slab thickness, and transverse crack spacing. It was also found that reducing the spacing of longitudinal reinforcement decreases the induced tensile stresses in the slab.

2.11. Rigid Pavement Fatigue Distress Models

Fatigue damage is the major distress in rigid pavements. Repeated application of traffic loading results in fatigue damage at the critical response location. It can be propagated through

bottom-up or top-down mechanisms due to traffic loading and environmental effects. The calculation of fatigue damage involves the summation of damage created by each load from each damage increment. Fatigue damage is determined according to Miner's hypothesis as given in the following expression:

$$FD = \sum_{i=1}^{k} \frac{n_i}{N_i} \quad (2\text{-}8)$$

Where,

FD = Total fatigue damage

n_i = Number of load applications on the pavement

N_i = Allowable number of load applications on the pavement

i = loading or seasonal condition

Various fatigue models have been developed to estimate the allowable number of load repetitions to failure in concrete pavement. The most widely used models include Vesic model, Darter model, Tepfers model, PCA Beam Fatigue Model, and MEPDG fatigue model.

Vesic and Saxena (1969) developed a model for fatigue damage created by axle loads by combining Westergaard plate theory and field results obtained from AASHO Road Test. This model is expressed as follows:

$$N_{2.5} = 225000 \times \left(\frac{MR}{\sigma}\right)^4 \quad (2\text{-}9)$$

Where,

$N_{2.5}$ = Number of axle passes to failure

MR = Modulus of rupture of concrete slab

σ = Maximum tensile stress of concrete slab

Darter and Barenberg (1977) developed a fatigue model using several laboratory fatigue tests on concrete beams. The model is given in the following expression:

$$\log(N_f) = f_1 - f_2\left(\frac{\sigma}{MR}\right) \quad (2\text{-}10)$$

Where,

N_f = Allowable load repetitions

MR = Modulus of rupture of concrete slab

σ = Induced maximum tensile stress in concrete slab

f_1 = Calibration coefficient (16.61)

f_2 = Calibration coefficient (17.61)

Tepfers and Kutti (1979) proposed a model for fatigue life of concrete pavement by considering combination of axle load and environmental effects. Tepfer fatigue model is expressed as follows:

$$\frac{\sigma_{max}}{MR} = 1 - \beta(1 - R)logN \quad (2\text{-}11)$$

Where,

N= Number of axle repetition to failure (reliability = 50%)

MR = Modulus of rupture of concrete slab

$$R = \frac{\sigma_{min}}{\sigma_{max}}$$

σ_{max} = Induced maximum flexural stress by loading

σ_{min} = Induced minimum flexural stress before loading caused by environmental effect

β = Calibration coefficient (0.0685 for concrete)

When the minimum flexural stress is taken to be zero, Tepfers model can be simplified to the following equation:

$$\frac{\sigma_{max}}{MR} = 1 - \beta log N \qquad (2\text{-}12)$$

This equation calculates a smaller number of load repetitions compared to the original model.

Portland Cement Association (PCA) suggests the use of the model developed by Packard and Tayabji (1983). This model was developed using concrete beams with 5% complete beam fractures. The PCA Beam Fatigue model uses the following expressions depending on the ratio of induced stress (σ) and modulus of rupture of concrete (MR):

$$log(N_f) = 11.737 - 12.077\left(\frac{\sigma}{MR}\right) \qquad \text{for } \frac{\sigma}{MR} \geq 0.55 \qquad (2\text{-}13)$$

$$N_f = \left(\frac{4.2577}{\frac{\sigma}{MR} - 0.325}\right)^{3.268} \qquad \text{for } 0.45 \leq \frac{\sigma}{MR} < 0.55 \qquad (2\text{-}14)$$

$$N_f = \text{unlimited} \qquad \text{for } \frac{\sigma}{MR} \leq 0.45 \qquad (2\text{-}15)$$

The Mechanistic-Empirical Pavement Design Guide (MEPDG) fatigue model was developed using several highway databases and determines the allowable number of load

applications to failure pavement with 50% slab cracking. The MEPDG fatigue model is expressed as follows:

$$\log\left(N_{i,j,k,l,m,n}\right) = C_1\left(\frac{MR_i}{\sigma_{i,j,k,l,m,n}}\right)^{C_2} + 0.4371 \quad (2\text{-}16)$$

Where,

$N_{i,j,k,l,m,n}$ = Allowable number of load applications at condition i, j, k, l, m, n

MR_i = Modulus of rupture of concrete at age i

$\sigma_{i,j,k,l,m,n}$ = Induced stress at condition i, j, k, l, m, n

C_1 = Calibration constant (2.0)

C_2 = Calibration constant (1.22)

i = Age, j = Month (accounts for change in base elastic modulus and modulus of subgrade reaction), k = Axle types, l = Load level, m = Temperature differential throughout the slab, and n = Traffic offset path (NCHRP, 2003).

CHAPTER 3: FINITE ELEMENT MODELING OF JPCP AND CRCP

3.1. Introduction

Finite Element Method proved to be a robust and powerful tool for solving complicated that are difficult to solve by analytical approaches. Finite Element Models (FEMs) are a widely accepted computational technique for analyzing concrete pavements. Although there exist various finite element programs developed specifically for analyzing and designing concrete pavements, they have some limitations in modeling such as the number of slabs, material property definitions, loading shapes, and conditions, etc. However, commercial finite element programs such as ABAQUS can be used to model concrete pavements more realistically. Therefore, in this study ABAQUS/CAE v. 6.14.3 was implemented to develop finite element models to identify critical stresses on PCC slabs.

Generally, FE models of rigid pavements consider the concrete slab as a linear elastic material. Several studies compared linear elastic FE predictions for pavement responses to those obtained from field measurement and found that linear elastic assumption produces acceptable results, and the results are in good agreement with each other (Kennedy, 1996; Hammons, 1997; Sargand and Beegle, 1998; and Lee, et al., 1998). Also, Shoukry and Williams (1999) backcalculated the layer moduli of rigid, flexible, and composite pavement structures using 3-D FEM. The surface deflections were measured using FWD sensors at different locations with different FWD loads. The plotted surface deflections versus different FWD loads indicated a linear relation. Also, it was observed that considering the linear elastic behavior for the base and subgrade layers is a valid assumption as the induced stresses in these layers are very small. However, in concrete pavement design, the subgrade soil is regularly represented by a Winkler foundation model. This is the simplest model for an idealized soil behavior which utilizes a series of

independent vertical springs with constant spring stiffness to simulate the soil. Westergaard (1925) called this spring constant the “modulus of subgrade reaction” which is known as the k value. Westergaard defined the modulus of subgrade reaction as the applied pressure required to create a unit deflection under the loaded area. The Winkler foundation considers that the vertical deflection of a point at subgrade surfaces is dependent upon the existing vertical stress applied at that point and there is no shear transfer at the surface, while elastic solid foundation yields a continuous deflection at the surface (Aljhayyish, 2019). Figure 3-1 shows the difference between Winkler and Elastic foundation. MEPDG recommends the use of the Winkler model for simulating the subgrade layer because of its simplicity and computational time requirements.

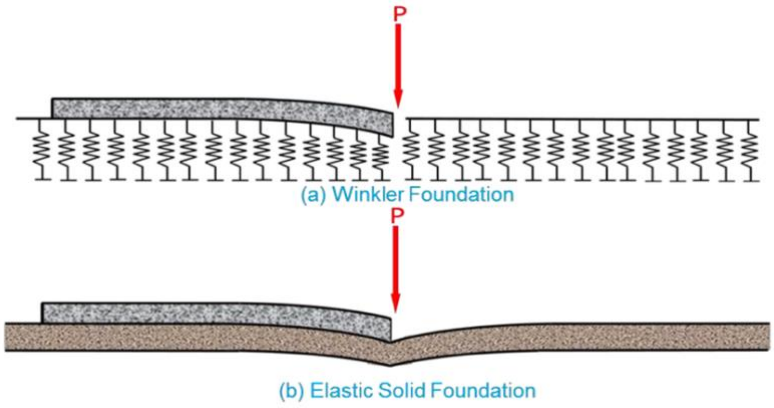

Figure 3-1. Winkler foundation vs. Elastic foundation

Various studies have been conducted to simulate the load transfer mechanisms across the joint. The load is transferred through aggregate interlock and dowel bars. The aggregate interlock mechanism transfers the load through the shear interaction of aggregate particles. Typically, this mechanism is ignored in concrete pavement design because this mechanism loses its effectiveness by wear and slab contraction (Kelleher and Larson, 1989). Measurements from field tests proved that the aggregate interlock mechanism is only effective when the joint opening is less than 1.0 mm (Maitra et al., 2009). Therefore, in JPCP design, dowel bars are considered as the only means

of the load transfer system across the transverse joints. The load transfer mechanism through dowel bars includes transferring the load between adjacent slabs without limiting free slab contraction. In previous FEM studies, dowel bars were modeled using spring and/or beam elements. Huang and Wang (1973) used linear elastic spring elements to simulate load transfer at the transverse joints. Tia et al. (1987) suggested the use of a combination of shear and torsional springs to model dowel bars behavior. Channakeshava et al. (1993) utilized beam elements along with spring elements to model dowel bars and interaction between dowel bars and surrounding concrete. Davids (2000) implemented quadratic beam elements for dowel bars and used springs sandwiched between dowel bars and concrete to define their interactions. Dere et al. (2006) modeled dowel bars as beam elements that are connected to concrete by two linear spring elements in horizontal and vertical directions. However, these approaches cannot realistically model the force generated between dowel bars and concrete slabs because the magnitude and directions of these forces are highly dependent on the load position of the concrete slab, and they vary from one dowel to another. William and Shoukry (2001) modeled dowel bars using eight-node solid brick elements. They divided the dowel bars into the sliding side and tied side. The sliding side is placed in a pre-drilled hole in the concrete slab and a friction interaction was defined between the bar and surrounding concrete surfaces to describe their relative movement. The other side of the dowel bar was embedded into the slab without the pre-drilling hole. Although this model requires assigning very fine mesh to dowel bars and surrounding concrete, it properly simulates their interaction and dowel bars load transfer mechanism. This concept was used in several studies to model concrete slab-dowel bars interaction (Khazanovich et al., 2001; Maitra et al., 2009; and Mackiewicz, 2015; Sadeghi and Hesami, 2018; Kim et al., 2018). Most of these studies considered the friction coefficients of 0.05 to define frictional interaction of dowel-concrete.

The interaction between the concrete slab and the underlying layer is typically modeled by friction interaction. According to AASHTO Pavement Design Guide (1993), the friction coefficient between the concrete slab and base course lies in the range of 0.9 to 2.2 depending on the types of base course. Various studies suggested the use of 1.5 for friction coefficient between concrete slab and base layer (Yoder & Witczak, 1975; Huang, 1993; and William et al., 2001).

Pavements are mostly subjected to moving traffic loads. The magnitude and contact area of the loads are affected by pavement surface roughness and vehicle suspension system. However, the dynamic analyses indicated that the dynamic response of concrete pavements is equal to or lower than their static response. Therefore, dynamic analysis is not generally necessary for concrete pavement design as it results in decreased pavement response (Chatti et al., 1994). In addition, Kim et al. (2000) studied the effect of the velocity of moving loads on JPCP response, and no significant change on the induced maximum tensile stress at the bottom of the slab was observed. The induced tensile stress in concrete pavement depends on the magnitude, location of loading, and axle configuration of vehicles (Hiller & Roesler, 2002). Therefore, concrete pavements should be evaluated under various load cases at different load locations to find the critical location in which maximum stress occurs in the concrete slab.

3.2. Development of JPCP FEM

3.2.1. General Assembly

The JPCP pavement structures were modeled as a multi-layered system consisting of an 8 inches Portland cement concrete (PCC) surface layer resting on 12 inches base layer, supported by natural subgrade soil. The surface layer consists of 9 slabs including 6 traveling slabs and 3 concrete shoulders. A full lane width of 12 ft was considered for traveling slabs 6 ft width for the

concrete shoulders. The length of slabs was taken to be 14 ft. Also, a small gap of 0.3 inches was considered between two slabs to simulate the joints in which dowel bars were the only means of load transfer. Dowel bars have a length of 18 inches with 1.25-inch diameter and they were placed in the mid-depth of the slab at the joints with 12 inches spacing. Besides, the slabs were connected to each other in lateral directions using 40 inches long tie bars with a dimeter of 0.625 inches. The spacing of tie bars was considered to be 40 inches. All slabs, shoulders, and dowels were modeled using solid elements, while beam element was used for tie bars. Base layer was also modeled using solid elements. However, according to literature, for analyzing concrete pavements, the subgrade layer is typically modeled as dense liquid Winkler foundation, instead of homogenous elastic solid, using spring connected to ground to ensure an accurate and more realistic result. To reduce the impact of boundary conditions and to provide realistic modeling, the middle slab is considered the slab of interest for evaluation. The assembled JPCP model is presented in Figure 3-2.

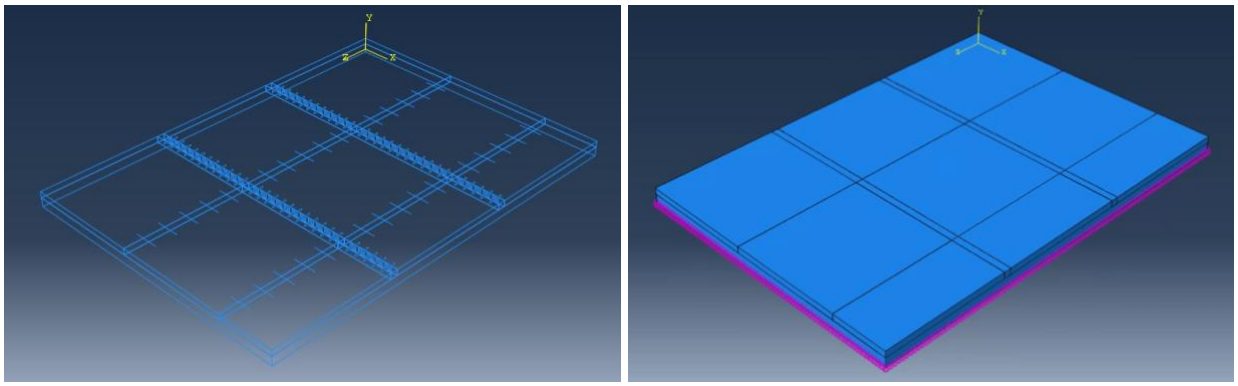

Figure 3-2. Finite element model of the JPCP structure

3.2.2. Material Models

Linear elastic material models were considered for all the parts in the models. Materials were characterized by their elastic modulus, Poisson's ratio, and density as presented in Table 3-1.

Table 3-1. Material properties

Part	Material	Modulus of Elasticity (psi)	Poisson's ratio	Density (pci)	Modulus of rupture (psi)	Modulus of subgrade reaction (pci)
Slab	Concrete	4,000,000	0.15	0.087	700	–
Base	Crushed stones	35,000	0.35	0.081	–	–
Dowel/ Tie bars	Steel	29,000,000	0.3	0.06	–	–
Subgrade	Natural Subgrade	–	–	–	–	120

3.2.3. Contact Interactions

Two contact interactions need to be defined in JPCP FEM. The first one is dowel-concrete interaction which accounts for the contact interactions between dowel and concrete around it. The second one is foundation-concrete interaction which refers to the interaction between PCC slabs and the base layer. These interactions in JPCP models were defined according to details provided in National Cooperative Highway Research Program (NCHRP) report on "Guidelines for Dowel Alignment in Concrete Pavements" (Khazanovich et. al., 2009). The dowel-concrete interaction was simulated using surface-to-surface contact technique with small sliding and constraint enforcement method of "node to surface". Besides, the depth of the adjustment zone was selected to be 0.1 inches. The depth of the adjustment zone lets ABAQUS adjust the position of the slave surface around the master surface (ABAQUS, 2014). No initial clearance between dowel and concrete was considered. For the contact property a "Tangential Behavior" with "Penalty" formulation with a friction coefficient of 0.05 and shear stress limit of 100 psi. was used, as well as a "Normal Behavior" with pressure-overclosure of "Hard contact" was implemented to minimize penetration of the dowel to the surrounding concrete at the interface and avoid transferring tensile stress across the interface.

The foundation-concrete interaction was defined using surface-to-surface contact with small sliding. The “node to surface” constrained enforcement with no adjustment zone was applied. A coefficient of friction of 1.5 with the possibility of separation was considered between concrete slabs and the base layer. This value was selected according to AASHTO pavement design guide recommendation (AASHTO, 1998). Besides, tie bars were simply embedded in concrete slabs to provide lateral support from adjacent slabs.

3.2.4. Meshing FEM

All layers were meshed using hexahedron 8-node reduced-integration 3-D linear brick elements (C3D8R). The size of mesh varied depending on the importance of the section. Considering the fact that the critical stress zones are located on middle traveling slabs, a fine mesh was assigned to this region. Meanwhile, meshing of all parts was refined to ensure that the model is computationally efficient. Dowel bars were also modeled using C3D8R elements, while 3-node beam elements (B31R) were used to model tie bars. The generated mesh for the model is presented in Figures 3-3 and 3-4.

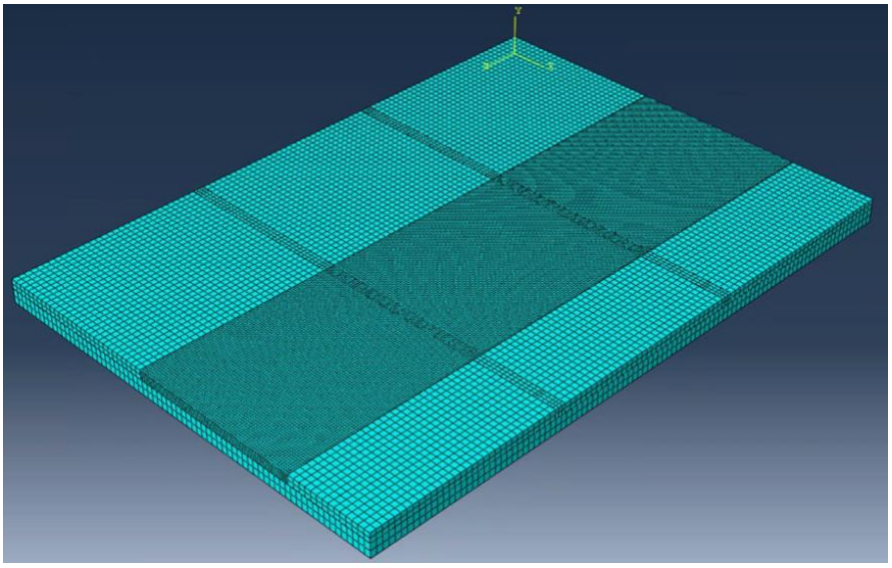

Figure 3-3. Finite element mesh used in the model

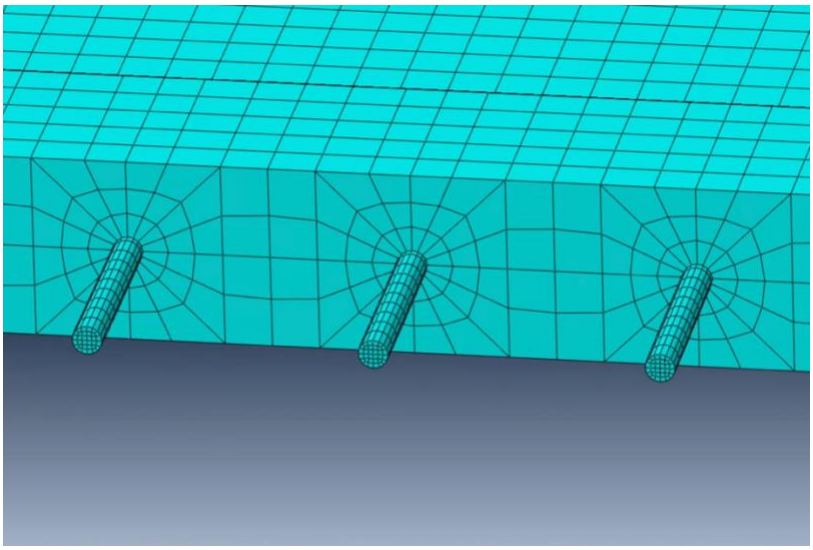

Figure 3-4. Finite element mesh at joint

3.2.5. Boundary Conditions

The boundary conditions for the model were assigned in a way that match those found in a real pavement structure. To simulate field conditions, the sides of the pavement model were constrained against all horizontal movements but allowed to move vertically. No boundary condition was applied at the bottom of the base layer as the subgrade was modeled using springs to ground to act as Winkler foundation.

3.2.6. Loading

For loading, a class 9 truck (single trailer 5-axle truck) with 80,000 lbs. gross weight is shown in Figure 3-5 was used. The axle and tire imprint dimensions of the truck as well as weight distribution over axles are represented in Figure 3-6. In FEM traffic loading can be simulated statically or dynamically. In this research, static analysis was performed as it is a widely accepted method for analyzing concrete pavements according to the literature. The truck was considered to run in the middle width of the lane, so the wheels were positioned 24 inches away from the edge of the slab. To obtain the critical locations of axles in which create the maximum stress at the

bottom of the slab, axle loads of the aforementioned truck were applied to the surface of the PCC slab and moved along the model. To do that, slabs were partitioned to provide the required surfaces to apply loads associated with each wheel (See Figure 3-7).

Figure 3-5. A typical class 9 truck.

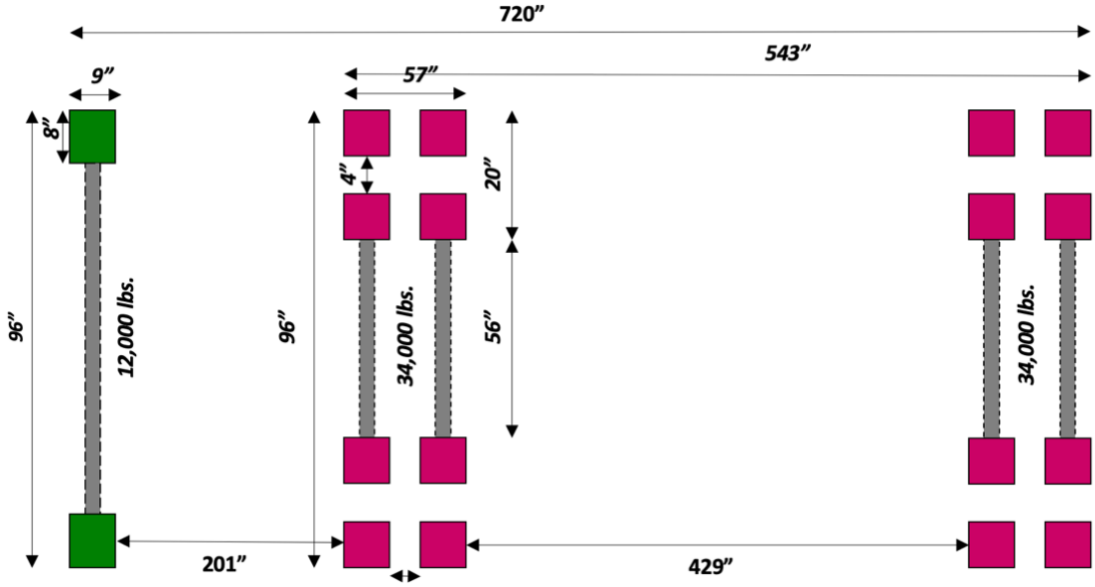

Figure 3-6. Dimensions and tire imprint of class 9 truck.

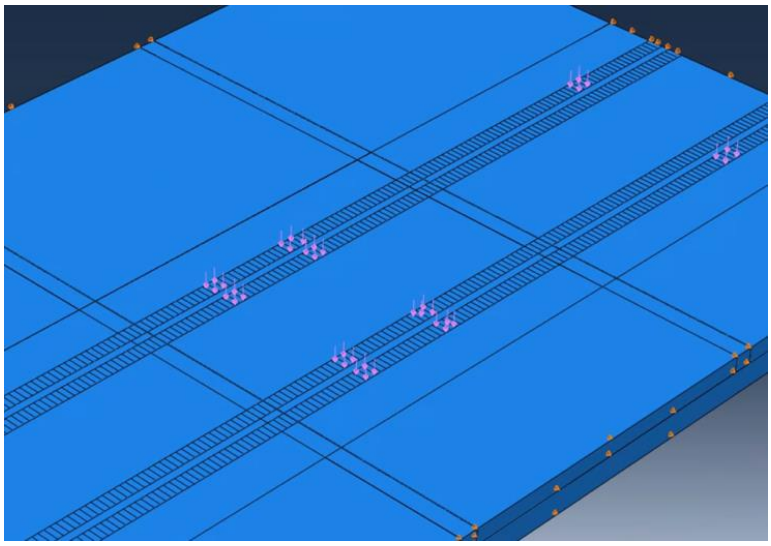

Figure 3-7. Surface partitions to applying loading on JPCP model

3.2.7. Locations of critical stresses

Using the developed JPCP FE model, stress analysis was performed to determine the maximum tensile stresses induced at the bottom of the concrete slab by the axle loads from the class 9 truck. After extensive runs of FE models by considering various locations for the truck axles along the slab, it was found that the maximum longitudinal stress is developed when the front wheels of the truck's tandem axle are located at the middle length of the slab. Figure 3-8 shows the distribution of the induced longitudinal stress in the slab. However, the maximum transverse stress is created at the joint when the front wheels of the truck's tandem axle are located at the joint, as depicted in Figure 3-9. Also, the lateral distribution of transverse and longitudinal stresses are presented in Figure 3-10. As can be seen, in this figure the maximum longitudinal stress is higher than those of transverse stress. Therefore, longitudinal tensile stress is the dominant induced stress at the bottom of the slab due to truck load which leads to the development of transverse bottom-up cracking in the slab. In addition, by evaluating the distributions of stresses from Figure 4-10, it is observed that the maximum longitudinal tensile stress is created 35 inches away from

the edge of the slab which is located between dual tires and closer to the inner tire. However, the maximum transverse tensile stress is developed 33 inches away from the edge of the slab which is corresponding to the edge of the outer tire of dual tires. Also, the variations of longitudinal tensile stress in the lateral direction are less than those of transverse tensile stress. As we move toward the edges of the slab, longitudinal stress is reduced from 162 psi to 80 psi, while this variation for transverse stress is intense as it decreases significantly away from the loading areas. Besides, the distribution of the induced stresses are shown in Figure 3-11. It is observed that the induced tensile stresses are transferred using dowel bars at the joints.

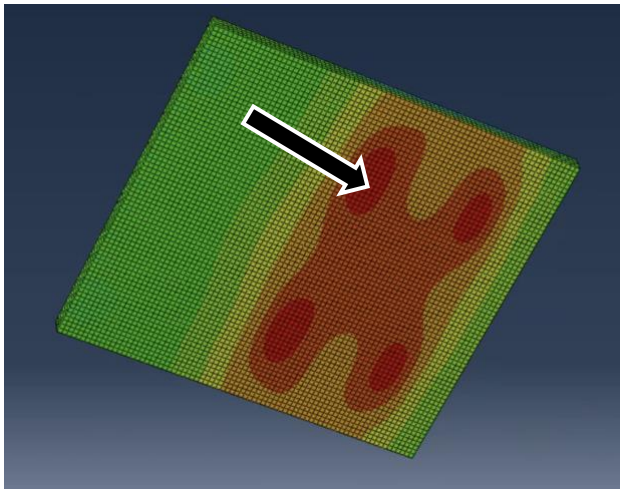

Figure 3-8. Maximum longitudinal tensile stress at the bottom of JPCP slab.

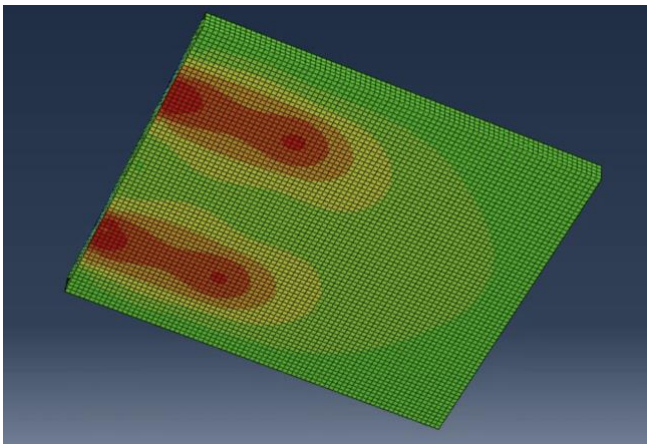

Figure 3-9. Maximum transverse tensile stress at the bottom of JPCP slab.

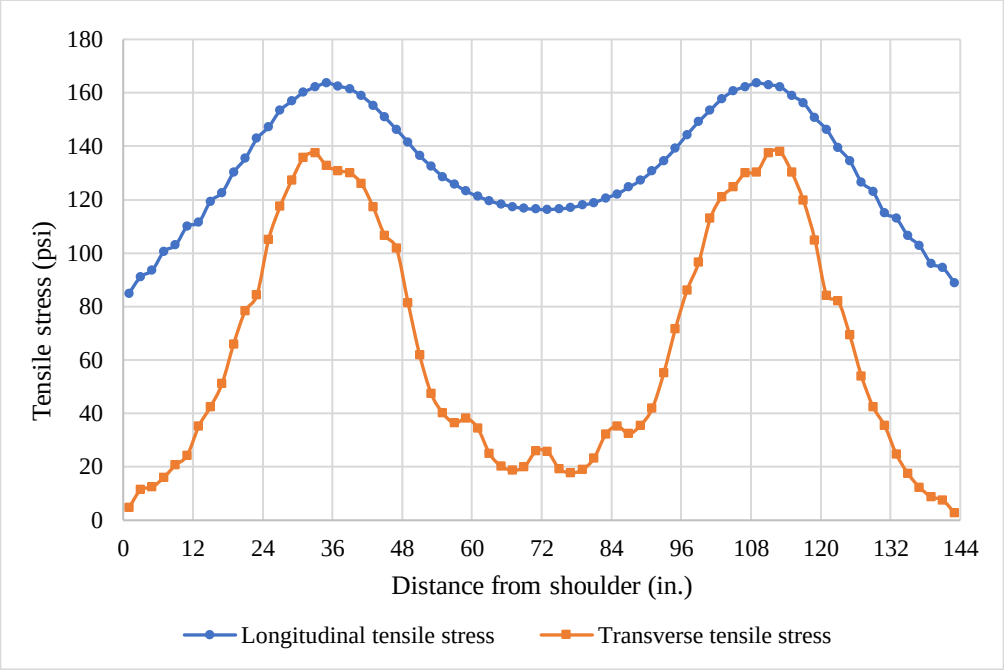

Figure 3-10. Lateral distribution of tensile stresses at the bottom of JPCP slab.

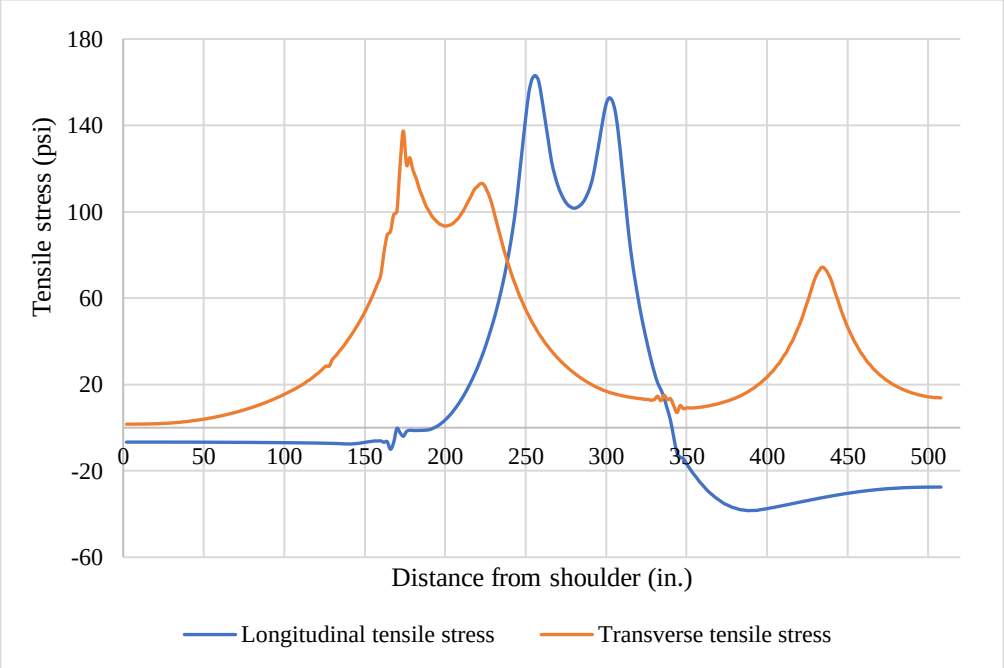

Figure 3-11. Distribution of induced tensile stresses at the bottom of slab along the model.

3.3. Development of CRCP FEM

3.3.1. General Assembly

Similar to JPCP, the CRCP pavement structure was modeled using a multi-layered system consisting of an 8 inches thick PCC surface layer and 12 inches thick base layer on top of natural subgrade soil. Transverse crack spacing was considered to occur every 5 ft. Therefore, the CRCP surface layer was modeled using 12 ft. × 5ft. slabs. A total of 24 slabs were considered for the surface layer including 16 traveling slabs and 8 concrete shoulder slabs. The width of shoulder slabs was taken to be 6 ft. Tie bars were modeled using beam elements with a diameter of 0.625 inches (#5 rebar) and a length of 30 inches. In addition, 480 ft. long #5 rebars were modeled using beam elements to go through all of the slabs in the length of the model. Rebars were placed with 5 inches spacing, while 30-inch intervals were considered for the tie bars (Roesler et. al, 2016). The base layer, also, was modeled using solid elements and dense liquid Winkler foundation was considered for the subgrade soil. The assembled JPCP model is presented in Figure 3-12.

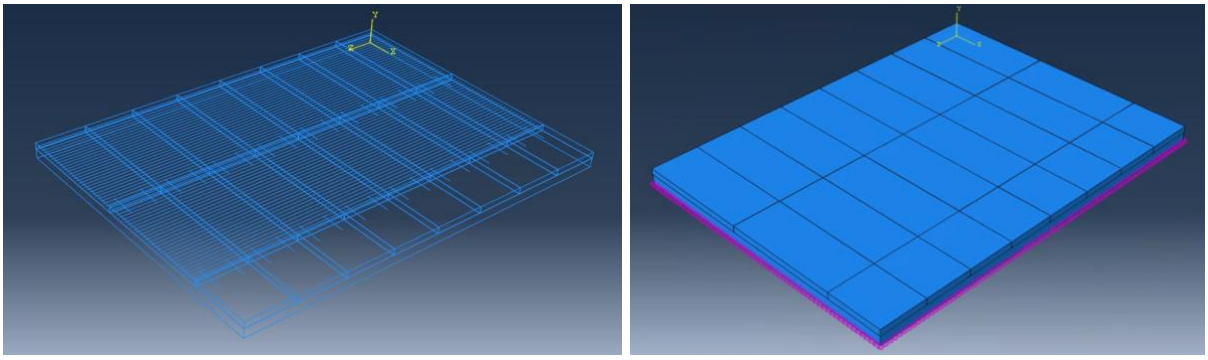

Figure 3-12. Finite element model of the CRCP structure

3.3.1. Material Models

Similar materials' characterization presented in table 3-1 were considered for the CRCP FE model.

3.3.2. Contact Interactions

The interaction between concrete slabs and the base layer was modeled using surface-to-surface contact technique with finite sliding and constraint enforcement method of “surface to surface”. A Tangential Behavior” with “Penalty” formulation with the friction of 1.5 along with “Normal Behavior” with pressure-overclosure of “Hard contact” was implemented. To simulate the aggregate interlock acting at crack surfaces, a “Tangential behavior” with coefficient friction of 3 was considered between PCC slabs. Moreover, rebars and tie bars were considered to be fully bonded with concrete according to Al-Qadi and Elseifi (2006), and they were embedded in the slabs.

3.3.3. Meshing FEM

Concrete slabs and base were meshed using C3D8R elements similar to the JPCP model. A similar meshing strategy was used to optimize the mesh size over the CRCP model. Reinforcement steel bars and tie bars were meshed using 3-node beam elements (B31R). The generated mesh for the model is illustrated in Figure 3-13.

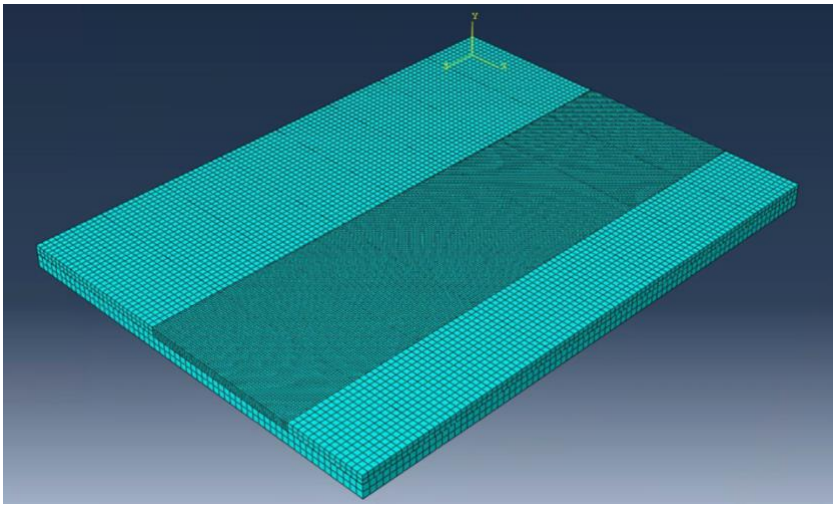

Figure 3-13. Generated finite element mesh used in the CRCP model.

3.3.4. Boundary Conditions

The boundary conditions were considered to constrain horizontal movements of layers, but the vertical movement was allowed. No boundary condition was needed for the bottom of the model as the subgrade was modeled as Winkler foundation.

3.3.5. Loading

Similar static loading from the class 9 truck shown in Figure 3-5 was applied to the CRCP model. The truck was considered to run in the center of the lane, so the wheels were positioned 24 inches away from the edge of slab. Similar to the JPCP model, one full pass of the truck was modeled to find the location in which maximum stress at the bottom of the slab is created. Figure 3-14 depicts surface partitions and applied load on the developed model.

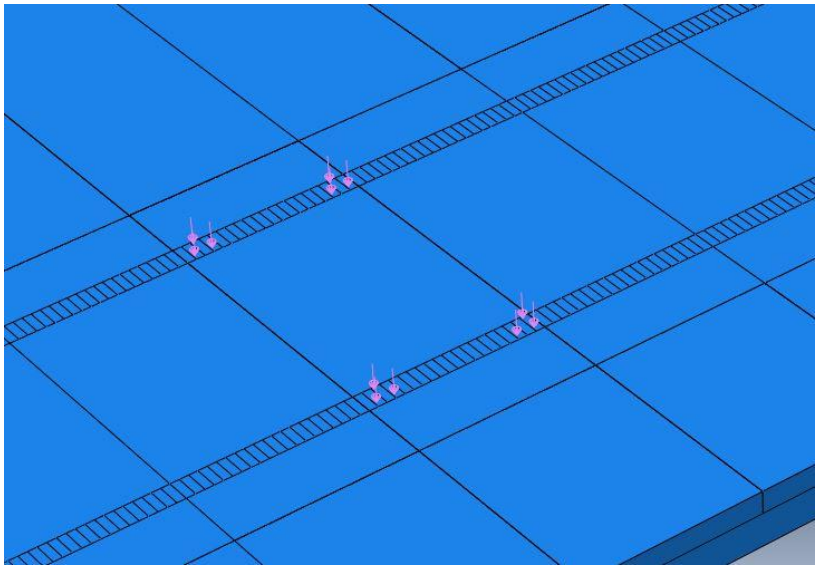

Figure 3-14. Surface partitions to applying loading on CRCP model.

3.3.6. Locations of critical stresses

The stress analysis of the developed FE model revealed that the maximum longitudinal tensile stress at the bottom of the slab is created when the front wheels of the truck's tandem axle

are located midway between two consecutive transverse cracks. The distribution of the longitudinal stress is illustrated in Figure 3-15. However, the developed maximum transverse tensile stress is associated with the condition that all tires of the truck's tandem axle are positioned between two consecutive cracks, and the front wheels of the truck's tandem axle are located at the edge of the crack. Figure 3-16 presents the distribution of the induced transverse stress at the bottom of the slab. The lateral distributions of longitudinal and transverse stresses associated with these two critical locations of the truck are shown in Figure 3-17. As can be seen in this figure, the maximum longitudinal and transverse stresses are created 37 inches away from the edge of the slab. Also, it can be seen that the magnitude of maximum longitudinal and transverse stress generated in the CRCP slab are roughly the same, but looking at their distributions, the variations of transverse stress are higher than those of longitudinal stress. The magnitude of transverse stress significantly decreases away from the loading area, but longitudinal stress distributes more uniformly. Moreover, the longitudinal distribution of the induced stresses are shown in Figure 3-18.

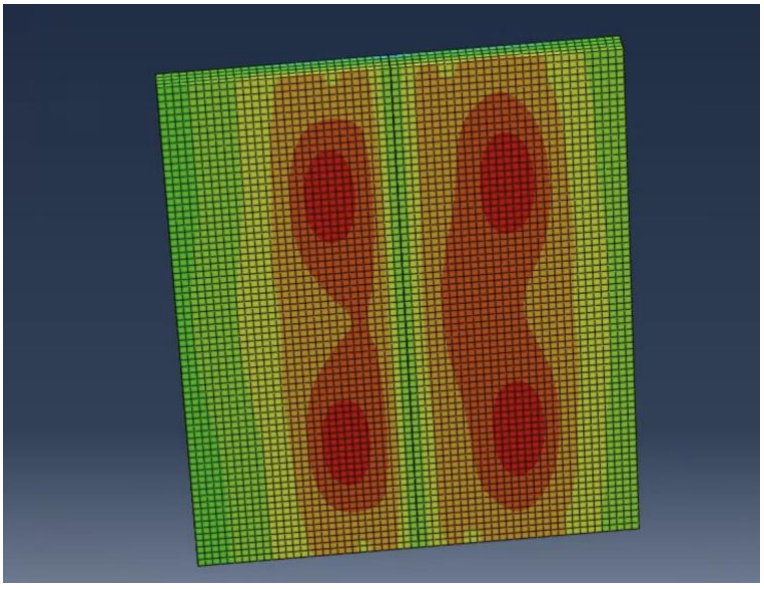

Figure 3-15. Maximum longitudinal tensile stress at the bottom of CRCP slab.

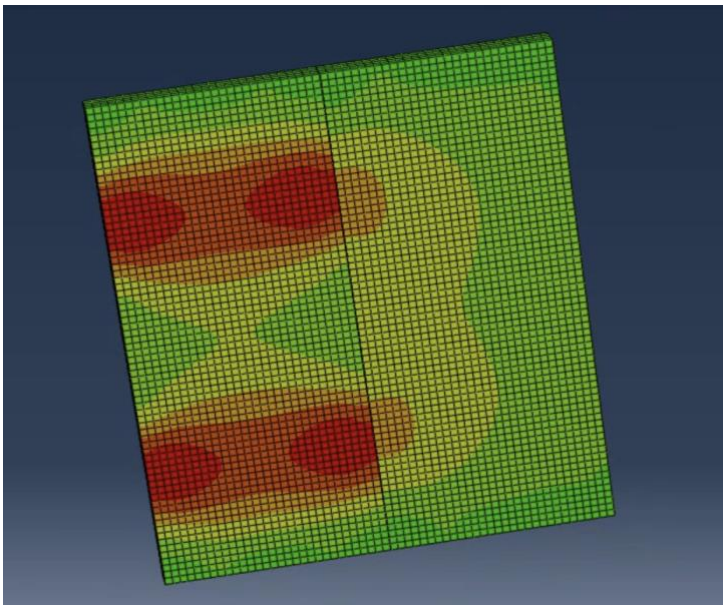

Figure 3-16. Maximum transverse tensile stress at the bottom of JPCP slab.

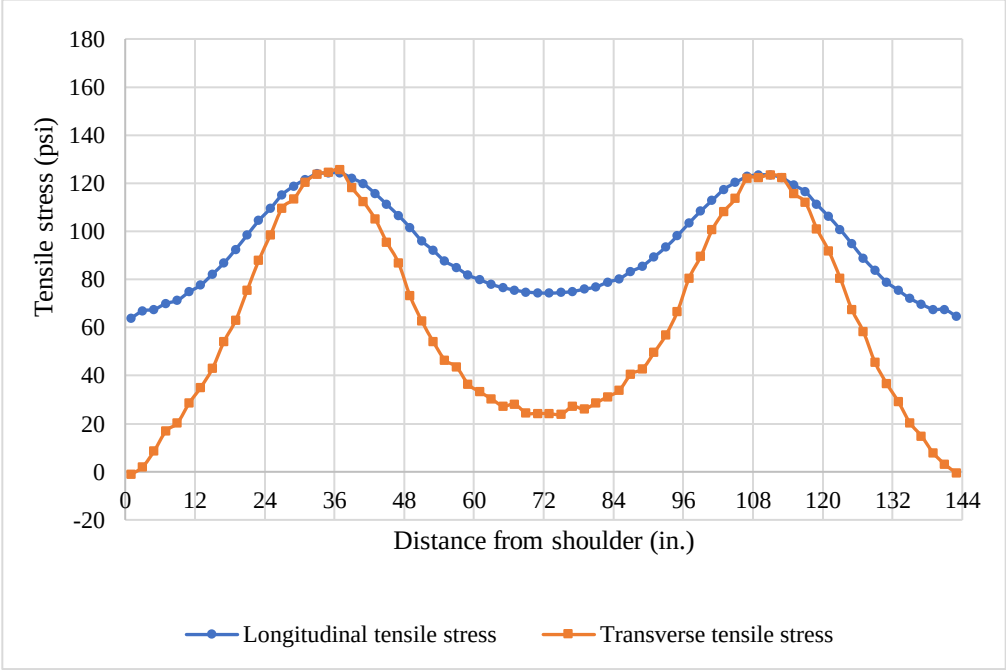

Figure 3-17. Lateral distribution of tensile stresses at the bottom of CRCP slab.

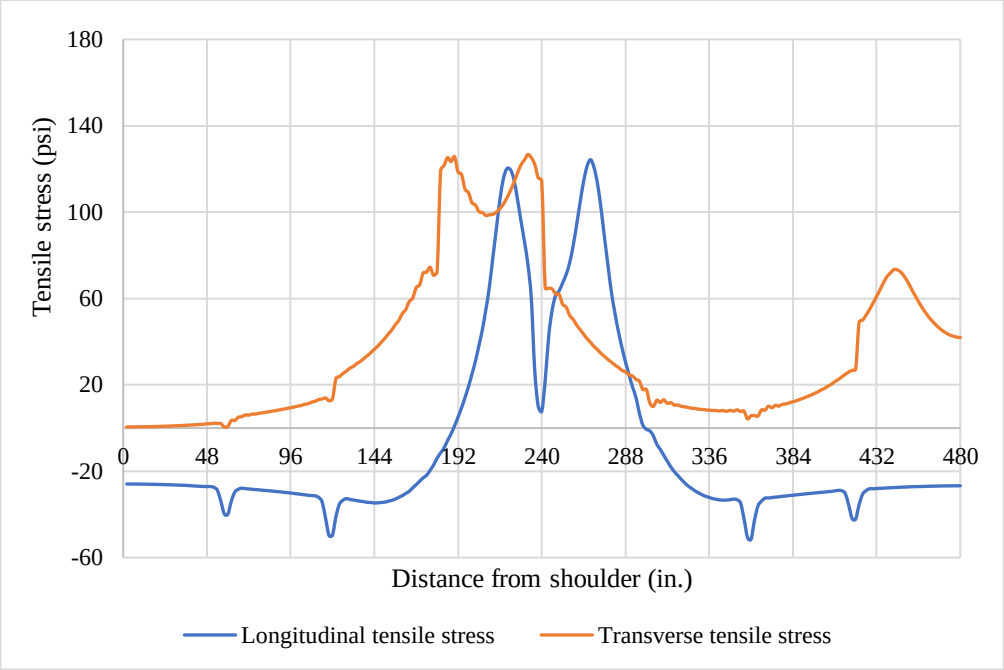

Figure 3-18. Distribution of induced tensile stresses at the bottom of CRCP slab along the model.

CHAPTER 4: DESIGN CONSIDERATIONS FOR IMPROVING PERFORMANCE OF CONCRETE PAVEMENTS

4.1. Introduction

This chapter focuses on the examination of various design considerations for improving the performance of JPCP and CRCP against truck platooning traffic. The design considerations include increasing the thickness of the PCC layer, thickening the PCC layer under the wheel path, using dowel bars with a larger diameter, and implementing larger diameter dowel bars and rebars within the wheel path in JPCP and CRCP, respectively. To do so, the critical positions of the truck are used for creating further FE models, and a parametric study is performed to evaluate the effectiveness of each of these considerations on the improvement of fatigue performance of pavements. In addition, to compare the performance of each design consideration under channelized traffic from truck platooning and regular traffic with wheel wander, further models will be developed for different lateral locations for the axle loads. These models will be utilized to determine the optimized concrete pavement structure showing better performance against truck platooning and enhanced expected service life.

4.2. JPCP design considerations

4.2.1. Impact of increasing the thickness of concrete slab

The selection of the thickness of slabs in the rigid pavement is governed by structural and economic factors. The slab thickness should be able to sustain traffic loads and the environmental conditions while it satisfies the lowest cost of construction. To evaluate the impact of JPCP slab thickness on pavement performance under truck platooning, the slab thicknesses of 8, 10, 12, and 15 inches are considered for FE modeling. To easier refer to these pavement structures in this manuscript, they are named JPCP-A1, JPCP-A2, JPCP-A3, and JPCP-A4, respectively.

Figure 4-1 shows the maximum tensile and maximum principal stresses (MPS) created in each pavement structure obtained from FE models. It should be noted that longitudinal and transverse stresses are developed in two different positions of axles as explained in section 3.2.7. Therefore, the maximum principal stresses corresponding to critical locations of longitudinal and transverse stresses are represented as MPS (L) and MPS (T), respectively. As can be observed in Figure 4-1, increasing the thickness of the concrete slab significantly reduces the induced stresses at the bottom of the slab. Increasing the thickness of the slab from 8 inches to 10 inches and 12 inches reduce the maximum longitudinal tensile stress by 22% and 36%, respectively. Comparing the results for JPCP-A1 and JPCP-A4 shows that doubling the thickness of slab decreases the longitudinal stress to more than half of its initial value. A similar conclusion can be drawn for transverse stress. Also, it was found that in the critical location of the loads, there is a negligible difference between the maximum principal stresses and normal tensile stresses which shows that the shear stress in these critical locations is close to zero. Therefore, in this study, normal stresses are used for bottom-up fatigue analysis. Since the longitudinal stress is larger than transverse stress, it is used for predicting bottom-up fatigue cracking.

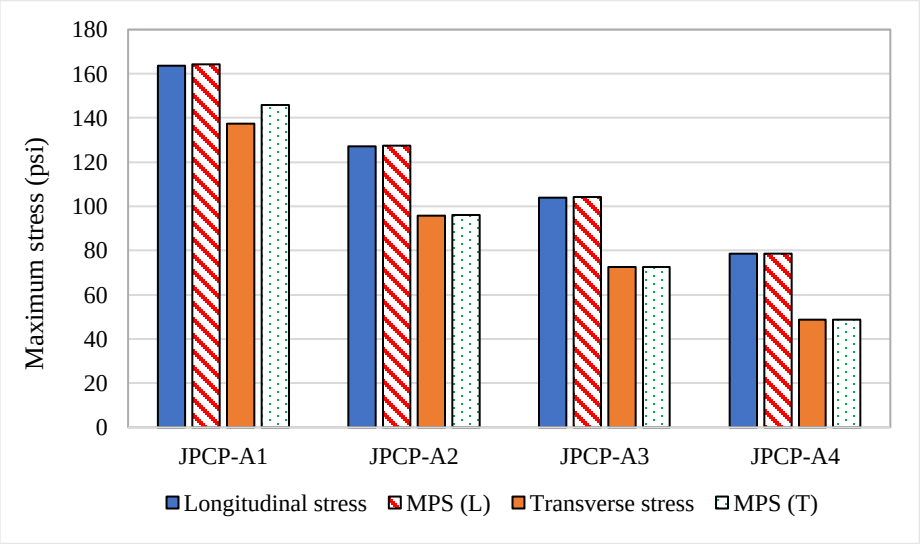

Figure 4-1. Effect of thickness of concrete slab on induced tensile stresses.

4.2.2. Impact of thickened PCC layer under the wheel path

Since the trucks in a platoon follow the leading truck, the axle loads will be concentrated only in the wheel path. Therefore, there might be a good chance to improve the performance of JPCP by increasing the thickness of the portion of the slab which is located under the wheel path. Thus, the thickness of the PCC slab under the wheel path is increased by 2 inches (JPCP-B1) and 4 inches (JPCP-B2) by cutting trenches with a 45-degree side slope in the base layer, as depicted in Figure 4-2. The bottom width of the trench was considered to be 20 in. similar to the width of dual tires.

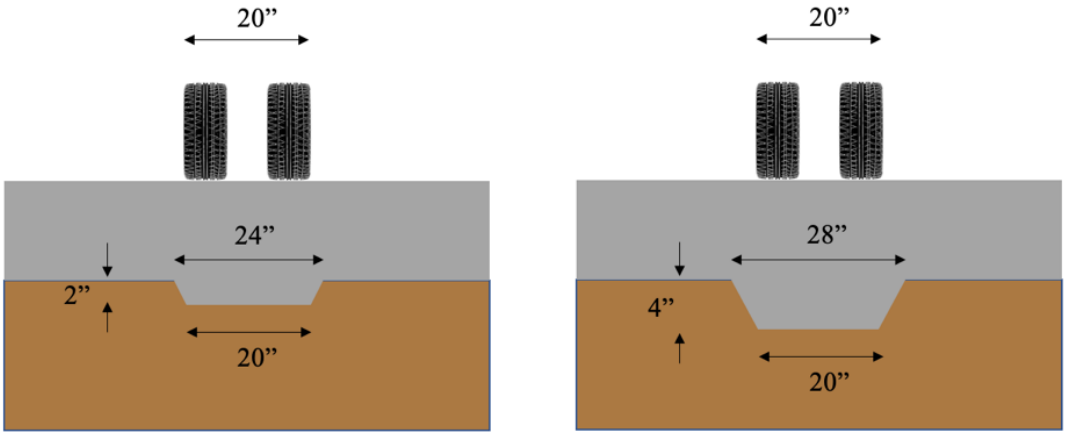

Figure 4-2. configuration of thickened PCC slab under the wheel path (a) 2 in. (b) 4 in.

After the initial evaluation of these models, it was observed that although the longitudinal and transverse stresses induced in the wheel path reduces compared to JPCP-A1, the transverse stresses created in the slab at the top edge of the trench is higher than those created under the wheel path (See Figure 4-3). These localized stress zones at the top edges of trenches make this design consideration ineffective in transverse stress reduction and increase the potential of bottom-up cracking starting from these points.

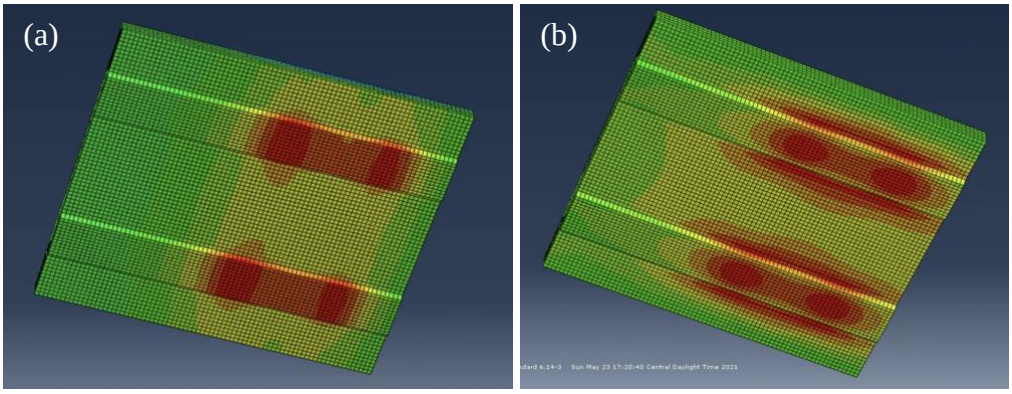

Figure 4-3. Induced (a) longitudinal and (b) transverse stresses at the edge of the trenches.

To address this stress concentration at the edge of the trenches, the width of the trenches can be increased. Therefore, a parametric study was conducted to find the minimum width of the trenches that produce lower transverse stress than those created under the wheel path at the bottom of the trench. To do so, the width of the bottom of the trench was increased from 20 in. to 24 in. and wider, until the induced transverse stress at the bottom of the trench is larger than those created at the edge of the trench. Figure 4-4 represents the result of the parametric study for JPCP-B1.

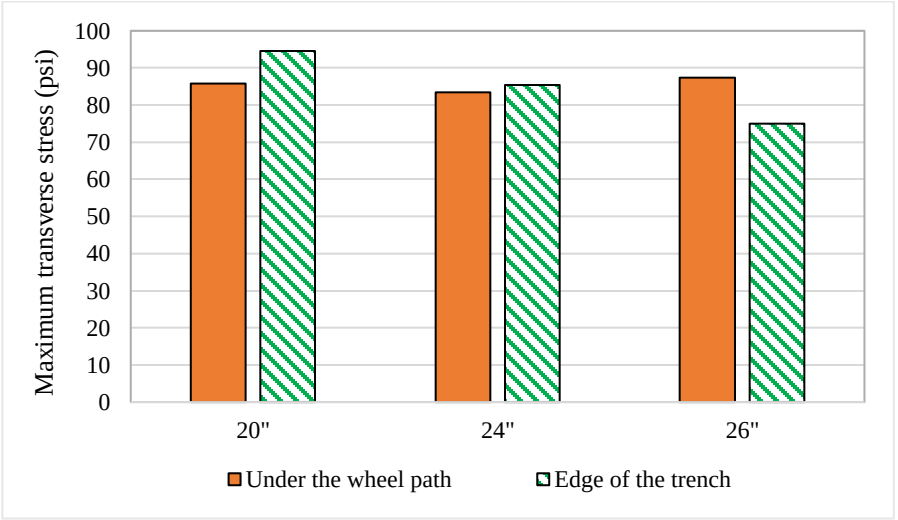

Figure 4-4. Transverse stresses created under different width of bottom of trench for JPCP-B1.

Figure 4-4 implies that increasing the width of the trench reduces the magnitude of transverse stress at the edge of the trench. It can be seen that when the bottom of the trench is 26

inches wide, the transverse tensile stress at the edge of the trench is lower than those induced under the wheel path. Figure 4-5 compares the transverse stress distributions for trench width of 20 inches and 26 inches. As can be seen, after increasing the bottom width of trenches to 26 inches, the maximum transverse stress is located at the bottom of the wheel path.

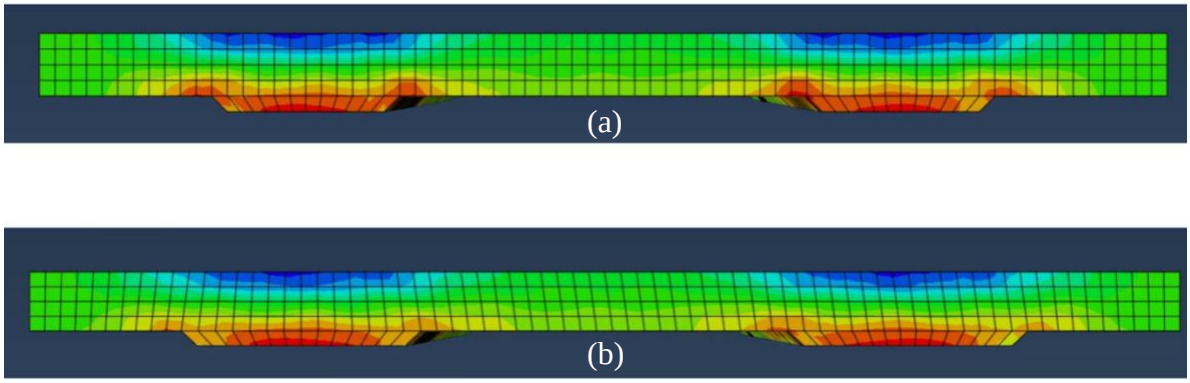

Figure 4-5. Comparing transverse stress distributions for (a) 20 in. and (b) 26 in. width of trench.

In addition, the longitudinal stresses for these cases are presented in Figure 4-6. As can be observed, the longitudinal stress decreases by increasing the width of the trench, but the maximum longitudinal stress is always less than those developed at the bottom of the trench.

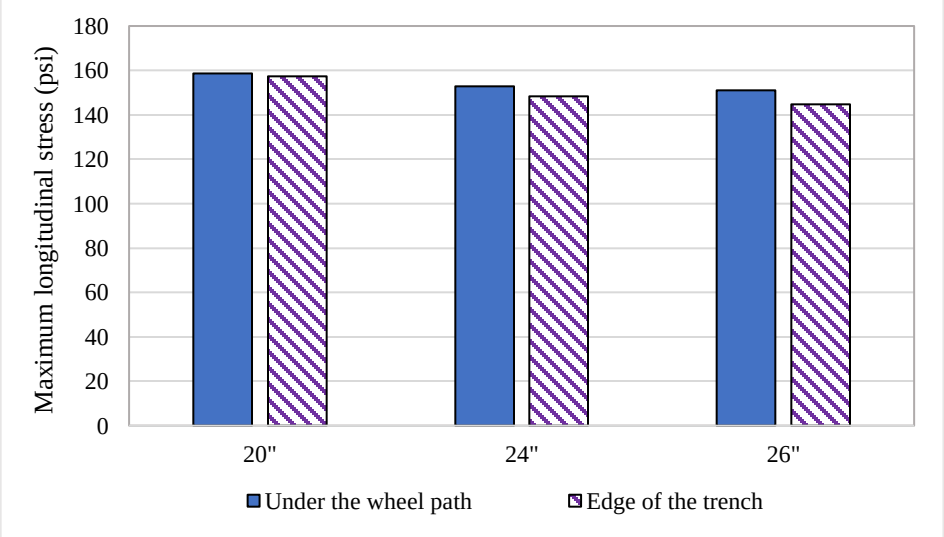

Figure 4-6. Longitudinal stresses created under different width of bottom of trench for JPCP-B1.

A similar analysis was conducted for JPCP-B2. The results are plotted in Figures 4-7 and 4-8. It indicates that a width of 32 inches for the bottom of the trench is required to get the maximum transverse stress under the wheel path. Also, Figure 4-8 proves that the longitudinal stress at the edge of the trench is always less than those created under the wheel path.

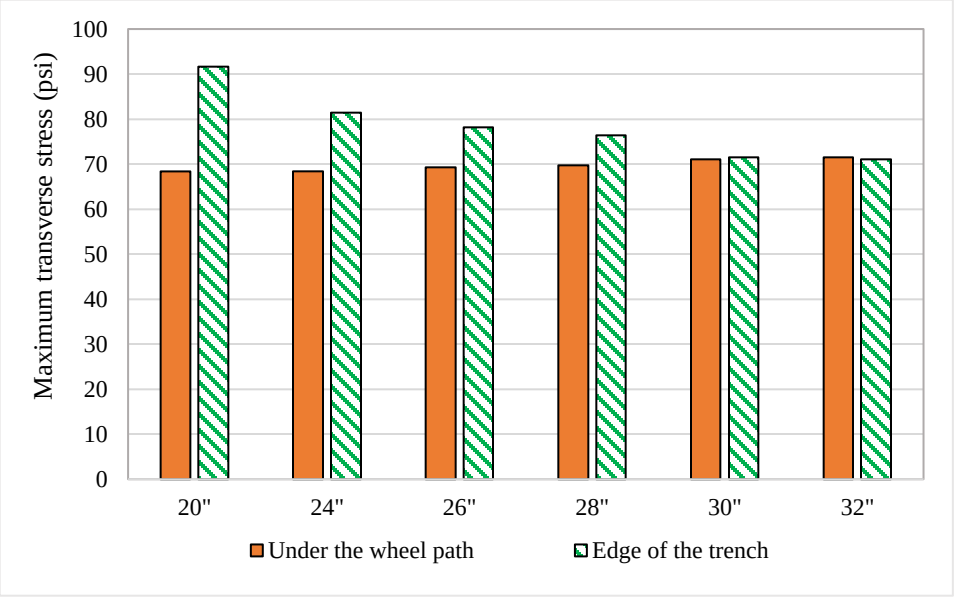

Figure 4-7. Transverse stresses created under different width of bottom of trench for JPCP-B2.

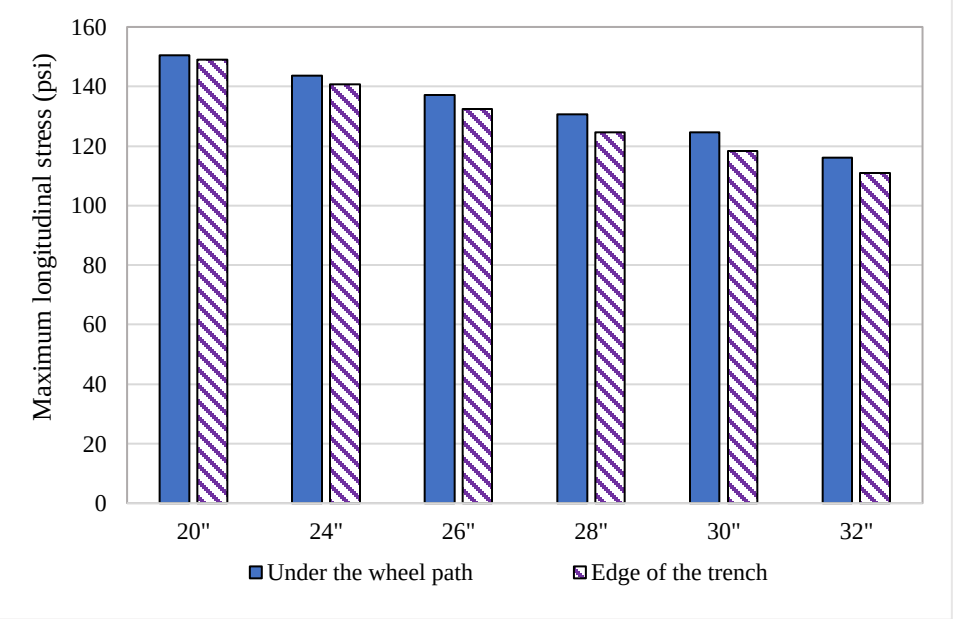

Figure 4-8. longitudinal stresses created under different width of bottom of trench for JPCP-B2.

According to the parametric study performed for the minimum width of the bottom of the trench, the width of 26 inches and 32 inches were selected for trenches in JPCP-B1 and JPCP-B2 structures, respectively. To evaluate the effectiveness of this measure on the reduction of induced stresses in JPCP, the results were compared to those obtained from JPCP-A1 (base structure). As shown in Figure 4-9, increasing the thickness of the slab under the wheel path by 2 inches and 4 inches. decrease the longitudinal stress by 7.7% and 29%, respectively. These reductions for transverse stress are 36% and 48%. Similar results were observed for maximum principal stresses. Comparing these results to those obtained from JPCP-A2 and JPCP-A3 reveals that, as expected, thickening the slab under the wheel path is effective in the reduction of stresses but not as much as increasing the thickness uniformly. The thickness of the slab for JPCP-A2 and JPCP-B1 are 10 inches under the wheel path, but the induced longitudinal stress in JPCP-A2 is 20% less than those developed in JPCP-B1. Similarly, comparing JPCP-A3 and JPCP-B2 reveals that 12 inches uniformly thick slabs produce 10% less longitudinal stress. It should be noted that the width of the trench in JPCP-B2 is 32 inches wide, so it reduces the difference between these two structures.

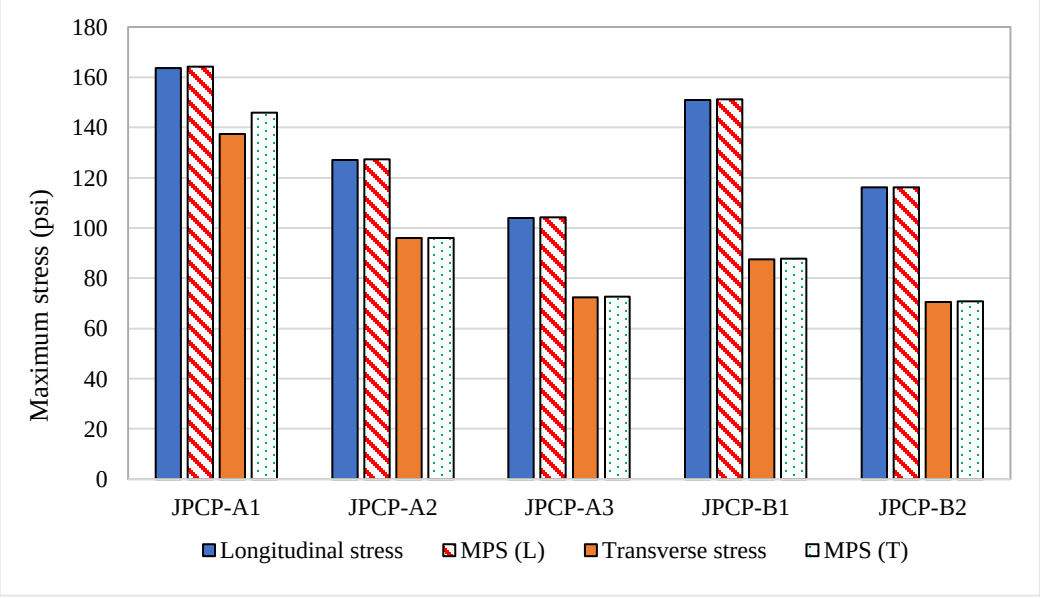

Figure 4-9. Effect of thickened slab under the wheel on induced tensile stresses.

4.2.3. Impact of dowel bar diameter

Dowel bars increase the load transfer efficiency by letting the leave slab carry the load before the load is over it. This decreases joint deflection and stresses in the adjacent slabs. In order to transfer the load between adjacent slabs, dowel bars are subjected to bending moments. The magnitudes of the bending moments generated in dowel bars are affected by their stiffness. Therefore, dowel bar diameter should have a considerable impact on the state of stresses induced in the concrete slabs. The most common dowel bars used in pavement construction have diameters of 1.25 inches and 1.5 inches. Thus, to study the impact of dowel bar diameter in stress reduction, the size of dowel bars in JPCP-A1 and JPCP-A2 are increased from 1.25 inches to 1.5 inches. These two models are referred as JPCP-C1 and JPCP C-2. The results from FEMs are plotted in Figure 4-10. It indicates that increasing the diameter dowel bars from 1.25 inches to 1.5 inches reduces the developed stresses in JPCP structures. Such a reduction in the longitudinal stress results from the fact that larger size dowel bars provide better load transfer and support from the adjacent slabs, so the bending of the slab due to load is decreased. Similar result was observed for transverse stress. It can be observed that using larger size dowel bars leads to 7.3% and 3.6% reduction in induced longitudinal stress in JPCP-C1 and JPCP-C2 structures, respectively. It shows that the effect of size of dowel bars in JPCP structures with thicker slabs decreases. This could be due to the fact that the bending in thicker slabs is lower than those developed in thinner slabs, so less load will be transferred by the dowel bars to the adjacent slab and the contribution of the dowel bars decreases. Therefore, the effect of increasing the size of dowel bar decreases in thicker slabs.

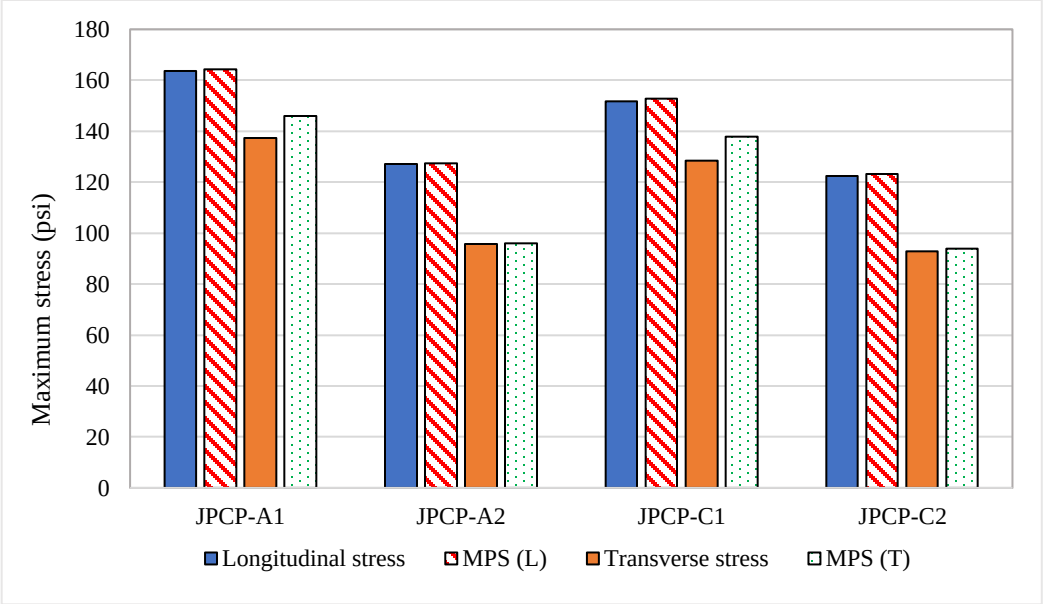

Figure 4-10. Effect of size of dowel bars on induced tensile stresses.

4.2.4. Impact of using dowel bars with larger diameter in the wheel path

Channelized loading associated with truck platooning and concentration of the wheel loads in a certain lateral position of the pavement surface provides this opportunity to examine the impact of increasing the diameter of dowel bars installed within the wheel path on the induced stress in the concrete. The distribution of the load through dowel bars across the joint was investigated by Friberg (1940) and it was found that the contributions of dowel bars closer to the location of the load are higher than those away from the load. Figure 4-11 illustrates the distribution of maximum principal stresses on concrete around the dowel bars. As can be seen, the maximum principal stress around dowel bars located in the wheel path is higher than those away from the wheel path, so dowel bars under the wheel path have higher contributions in load transfer. Therefore, instead of replacing all dowel bars at the joint, the 1.25 inches dowel bars located in the wheel path are replaced with 1.5 inches diameter dowel bars in JPCP-A1 and JPCP-A2. These pavement structures are called JPCP-D1 and JPCP-D2, respectively.

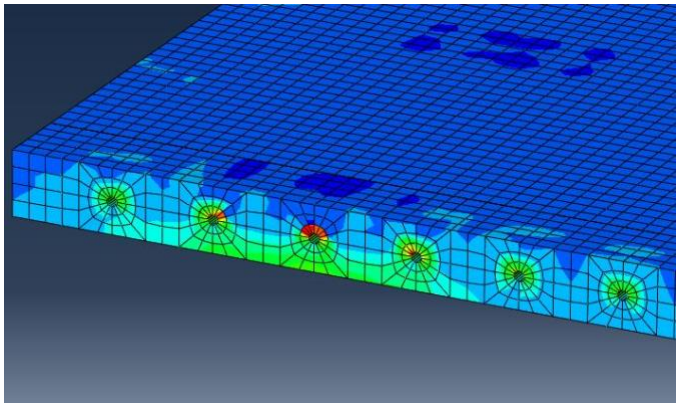

Figure 4-11. Maximum principal stress distribution on concrete around dowel bars.

Figure 4-12 compares the results from JPCP-D1 and JPCP-D2 with JPCP-A and JPCP-C structures. As can be observed, for the same slab thickness, replacing only the dowel bars in the wheel path with a larger diameter reduces the tensile stresses at the bottom of wheel path. However, this reduction is 5% for the longitudinal stress in pavement with 8 inches thick slab which is 2% less than those created by replacing all the dowel bars. Also, negligible change in transverse stress was observed by comparing the results from replacing dowel bars in the wheel path with replacing all of the dowel bars. Therefore, it can be concluded that using larger size dowel bars outside the wheel path has a minor effect on the reduction of maximum stresses at the bottom of the slab.

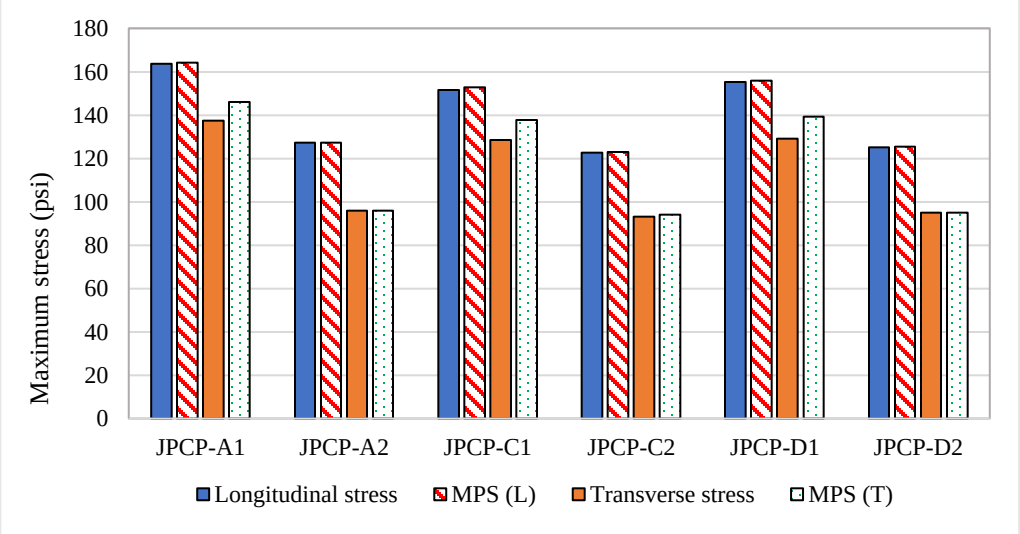

Figure 4-12. Effect of using larger size dowel bars in the wheel path on induced tensile stresses.

4.2.5. Impact of placing a thin asphalt layer under the concrete slabs

Base erodibility is one of the factors that significantly impacts the initiation and propagation of pavement distresses. It has been observed that JPCP pavement with treated base experiences less faulting compared to granular (untreated) bases. Utilizing a treated base such as an asphalt layer directly beneath the JPCP slab is the most common practice to eliminate base erosion and reduce the potential of pumping. Therefore, a 2-inch thick asphalt layer was modeled between the concrete slab and base layer. The asphalt layer was modeled with linear elastic behavior with the modulus of elasticity of 400,000 psi and a Poisson ratio of 0.3. The aforementioned design considerations were applied to the developed model. However, the trenches under the wheel path cannot be provided in the asphalt base layer. A similar naming convention was used for the developed models with asphalt base in which JPCP-A-AB represents structures with different slab thickness, JPCP-C-AB shows structures with larger size dowel bars, and JPCP-D-AB represents structures with larger size dowel bars in the wheel path.

Figure 4-13 summarizes the results obtained from analyzing the developed models. As can be seen, a similar reduction discussed in the previous sections was observed for JPCP structures with the asphalt base. Comparing the induced stress in JPCP with asphalt base with those with granular base shows that asphalt base reduces the magnitude of induced stresses. Also, it can be seen that increasing the thickness has the highest impact on stress reduction and JPCP with 15 inches slab thickness produces the least stresses. It can also be observed that although increasing the slab thickness from 8 inches to 10 inches in conjunction with replacing dowel bars with a larger diameter is an effective method for decreasing the induced stresses at the bottom of the slab, increasing the thickness alone to 12 inches is much more effective in stress reduction. Hence, a cost analysis is required to find a cost-effective alternative.

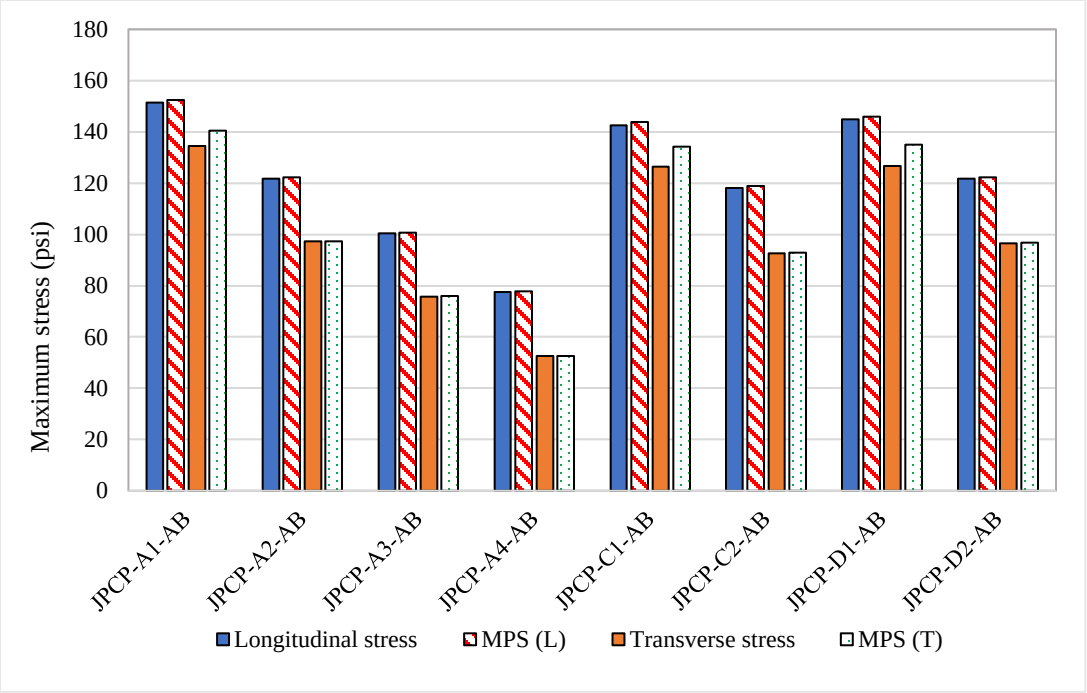

Figure 4-13. Induced stresses in JPCP structures with asphalt base.

4.3. Effect of lateral positions of the wheels in the induced stress in JPCP

To compare the stress created by channelized traffic results from truck platooning and normal traffic with wheel wander and to evaluate the performance of the discussed pavement structures under the different lateral positions of the wheels, the axle loads are moved toward the edge of the slab with 6 inches increments. Therefore, wheel wander of 6 inches, 12 inches, 18 inches, and 24 inches were modeled by positioning the edge of the outer tires 18 inches, 12 inches, 6 inches from the edge of and at the edge of the slab. Figures 4-14 and 4-15 depict the longitudinal and transverse stress distributions at the bottom of JPCP-A1 structure. As illustrated, the magnitude of the stresses significantly varies as the wheel wander increases. In addition, the maximum longitudinal stress occurs closer to the edge of the slab, while the transverse stress decreases as the vehicle is located at the edge of the slab.

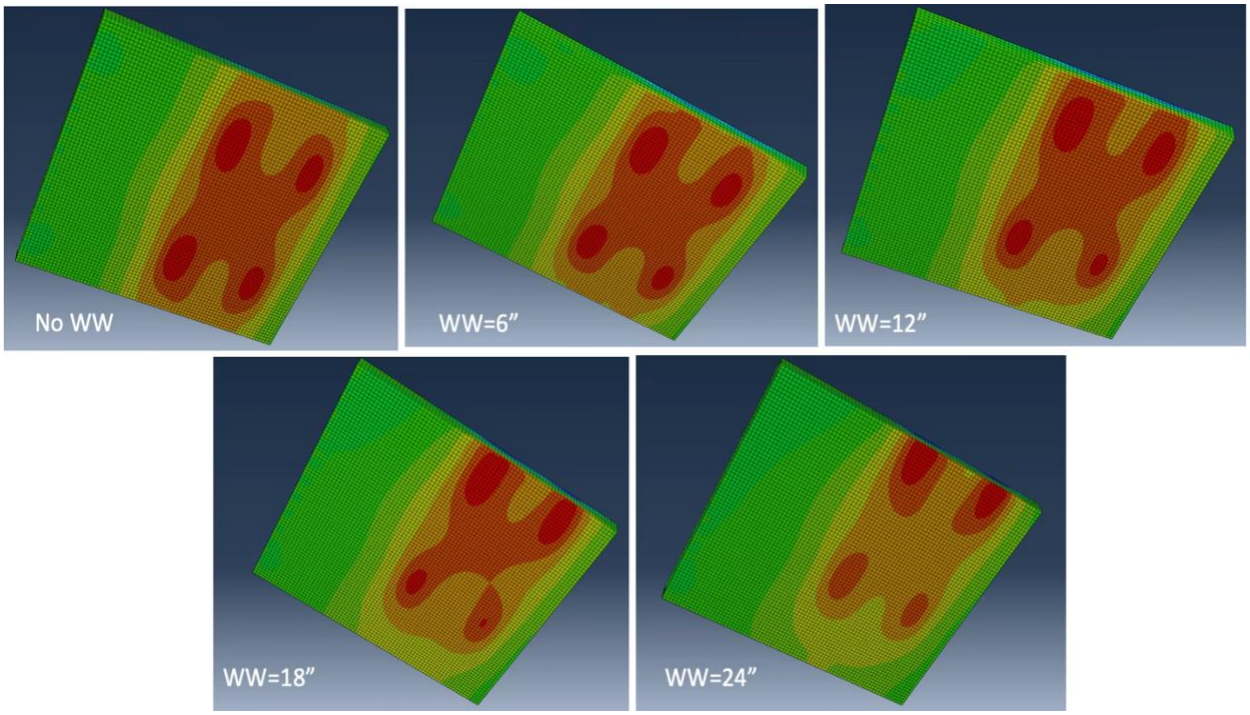

Figure 4-14. Longitudinal stress distributions under different levels of wheel wander.

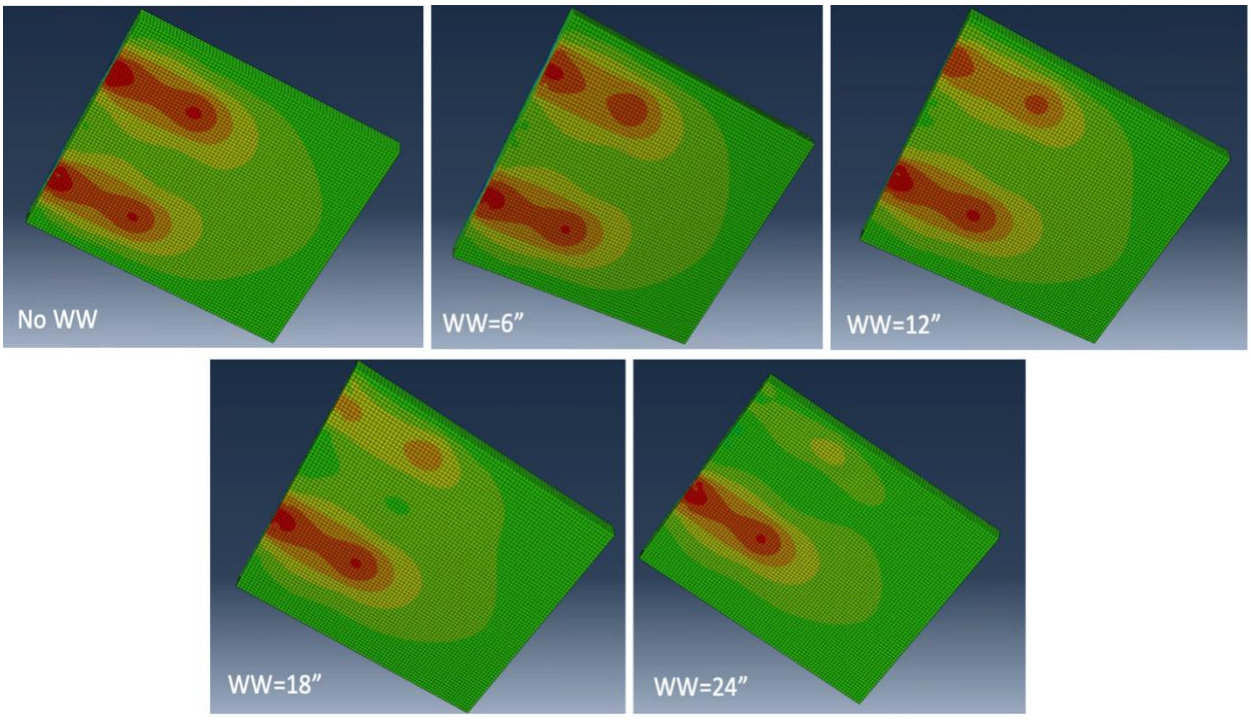

Figure 4-15. Transverse stress distributions under different levels of wheel wander.

Figures 4-16 and 4-17 represent the effect of wheel wander on magnitudes of critical longitudinal and transverse tensile stresses at the bottom of the pavement structures. As can be observed in Figure 4-16, wheel wander increases the induced longitudinal stresses at the bottom of the slab, and the maximum tensile stress is created when the load is located at the edge of the slab. In addition, it is found that wheel wander has the same impact on all of the pavement structures except on structures with thickened slabs under the wheel path (JPCP-B1 and JPCP-B2). The trends of increasing longitudinal stress in JPCP-B1 and JPCP-B2 by wheel wander show that wheel wander of 12 inches and 18 inches significantly increases the induced longitudinal stresses. This is due to the fact that in these cases, the loads are located outside of the thickened portion of the slab which leads to a jump in the magnitude of the longitudinal stresses. According to the results presented in Figure 4-17, the transverse stress increases with increasing wheel wander and then decreases when the load is located at the edge of the slab. The reason for this decrease is the presence of tie bars at the edge of the slab which contributes to the reduction of stresses in the transverse direction. Although a similar trend was observed for all of the pavement structures, JPCP-B1 and JPCP-B2 show a significant increase in magnitudes of transverse stresses at 12 inches and 18 inches wheel wander. The reason for this increase is that in these two cases the loads are located at the edge of the trenches which intensifies the transverse stress concentration at the top edge of the trench. Thereby, this design consideration will be less effective when the pavement is subjected to traffic with a wheel wander of larger than 6 inches. A similar trend was observed on JPCP structures with an asphalt base, as shown in Figures 4-18 and 4-19. However, the level of induced stresses is lower owing to the presence of a high modulus asphalt base.

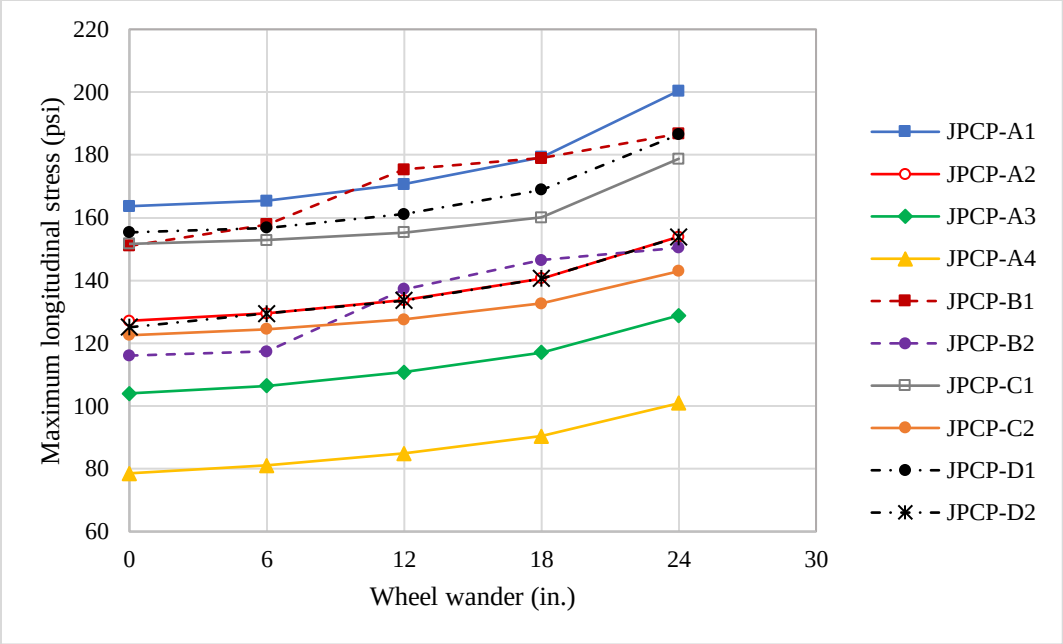

Figure 4-16. Effect of wheel wander on longitudinal tensile stress at the bottom of slab.

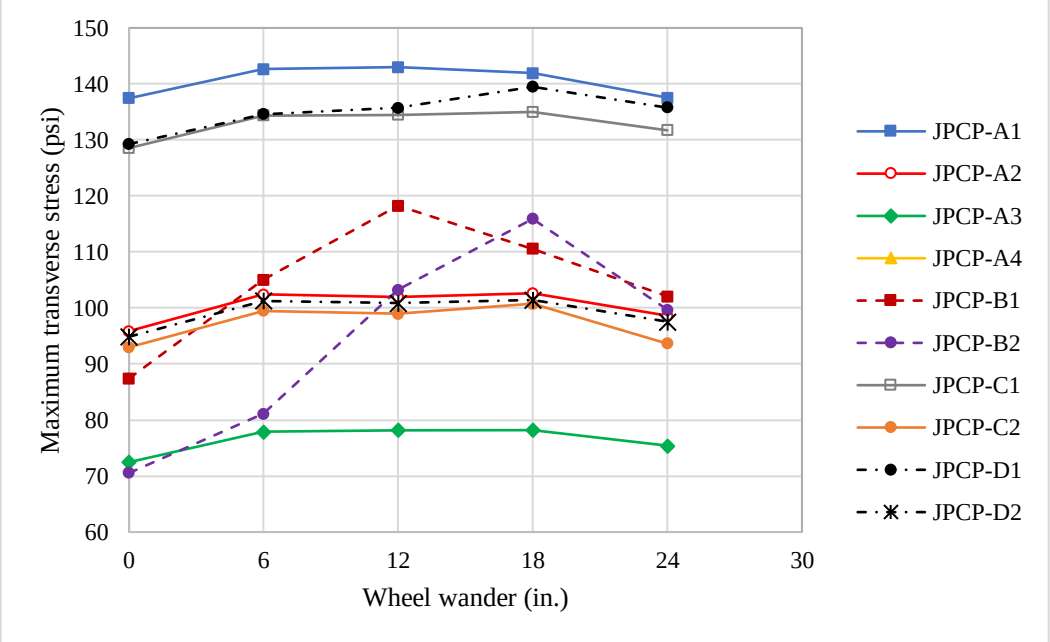

Figure 4-17. Effect of wheel wander on transverse tensile stress at the bottom of slab.

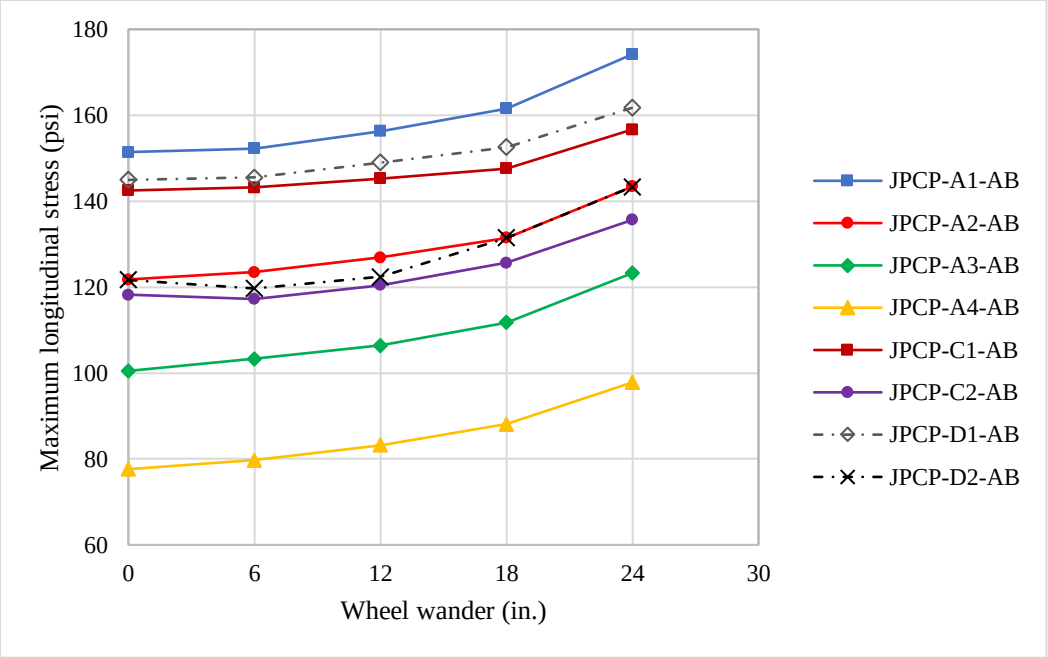

Figure 4-18. Effect of wheel wander on longitudinal stress at the bottom of slab in JPCP structures with asphalt base.

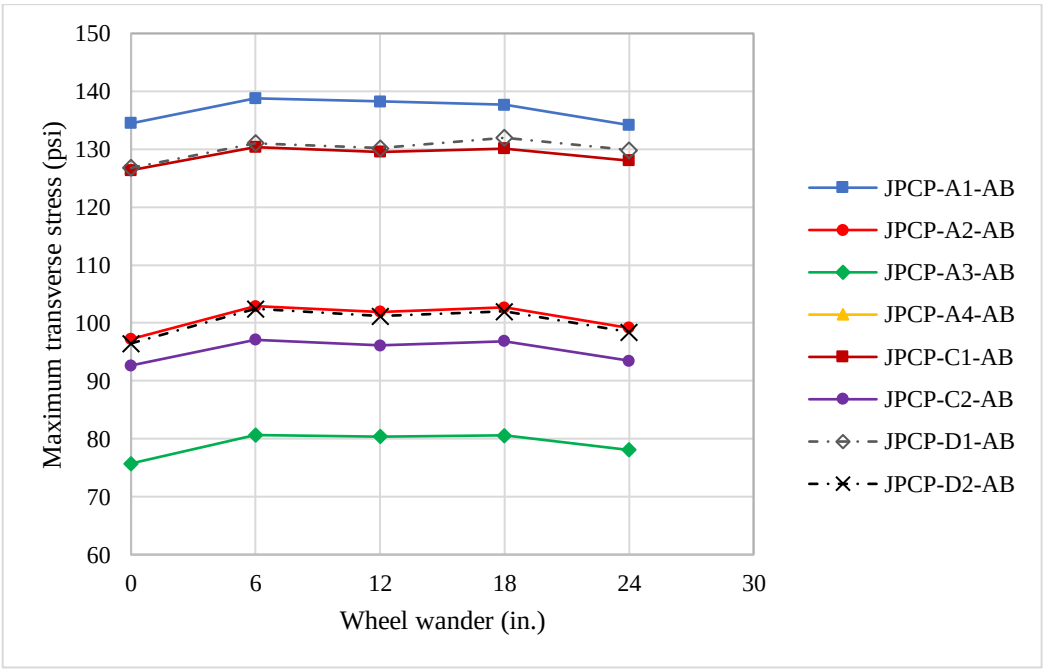

Figure 4-19. Effect of wheel wander on transverse stress at the bottom of slab in JPCP structures with asphalt base.

4.4. CRCP design considerations

4.4.1. Impact of increasing thickness of concrete slab

In order to evaluate the impact of slab thickness on CRCP performance under truck platooning traffic, the slab thickness in the FE model is increased from 8 to 10 and 12 inches. These pavement structures are named CRCP-A1, CRCP-A2, and CRCP-A3, respectively. The impact of the increasing thickness of concrete slabs on induced stresses at the bottom of the slab is illustrated in Figure 4-20. In this figure, MPS (L) and MPS (T) represent the maximum principal stresses at two critical locations of loads where the longitudinal stress and transverse stress are developed, respectively. According to this figure, the induced stresses significantly reduce as the thickness of the slab increases. The calculated longitudinal stress reduces by 18% and 37% when the thickness of the concrete slab is increased by 2 inches and 4 inches, respectively. A similar reduction trend was observed for transverse and maximum principal stresses. Moreover, it can be seen that the maximum principal stresses are very close to tensile stresses which means the shear stress in this location is negligible. Also, it is observed that transverse stress in CRCP-A1 is slightly higher than longitudinal stress, while by increasing the thickness to 10 inches and 12 inches the longitudinal stress becomes higher than transverse stress. Thereby, to have a better comparison, for all of the structures the longitudinal stress was considered as dominant stress for bottom-up fatigue analysis.

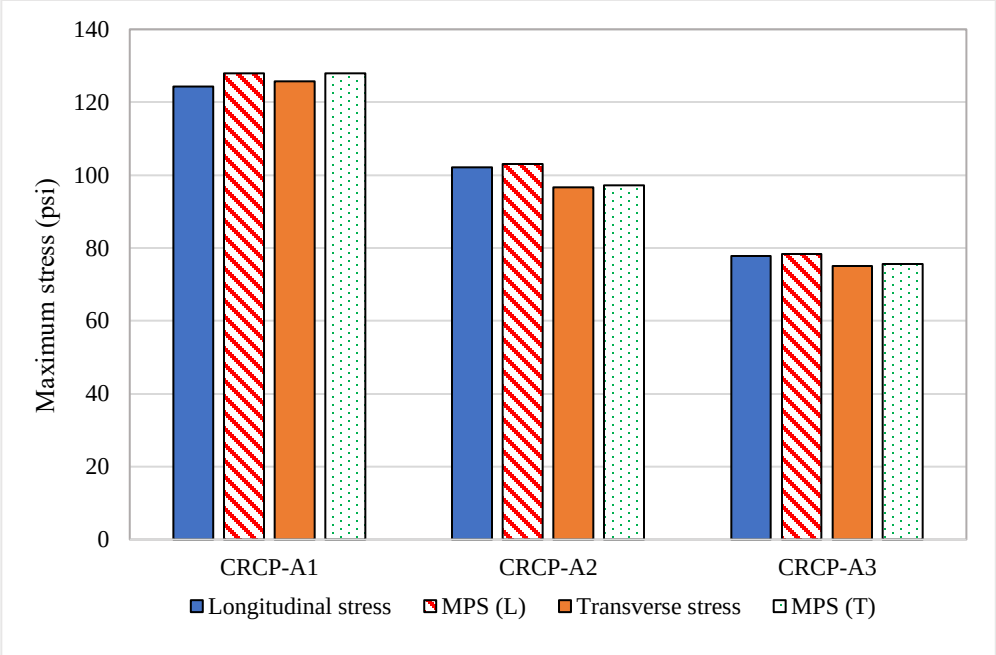

Figure 4-20. Effect of thickness of concrete slab on induced tensile stresses in CRCP.

4.4.2. Impact of thickened PCC layer under the wheel path

Lack of wheel wander in truck platooning traffic provides the opportunity of increasing the thickness of the PCC slab in the wheel path instead of uniformly increasing the thickness of the slab. This measure leads to reducing the cost of construction of pavement which may withstand better against channelized traffics. Similar to what was shown in Figure 4-2 for JPCP, the thickness of CRCP slab is increased by providing two trenches in the base layer under the wheel path with depths of 2 inches (CRCP-B1) and 4 inches (CRCP-B2). Similar to what is discussed in section 4.3.2 for JPCP, a stress concentration was observed at the top edge of the trench which makes the edge of the trench a critical location for transverse stress (See Figure 4-21). However, the stress concentration does not occur for longitudinal stress, and the maximum stress is developed at the bottom of the trench under the wheel path.

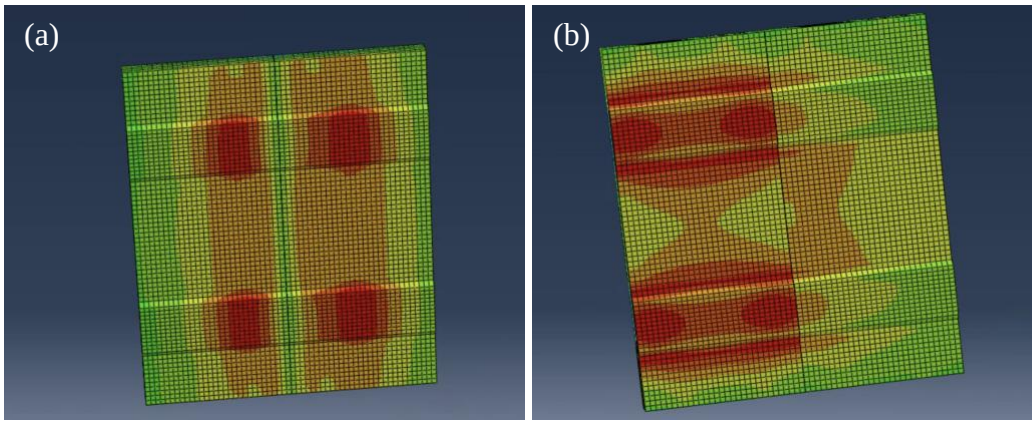

Figure 4-21. Induced (a) longitudinal and (b) transverse stresses at the top edge of the trench.

A parametric study was performed to find the required width for the bottom of the trench to avoid stress concentration at the edge of the trenches. Figure 4-22 shows the effect of increasing the bottom width of 2-inch-deep trenches. As can be seen, increasing the width of the trench reduces the transverse stress at the edge of the trench, while this reduction for stresses under the wheel path is negligible. It is observed that providing a trench with a bottom width of 26 inches causes the maximum transverse stress to occur at the bottom of the wheel path for CRCP-B1.

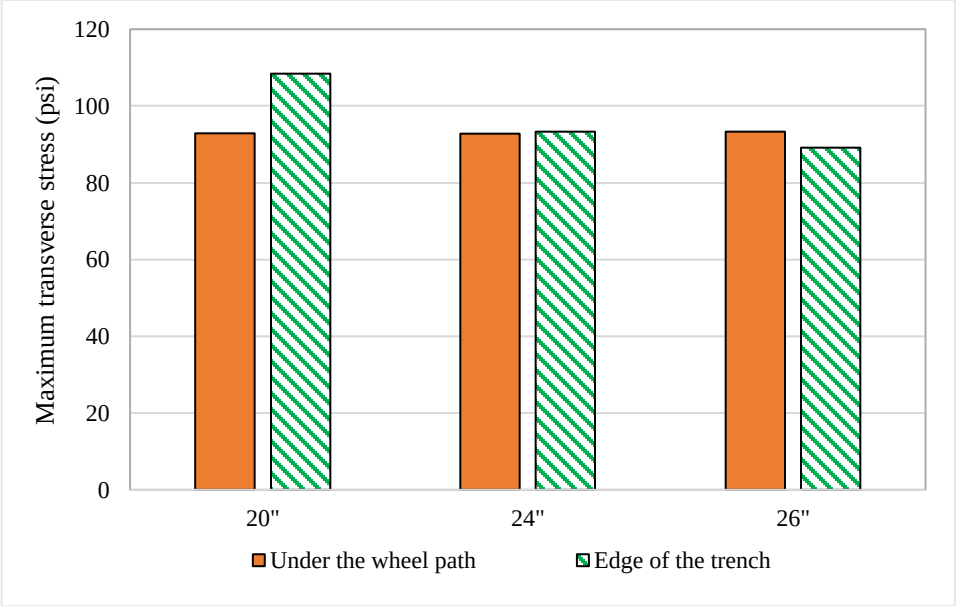

Figure 4-22. Transverse stresses created under different bottom width of trench for CRCP-B1.

The distribution of transverse stress in concrete slab for trench width of 20 inches and 26 inches are shown in Figure 4-23. According to this figure, the localized stress generated at the edge of the trench is removed when the width of the trench is increased to 26 inches. Also, as illustrated in Figure 4-24, the developed longitudinal stress decreases by increasing the width of the trench, but the maximum longitudinal stress always occurs at the bottom of the trench and under the wheel path.

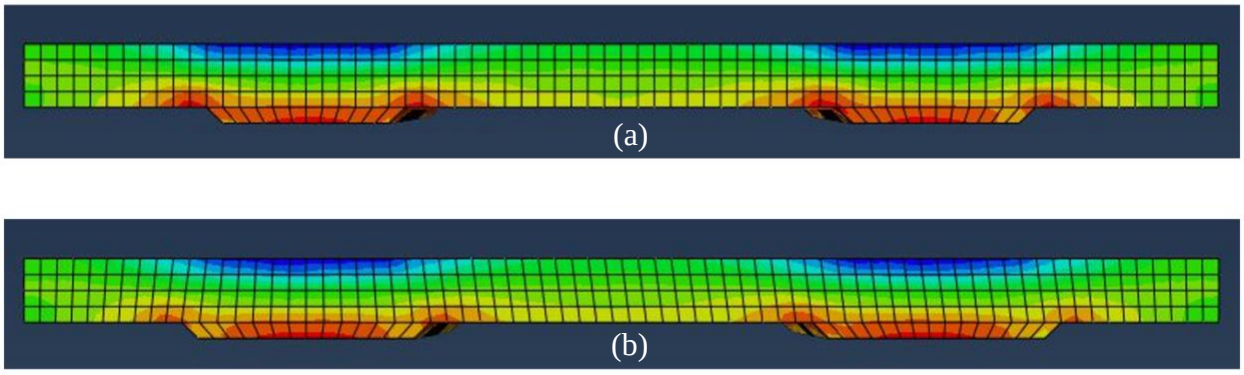

Figure 4-23. Comparing transverse stress distributions for (a) 20 in. and (b) 26 in. for bottom width of trench.

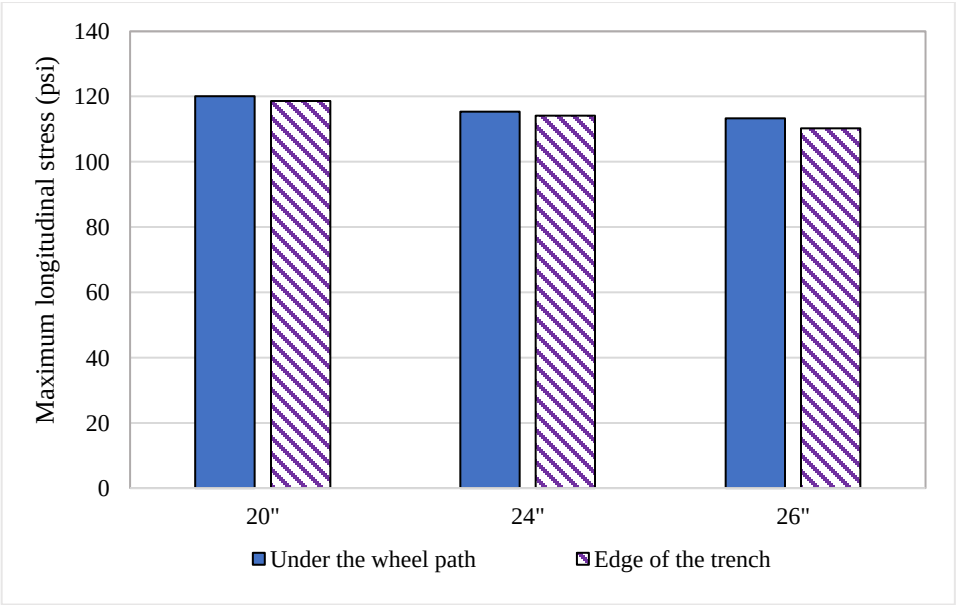

Figure 4-24. Longitudinal stresses created under different bottom width of trench for CRCP-B1.

Figures 4-25 and 4-26 represent the parametric analysis for CRCP with 4 inches trench (CRCP-B2). The results show that a minimum width of 32 inches is required for the bottom of the trench to have the maximum transverse stress under the wheel path. Also, Figure 4-26 confirms that the longitudinal stress is always created under the wheel path.

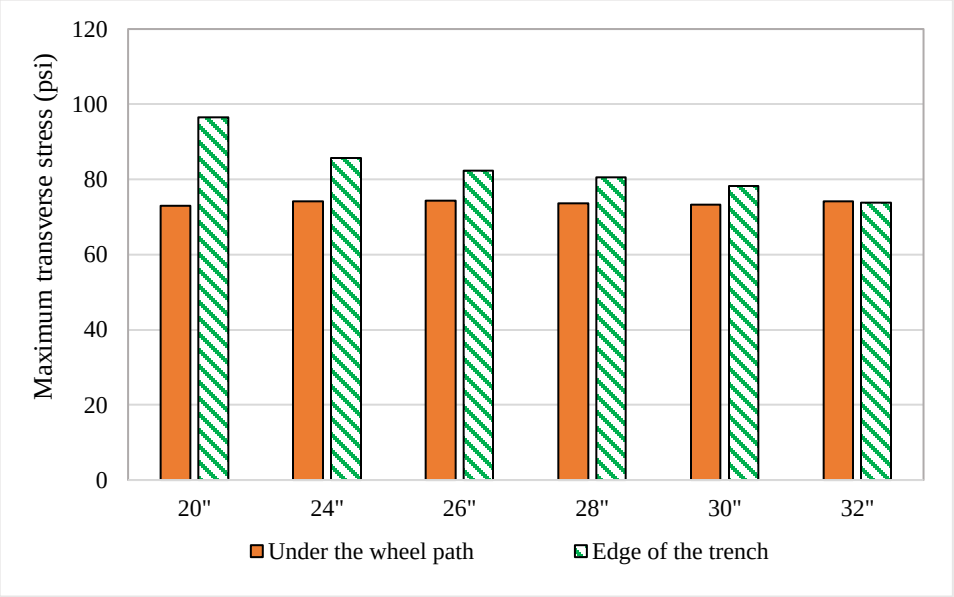

Figure 4-25. Transverse stresses created under different bottom width of trench for CRCP-B2.

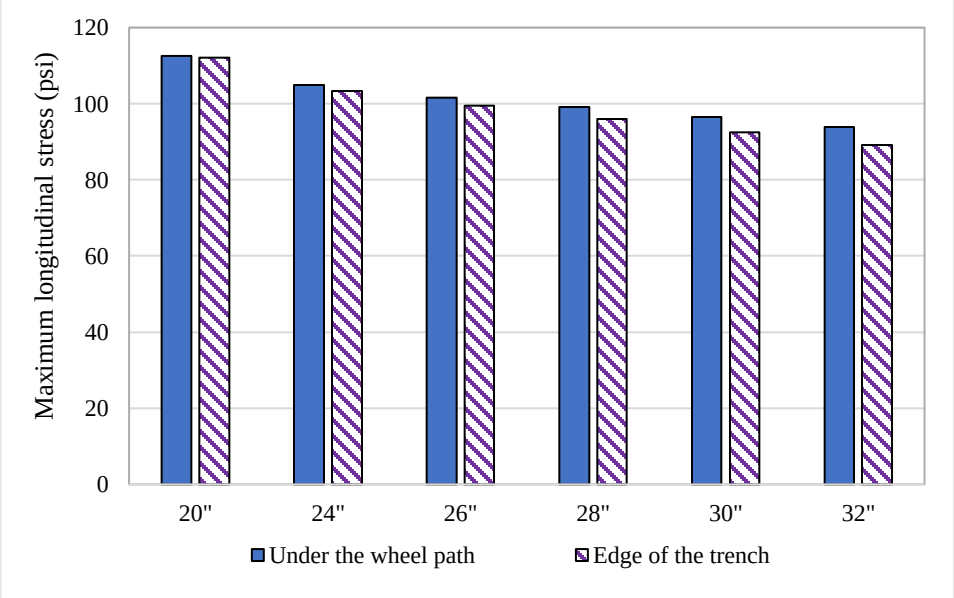

Figure 4-26. longitudinal stresses created under different bottom width of trench for CRCP-B2.

According to the results obtained from the parametric study, 26 inches and 32 inches were selected for the bottom width of trenches for CRCP-B1 and CRCP-B2 structures, respectively. To evaluate the effectiveness of the thickened slab under wheel path on reduction of induced stresses in CRCP, the results were compared to those structures with a uniform increase in slab thickness. As shown in Figure 4-27, compared to CRCP-A1, increasing the thickness of the slab under the wheel path by 2 inches and 4 inches decrease the longitudinal stress by 8.7% and 24%, respectively. However, comparing CRCP-B1 with CRCP-A2 reveals that providing 2 inches trenches under the wheel path is 10% less effective in the reduction of longitudinal stress under the wheel path.

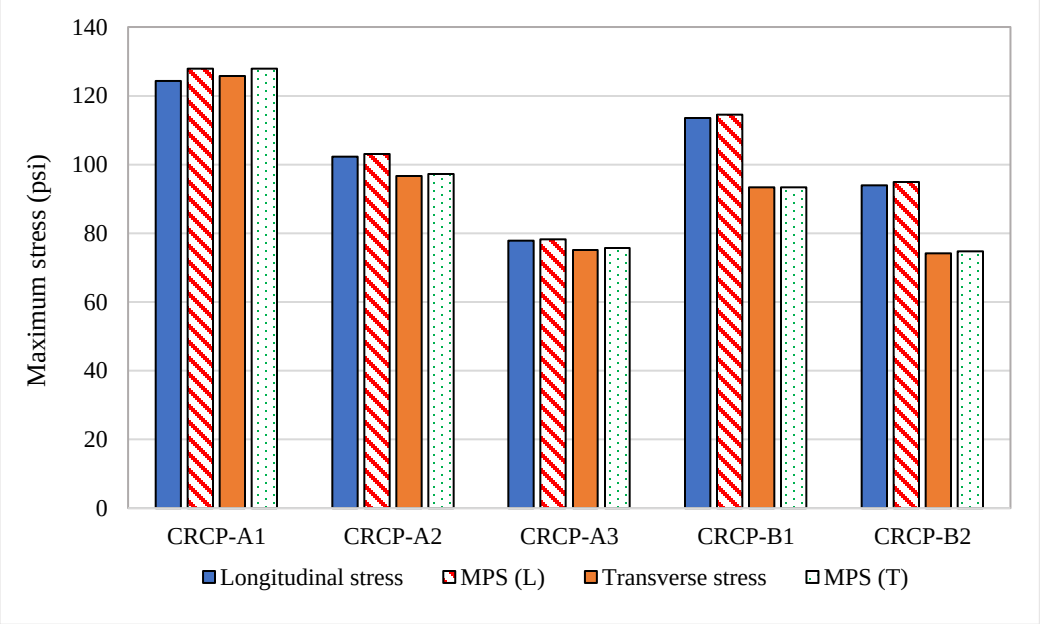

Figure 4-27. Effect of thickened slab under the wheel on induced tensile stresses.

4.4.3. Impact of increasing the size of rebars

Sufficient longitudinal steel content in CRCP controls the crack spacing, keeps transverse cracks tight, and maintains higher load transfer across the cracks. Therefore, adequate longitudinal steel content is an important factor that affects the performance of CRCP. The longitudinal

reinforcement steel can constitute 0.6 to 0.8 percent of the slab cross-section area. CRCP needs a large number of rebars, so using larger size rebars significantly increases the cost of construction. For instance, installing #6 rebars instead of #5 rebars in CRCP increases the required steel weight by 54% in a unit length of the pavement. Therefore, replacing all rebars with a larger size is not a cost-efficient way to improve the performance of CRCP. Since the damage created from truck platooning concentrates in a certain lateral location, to improve the load transfer efficiency across the cracks, only the rebars under the wheel path are replaced with a larger size. Thus, #5 rebars located under the wheel path are replaced with #6 rebars in CRCP-A1 and CRCP-A2, and they are called CRCP-C1 and CRCP-C2 respectively. Figure 4-28 compares the calculated tensile stresses caused by increasing the diameter of rebars. As can be observed, increasing the size of rebars under the wheel path from #5 to #6 has minimal effect on the reduction of tensile stresses at the bottom of the wheel path. The longitudinal tensile stress decreases by 1% and 1.8% for 8 inches and 10 inches slabs, respectively.

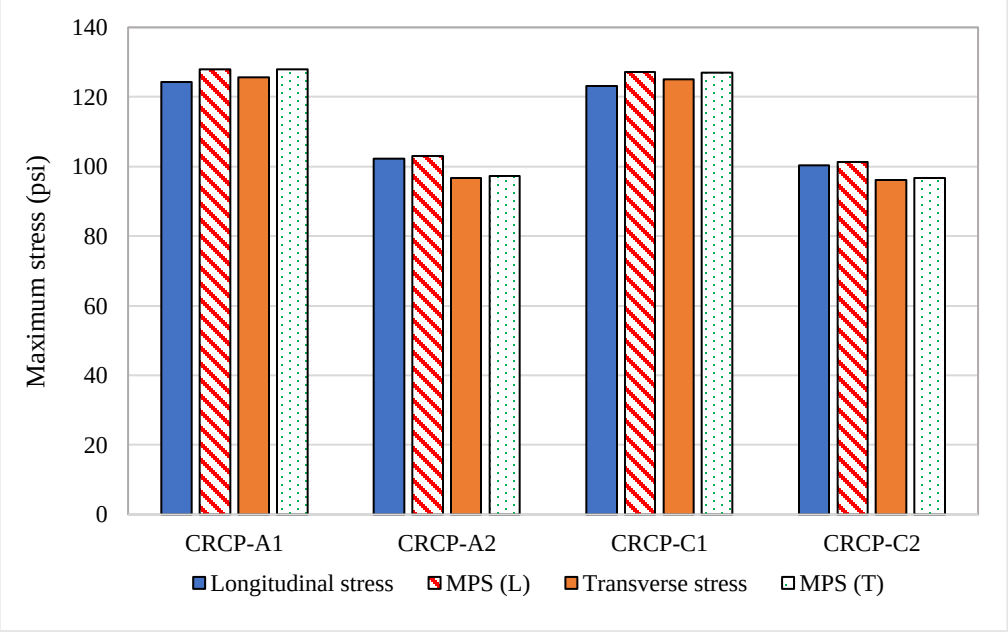

Figure 4-28. Effect of using rebars with larger size in the wheel path on induced tensile stresses.

4.5. Effect of lateral positions of the wheels in the induced stress in CRCP

In order to determine the impact of wander on the discussed CRCP pavement structures and evaluate their performance under different lateral wander of the loads, further FEMs were developed by moving the loads toward the edge of the slab with 6 inches increments. Figures 4-29 and 4-30 depict the induced longitudinal and transverse stress distributions at the bottom of CRCP-A1 under different levels of wheel wander.

Figures 4-31 and 4-32 compare the impact of wheel wander on the induced maximum longitudinal and transverse tensile stresses at the bottom of the discussed pavement structures. The results prove that wheel wander increases the induced stresses at the bottom of the slab and the maximum longitudinal tensile stress is created when the load is located at the edge of the slab. However, pavements with non-uniform thickness are more susceptible to wheel wander and experience higher variation in longitudinal stresses due to wheel wander. Also, Figure 4-32 shows an increase followed by a decrease in transverse stress due to wheel wander. The lower magnitudes of transverse stresses with 24 inches wheel wander are due to the presence of tie bars across the longitudinal joint of the slab. In addition, it can be observed that the transverse tensile stress significantly changes in pavement structures with a trench under the wheel path (CRCP-B1 and CRCP-B2) when it is subjected to wheel wander. For the pavement with trench depth of 2 inches (CRCP-B1), the maximum transverse stress is created with 12 inches wheel wander, while the maximum stress for trench depth of 4 inches (CRCP-B2) is induced with 18 inches wheel wander. The reason for this increase is that the load in these two cases is located at the edge of the trench. This leads to the conclusion that this design consideration will be less effective when the pavement is subjected to traffic with wheel wander.

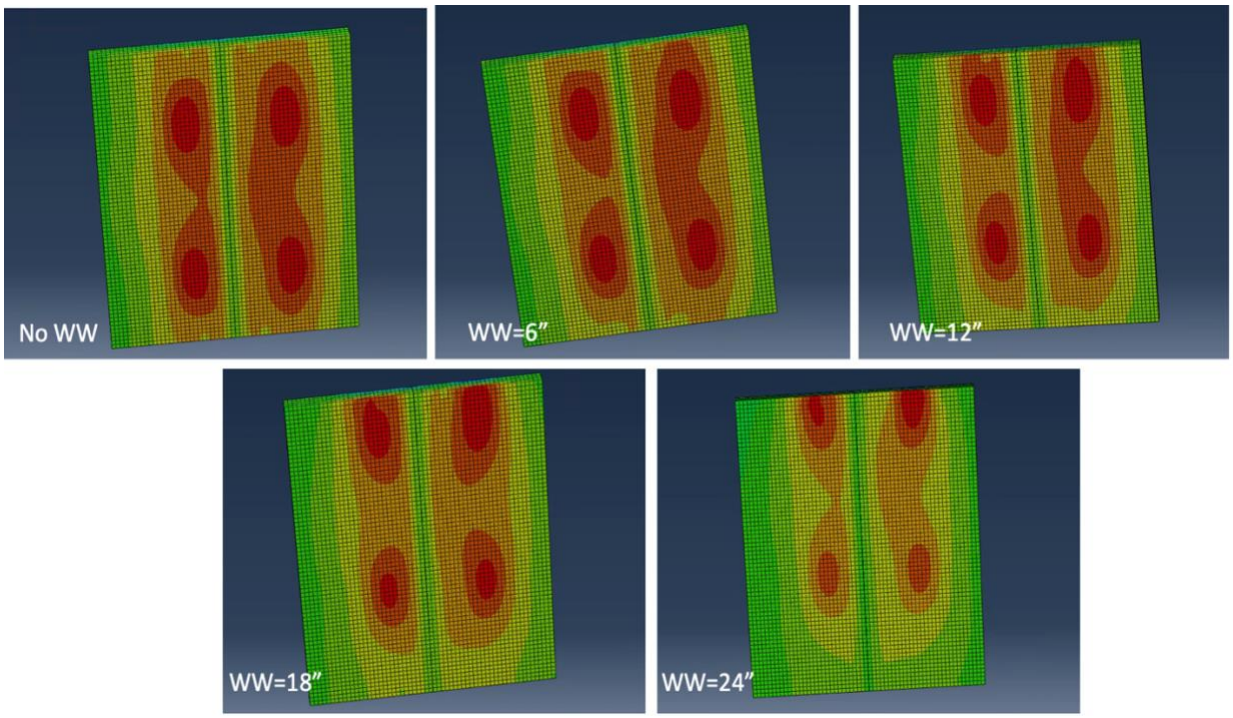

Figure 4-29. Longitudinal stress distributions in CRCP under different levels of wheel wander.

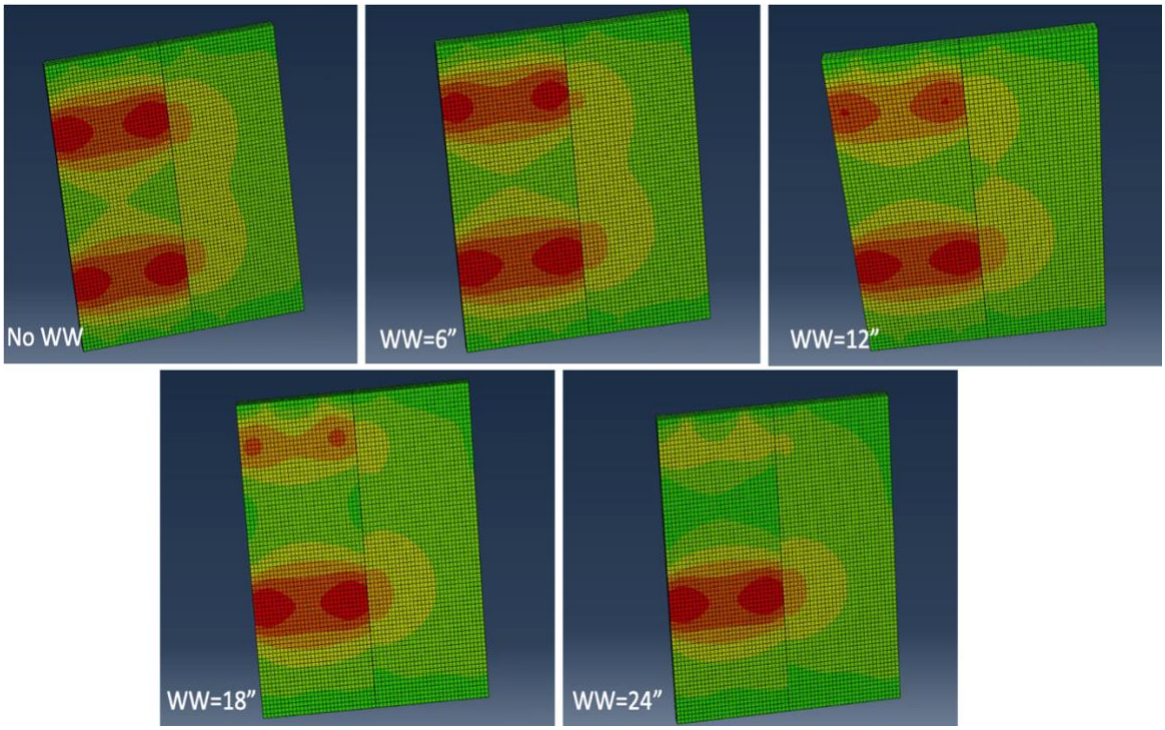

Figure 4-30. Transverse stress distributions in CRCP under different levels of wheel wander.

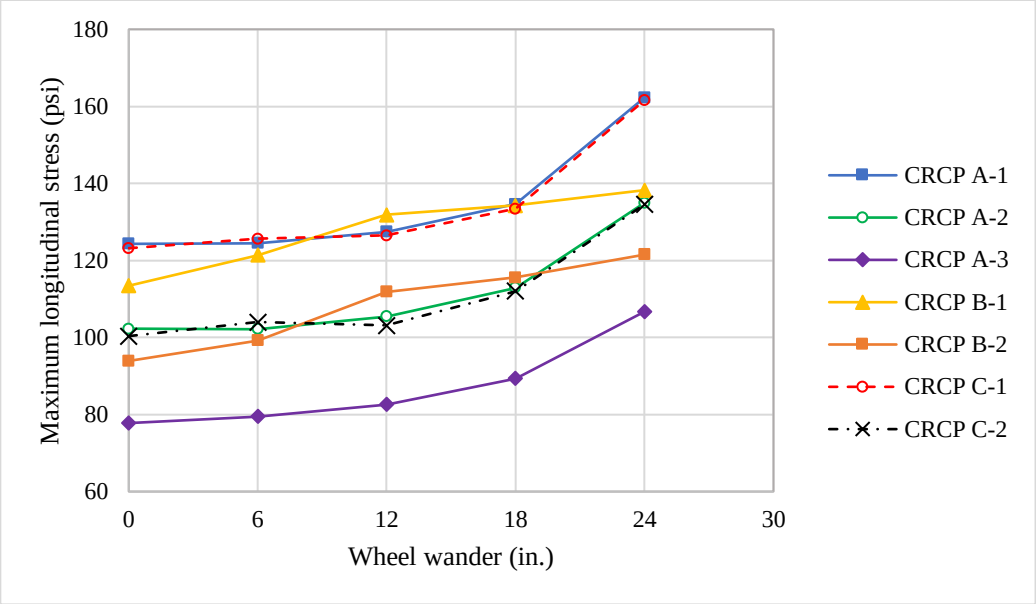

Figure 4-31. Effect of wheel wander on longitudinal tensile stress at the bottom of slab.

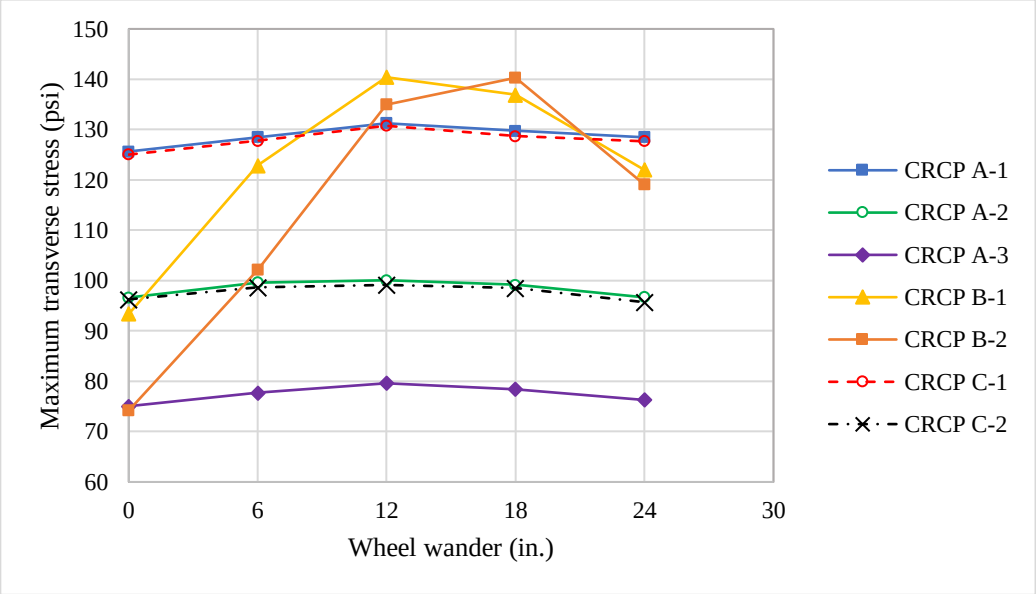

Figure 4-32. Effect of wheel wander on transverse tensile stress at the bottom of slab.

4.6. Fatigue damage analysis

To determine the fatigue performance of the discussed pavement structures under channelized traffic of truck platooning and normal traffic with wheel wander, the maximum induced longitudinal tensile stresses at the bottom of concrete slab computed by FE models are

used. The bottom-up fatigue damages are calculated based on Darter (Eq. 3-10), Tepfers (Eq. 3-12), and MEPDG (Eq. 3-16) fatigue models discussed in chapter 2. These fatigue models calculate the allowable number of load repetitions on the different probabilities of failures. Also, the relative damage is calculated for one pass of the truck based on Miner's hypothesis (Eq. 3-8).

4.6.1. Fatigue performance under channelized traffic

Table 4-1 summarizes the allowable load repetitions calculated by three fatigue models for JPCP structures with the granular base. As can be seen in this table, Darter and Tepfers fatigue models compute the allowable load repetitions close to each other. However, the calculated allowable load repetitions by MEPDG model for low values of stresses are significantly higher than those calculated by two other models, while it computes the allowable load repetitions in structures with higher stresses close to two other models. In addition, to compare the effectiveness of each of the design considerations in increasing the fatigue life of pavement under the channelized traffic, the relative fatigue life was computed by dividing allowable load repetitions to that calculated for the reference pavement structure (JPCP-A1). The results are presented in Table 4-1. As can be observed, increasing the thickness of the slab significantly increases the fatigue life of the pavement. For instance, increasing the slab thickness from 8 inches (JPCP-A1) to 12 inches (JPCP-A3) enhances the life pavement 31.63 and 17.52 times according to Darter and Tepfers models, respectively. However, MEPDG calculates this increase as 500 million times. It appears that MEPDG provides an unrealistic result for the discussed pavement structure.

To study the impact of implementing these three fatigue models in the damage calculation, the allowable load repetitions by each of these models are calculated in the stress range of 80 to 250 psi. The results are plotted in Figure 4-33. As shown, in the case of small stresses, the calculated allowable load repetitions by MEPDG are significantly higher than those calculated by

the other two models, and any change in low stresses results in considerable change in calculated load repetitions. Conversely, when the stress is higher than 200 psi, MEPDG curve gets parallel to Darter and Tepfers models and produces lower load repetitions. It can be concluded that the calibration coefficients in MEPDG formula result in unrealistic results in a lower range of stresses, so it cannot be used for fatigue analysis in the discussed pavement structures.

Table 4-1. Calculated allowable load repetitions for JPCP structures with granular base.

Pavement Structure	Critical tensile stress (psi)	Darter fatigue model		Tepfers fatigue model		MEPDG fatigue model	
		Allowable load repetitions	Relative life	Allowable load repetitions	Relative life	Allowable load repetitions	Relative life
JPCP-A1	163.65	3.11E+12	1.00	1.53E+11	1.00	1.64E+12	1.00
JPCP-A2	127.15	2.58E+13	8.28	8.85E+11	5.77	2.90E+16	1.76E+04
JPCP-A3	104.02	9.84E+13	31.63	2.69E+12	17.52	8.10E+20	4.94E+08
JPCP-A4	78.55	4.30E+14	138.32	9.13E+12	59.54	1.89E+29	1.15E+17
JPCP-B1	151.00	6.48E+12	2.08	2.81E+11	1.84	2.69E+13	16.40
JPCP-B2	116.05	4.90E+13	15.76	1.51E+12	9.84	2.25E+18	1.37E+06
JPCP-C1	151.64	6.24E+12	2.00	2.73E+11	1.78	2.30E+13	14.04
JPCP-C2	122.54	3.37E+13	10.82	1.10E+12	7.20	1.59E+17	9.68E+04
JPCP-D1	155.31	5.04E+12	1.62	2.29E+11	1.49	9.80E+12	5.97
JPCP-D2	125.08	2.91E+13	9.34	9.77E+11	6.37	6.11E+16	3.72E+04

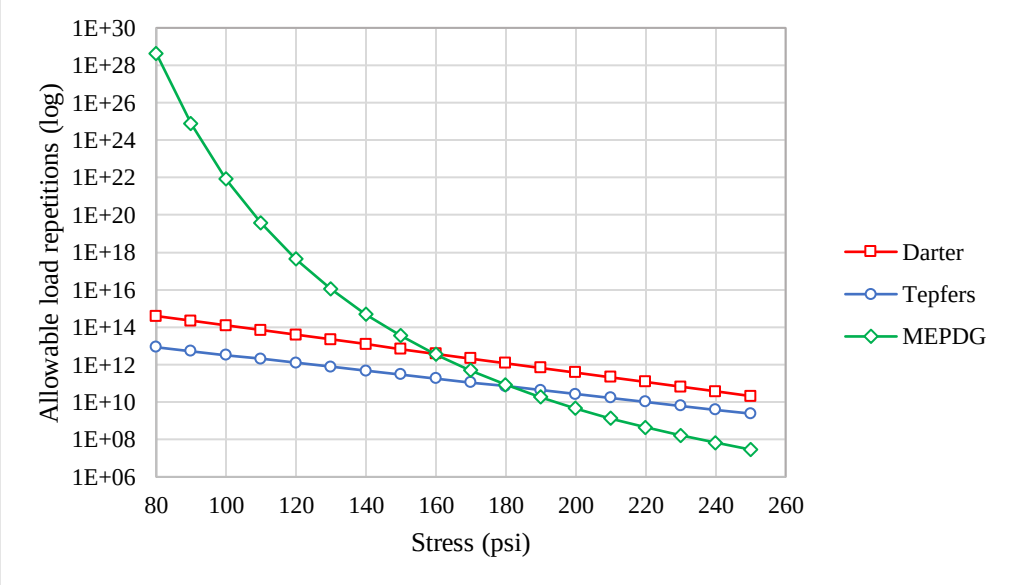

Figure 4-33. Comparing allowable load repetitions by Darter, Tepfers, and MEPDG models.

To further discuss the effectiveness of each of these design considerations, the relative lives calculated by Darter and Tepfers models are plotted in Figure 4-34. As can be seen, Tepfers model reflects less change in the life of pavements by changing the pavement structure. However, a similar trend was observed by these two models. For the sake of discussion, the results from Tepfers model are used to assess the fatigue life of the pavements. Figure 4-35 shows the structure of each design alternative and their relative life based on Tepfers model. As shown, increasing the thickness of the slab is the most effective method to improve the fatigue performance of JPCP structures under channelized traffic. In addition, thickening slabs by providing 2 inches and 4 inches trench under the wheel path of channelized traffic increase the fatigue life by 1.84 and 9.84 times. These increases in the life of pavement are much less than those provided by the equivalent uniformly thickened pavements (JPCP-A2 and JPCP-A3) which enhance the life by 5.77 and 17.52 times. Likewise, replacing dowel bars with a larger size in structures with 8 inches and 10 inches thick slabs leads to increasing the fatigue life of these pavements subjected to channelized traffic by 1.78 and 7.20 times, respectively. However, replacing only dowel bars located at the wheel path in these pavement structures results in improving the life of the pavement by 1.49 and 6.37 times. Thereby, it can be concluded that even though replacing dowel bars in the wheel path has the lowest impact on life improvement of JPCP among all design considerations, replacing dowel bars outside the wheel path does not have a considerable impact on improving the life of pavement to withstand again channelized traffic.

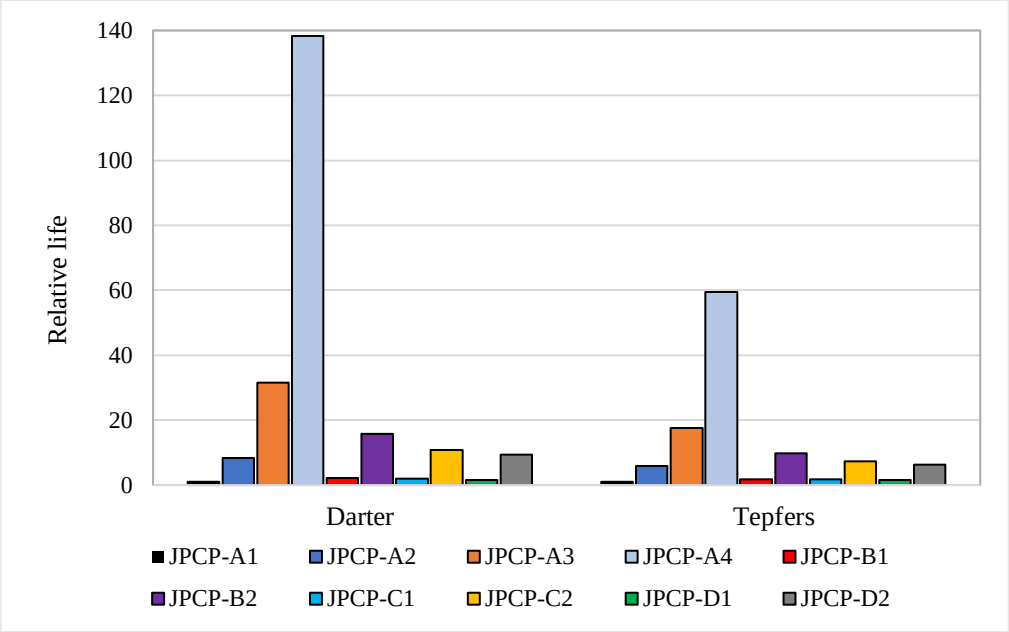

Figure 4-34. Effect of different design considerations in increasing fatigue life of JPCP with granular base under the channelized traffic based on Darter and Tepfers models.

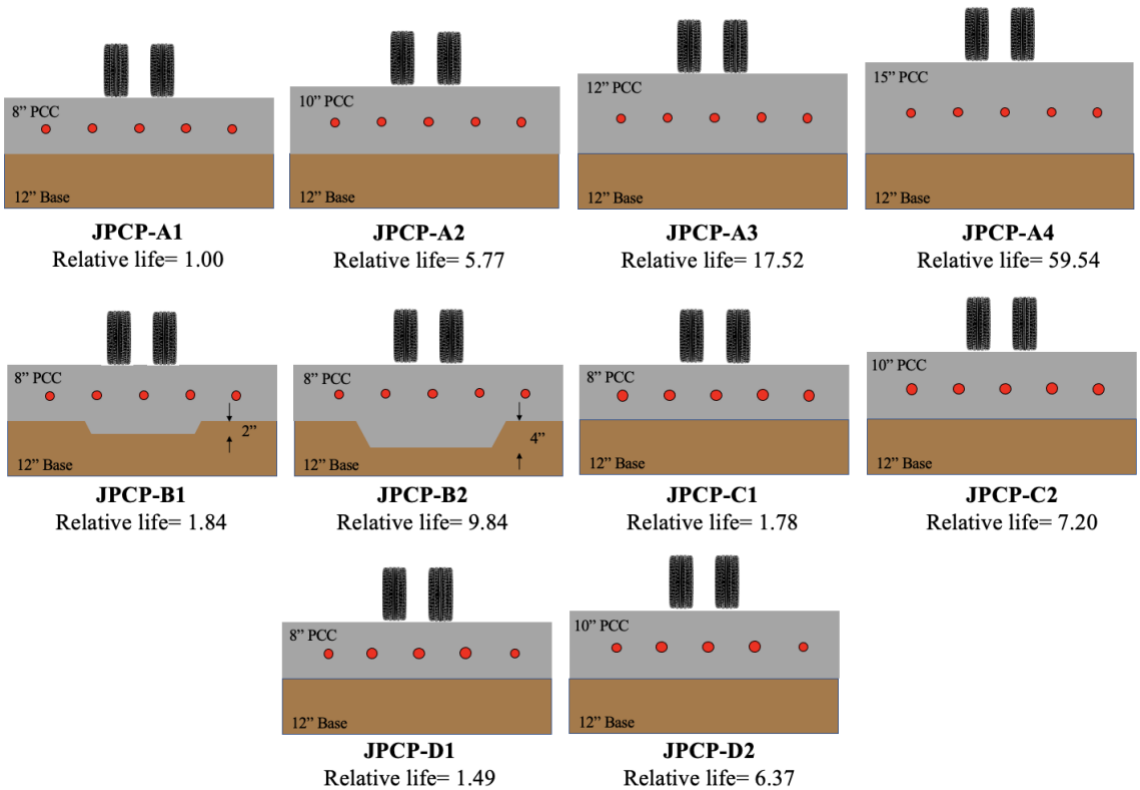

Figure 4-35. Graphical illustration of the effect of different design considerations in increasing fatigue life of JPCP with granular base under the channelized traffic based on Tepfers model.

A similar evaluation is conducted on JPCP structures with asphalt base. The results are presented in Table 4-2. Since the stress levels induced in JPCP with asphalt base are lower than those induced in JPCP with granular base, MEPDG fatigue model does not work on these pavement structures as well. Therefore, Darter and Tepfers models are used to study the effectiveness of each design consideration on improving the fatigue performance of the pavement under channelized traffic. As expected, increasing the slab thickness has the highest impact on increasing the life, and JPCP-A4-AB is capable of carrying the highest channelized load repetitions. Figure 4-36 illustrates the relative life of each pavement structure based on Darter and Tepfers models. As can be seen, increasing thickness from 8 inches to 15 inches improves the life of the pavement by 71.91 times based on Darter model. However, Tepfers model calculates this improvement by almost half of this value. JPCP-D1-AB, however, shows only 45% and 36% improvement in the life of pavement based on Darter and Tepfers models respectively. To better understand the improvement in fatigue life of each design alternative based on Tepfers model, their relative life is presented in Figure 4-37.

Table 4-2. Calculated allowable load repetitions for JPCP structures with asphalt base.

Pavement Structure	Critical tensile stress (psi)	Darter fatigue model		Tepfers fatigue model		MEPDG fatigue model	
		Allowable load repetitions	Relative life	Allowable load repetitions	Relative life	Allowable load repetitions	Relative life
JPCP-A1-AB	151.43	6.32E+12	1.00	2.76E+11	1.00	2.43E+13	1.00
JPCP-A2-AB	121.78	3.52E+13	5.57	1.15E+12	4.15	2.13E+17	8.77E+03
JPCP-A3-AB	100.49	1.21E+14	19.12	3.18E+12	11.54	6.17E+21	2.54E+08
JPCP-A4-AB	77.62	4.54E+14	71.91	9.54E+12	34.61	4.97E+29	2.05E+16
JPCP-C1-AB	142.49	1.06E+13	1.68	4.24E+11	1.54	2.42E+14	9.96
JPCP-C2-AB	118.19	4.33E+13	6.86	1.36E+12	4.94	9.05E+17	3.73E+04
JPCP-D1-AB	144.96	9.19E+12	1.45	3.76E+11	1.36	1.24E+14	5.11
JPCP-D2-AB	121.67	3.54E+13	5.60	1.15E+12	4.17	2.22E+17	9.14E+03

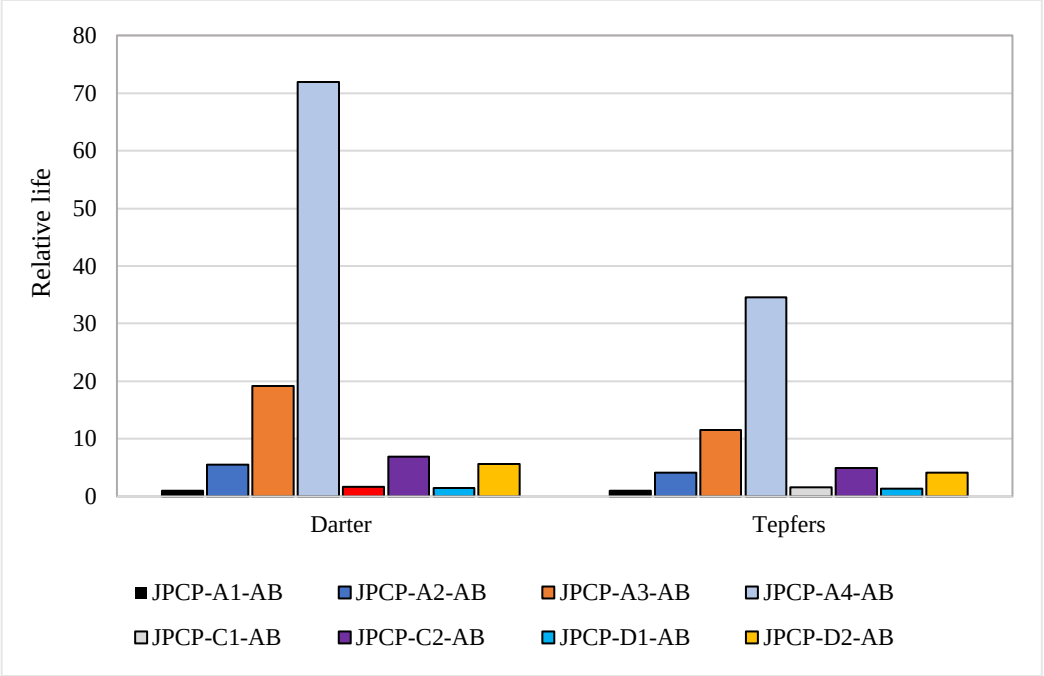

Figure 4-36. Effect of different design considerations in increasing fatigue life of JPCP with asphalt base under the channelized traffic based on Darter and Tepfers models.

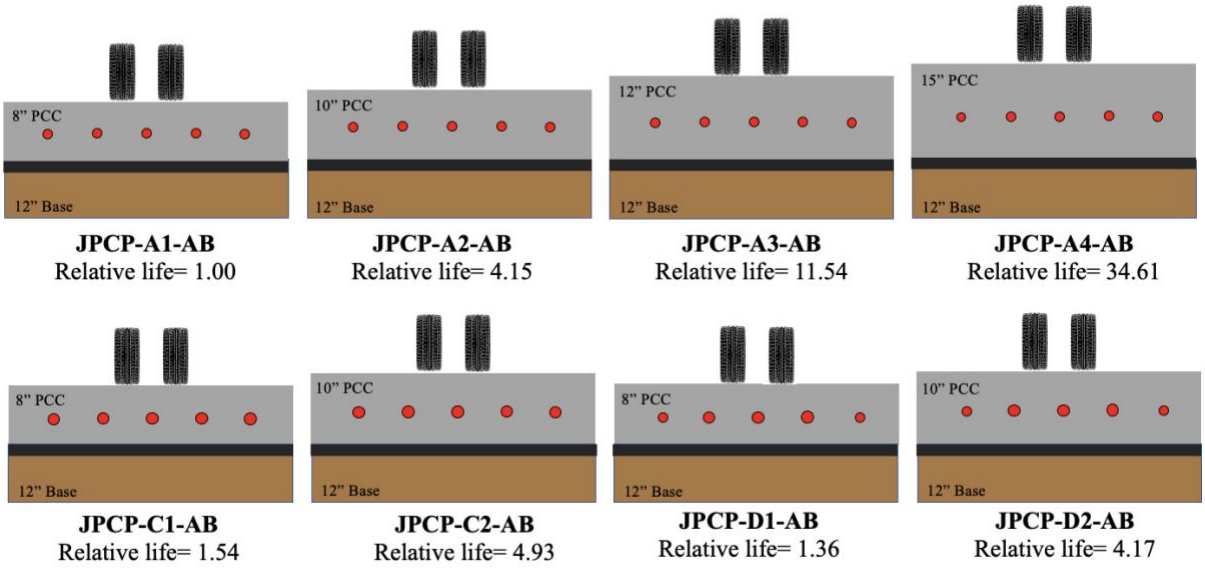

Figure 4-37. Graphical illustration of the effect of different design considerations in increasing fatigue life of JPCP with asphalt base under the channelized traffic based on Tepfers model.

Table 4-3 represents the allowable load repetitions for CRCP structures, and their relative life calculated by the three fatigue models. It can be seen that similar to JPCP structures, the application of MEPDG fatigue model on the CRCP structures produces unrealistic results. Thereby, only Darter and Tepfers fatigue models were used to compare the effectiveness of each design considerations in improving the longevity of CRCP under channelized traffic. To do so, the relative lives are calculated and plotted in Figure 4-38. Comparing these values reveals that increasing the thickness of the slab has the highest effectiveness in improving the fatigue life of CRCP, while replacing rebars in the wheel path with a larger size has the lowest effectiveness. Also, it was found that replacing rebars in the wheel path has a negligible effect on life improvement in CRCP with 8 inches slab. Also, thickening the slab under the wheel path by 2 inches and 4 inches, respectively, contributes to increasing the life of the pavement by 1.69 and 4.30 times according to Tepfers model. Darter model computes these values as 1.88 and 5.82. For better comparison, the structure of each design alternative and their relative life computed based on Tepfers model are depicted in Figure 4-39.

Table 4-3. Calculated allowable load repetitions for CRCP structures.

Pavement Structure	Critical tensile stress (psi)	Darter fatigue model		Tepfers fatigue model		MEPDG fatigue model	
		Allowable load repetitions	Relative life	Allowable load repetitions	Relative life	Allowable load repetitions	Relative life
CRCP-A1	124.304	3.040E+13	1.00	1.014E+12	1.00	8.134E+16	1.00
CRCP-A2	102.222	1.092E+14	3.59	2.929E+12	2.89	2.237E+21	2.75E+04
CRCP-A3	77.78	4.501E+14	14.81	9.472E+12	9.34	4.209E+29	5.17E+12
CRCP-B1	113.428	5.708E+13	1.88	1.710E+12	1.69	7.197E+18	88.48
CRCP-B2	93.91	1.768E+14	5.82	4.366E+12	4.30	4.259E+23	5.24E+06
CRCP-C1	123.17	3.246E+13	1.07	1.071E+12	1.06	1.246E+17	1.53
CRCP-C2	100.361	1.217E+14	4.00	3.203E+12	3.16	6.662E+21	8.19E+04

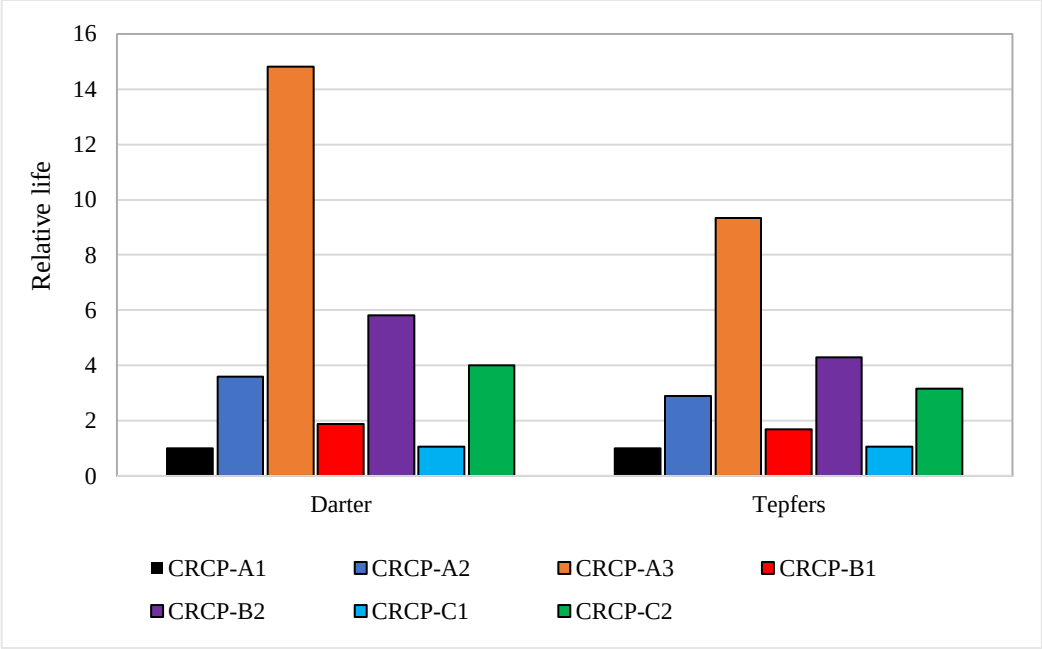

Figure 4-38. Effect of different design considerations in increasing fatigue life of CRCP subjected to channelized traffic based on Darter and Tepfers models.

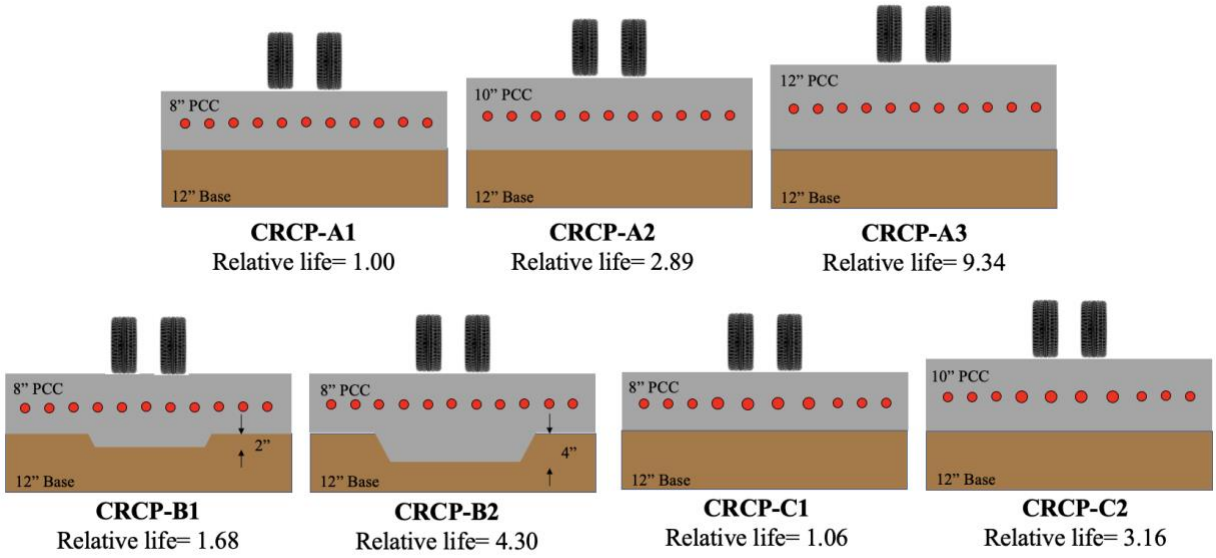

Figure 4-39. Graphical illustration of the effect of different design considerations in increasing fatigue life of CRCP subjected to channelized traffic based on Tepfers models.

4.6.2. Impact of wheel wander on induced fatigue damage

In order to compare the damage created by channelized traffic from truck platooning and normal traffic with wheel wander, the pavement structures are analyzed under 1,000,000 passes of traffic. Since wheel wander was simulated with 6 inches increments, therefore the number of passes should be distributed in 9 different lateral positions including no wander, 6, 12, 18, 24 inches wander to the left and to the right. Each of these lateral positions of the wheels produces maximum tensile stress in different points at the bottom of the slab, as shown in Figure 4-40. In this figure, the response point zero is the location where the maximum tensile stress is developed by the traffic runs at the center of the lane (no wheel wander). The negative values show the points in which the maximum tensile stress is induced by the lateral wander to the left of the lane towards the concrete shoulder. The total damage accumulated in any of these points is derived from the damages created by total passes of traffic from all 9 lateral positions of the wheels. This computation can be performed by matrix multiplication which is explained in the following steps:

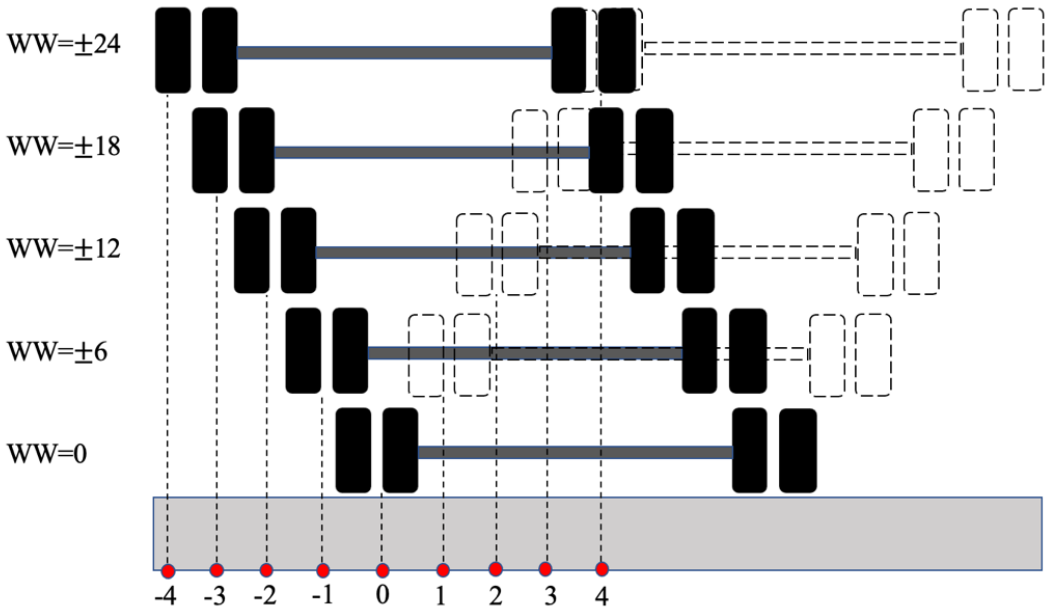

Figure 4-40. Response points for different lateral location of the wheels.

Step 1: Normal distribution of traffic

The first step is to construct a matrix representing the distribution of the total number of passes over each lateral position of the vehicle. As previously mentioned, a normal distribution best describes the wheel wander, in which most passes occur around a mean and the values decrease by increasing the distance from the mean. However, since the slabs are laterally limited by longitudinal joints, a truncated normal distribution should be implemented. A truncated distribution is a conditional distribution that results from restricting the domain of distribution. In a truncated distribution, the occurrences are limited to values that lie above or below a given threshold (truncation point) or within a specified range. The truncation upper and lower boundaries are chosen to be a certain number of deviations from the mean, which makes the data sample more compact and efficient. The formula of the truncated normal distribution is given in the following equation:

$$g(x,\mu,\sigma,L,U) = \frac{f(\frac{x-\mu}{\sigma})}{\sigma\,(F\left(\frac{U-\mu}{\sigma}\right)-F\left(\frac{L-\mu}{\sigma}\right))} \tag{4-1}$$

Where,

x = normally distributed random variable (e.g., the lateral position of the wheel).

σ = standard deviation of x.

μ = mean of x.

f = probability density function of the standard normal distribution.

F = cumulative density function of the standard normal distribution.

L = lower bound; $-\frac{l_w-A_w+T_w}{2}$

U = upper bound; $\frac{l_w - A_w + T_w}{2}$

A_w = axle width that depends on the tire type.

l_w = lane width.

T_w = Total width of dual tires or width of tire for single tire axle.

It should be noted that in this study for the purpose of wheel wander, the lower and upper bounds of truncation are considered symmetric relative to the center value. The total number of passes is divided into nine six-inch wide segments. The number of passes in each of these segments (X_i) can be computed using the following equation:

$$X_i = \frac{f\left(\frac{(x+3)-\mu}{\sigma}\right) - f\left(\frac{(x-3)-\mu}{\sigma}\right)}{\sigma\left(F\left(\frac{U-\mu}{\sigma}\right) - F\left(\frac{L-\mu}{\sigma}\right)\right)} \times N_p \quad (4\text{-}2)$$

In which, N_p is total number of passes. The traffic distribution matrix (ND) can be assembled as follows:

$$ND = [X_{-4} \;\; X_{-3} \;\; X_{-2} \;\; X_{-1} \;\; X_0 \;\; X_1 \;\; X_2 \;\; X_3 \;\; X_4]_{1\times 9} \quad (4\text{-}3)$$

Step 2: Fatigue damage calculation

The second step in this method is to evaluate the impact of different lateral positions of the vehicle on induced damage in each response points shown in Figure 4-36. To do so, for each lateral position of the loads, the induced stresses in each of the 9 response points are extracted from FEM and the fatigue damage is calculated for one pass of traffic. The computed values are used to construct the fatigue damage matrix (FD) as follows:

$$FD = \begin{bmatrix} Y_{-4,-24} & Y_{-3,-24} & Y_{-2,-24} & Y_{-1,-24} & Y_{0,-24} & Y_{1,-24} & Y_{2,-24} & Y_{3,-24} & Y_{4,-24} \\ Y_{-4,-18} & Y_{-3,-18} & Y_{-2,-18} & Y_{-1,-18} & Y_{0,-18} & Y_{1,-18} & Y_{2,-18} & Y_{3,-18} & Y_{4,-18} \\ Y_{-4,-12} & Y_{-3,-12} & Y_{-2,-12} & Y_{-1,-12} & Y_{0,-12} & Y_{1,-12} & Y_{2,-12} & Y_{3,-12} & Y_{4,-12} \\ Y_{-4,-6} & Y_{-3,-6} & Y_{-2,-6} & Y_{-1,-6} & Y_{0,-6} & Y_{1,-6} & Y_{2,-6} & Y_{3,-6} & Y_{4,-6} \\ Y_{-4,0} & Y_{-3,0} & Y_{-2,0} & Y_{-1,0} & Y_{0,0} & Y_{1,0} & Y_{2,0} & Y_{3,0} & Y_{4,0} \\ Y_{-4,6} & Y_{-3,6} & Y_{-2,6} & Y_{-1,6} & Y_{0,6} & Y_{1,6} & Y_{2,-6} & Y_{3,6} & Y_{4,6} \\ Y_{-4,12} & Y_{-3,12} & Y_{-2,12} & Y_{-1,12} & Y_{0,12} & Y_{1,12} & Y_{2,12} & Y_{3,12} & Y_{4,12} \\ Y_{-4,18} & Y_{-3,18} & Y_{-2,18} & Y_{-1,18} & Y_{0,18} & Y_{1,18} & Y_{2,18} & Y_{3,18} & Y_{4,18} \\ Y_{-4,24} & Y_{-3,24} & Y_{-2,24} & Y_{-1,24} & Y_{0,24} & Y_{1,24} & Y_{2,24} & Y_{3,24} & Y_{4,24} \end{bmatrix}_{9\times9} \quad (4\text{-}4)$$

In this matrix, $Y_{i,j}$ represents the calculated damage in response point i result from the load with wheel wander of j. For example, $Y_{2,-12}$ presents the damage created in point 2 when the vehicle runs with 12 inches wander to the left side of from the center of the lane.

Step 3: Calculating the accumulated fatigue damage

The final step in the proposed method is to obtain the damage index matrix (DI) by multiplying the truncated normal distribution matrix (ND) by the fatigue damage matrix (FD). The resulting matrix will include the accumulated fatigue damage induced at each of the response points.

$$DI = ND \times FD = [DI_{-4} \quad DI_{-3} \quad DI_{-2} \quad DI_{-1} \quad DI_0 \quad DI_1 \quad DI_2 \quad DI_3 \quad DI_4] \quad (4\text{-}5)$$

Where, DI_n represents the accumulated fatigue damage in point n from total traffic. To simulate the impact of wheel wander on fatigue damage development in the discussed pavement structures, the matrix multiplication method is applied to these structures. Considering a normal distribution of 10 inches for the wheel wander, 1,000,000 pass of traffic is distributed over nine six-inch-wide segments in lateral direction. Figure 4-41 depicts the truncated normal distribution

of this traffic. As can be seen, with 10 inches standard deviation for wheel wander, only in 235,823 passes, the vehicles run through the center of the slab and 14,397 of them pass through last segment at the edge of slab. Using this figure, the normal distribution matrix can be assembled as follows:

$$ND = [9{,}800 \quad 49{,}800 \quad 119{,}200 \quad 201{,}300 \quad 239{,}800 \quad 201{,}300 \quad 119{,}200 \quad 49{,}800 \quad 9{,}800]$$

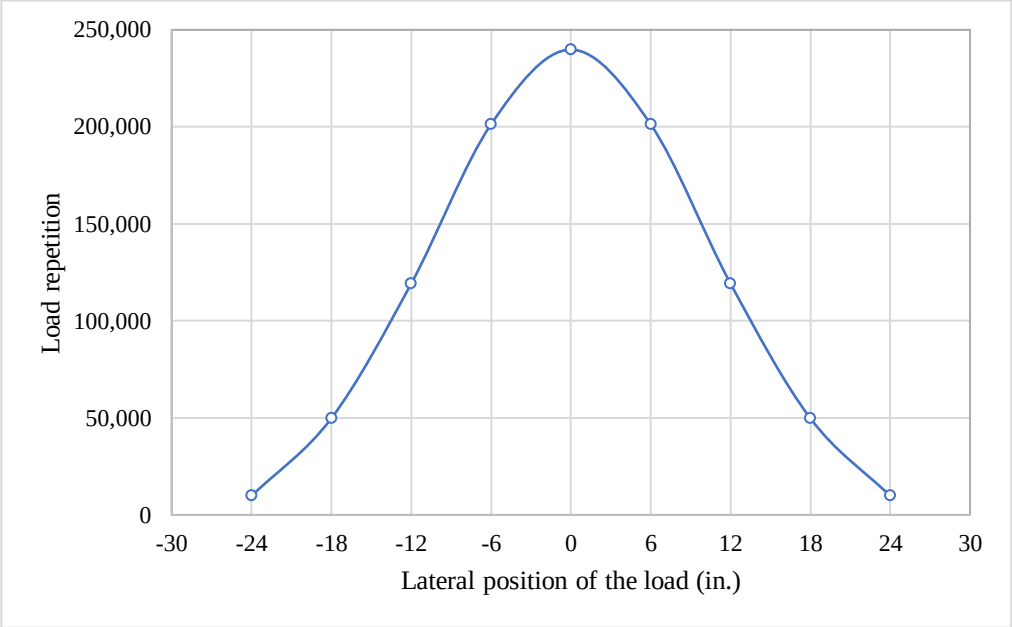

Figure 4-41. Normally distributed 1,000,000 passes of traffic.

After evaluation of JPCP-A1 structure under the loads with wheel wander of 0, ±6, ±12, ±18, and ±24 in., it was found that the maximum tensile longitudinal stresses are created in 3, 15, 23, 27, 35, 41, 47, 53, and 59 in. from the edge of the slab. Therefore, the stresses induced in these response points by all 9 load cases are extracted and used for damage calculation. As mentioned previously, the MEPDG provides unrealistic results for the pavement structures discussed in this model, and Tepfers model calculates the allowable number of passes smaller compared to Darter model. In this study, to have more conservative results, Tepfers model is used for fatigue damage calculation. Tables 4-4 and 4-5 represent the induced stresses and the damage calculated by Tepfers model in JPCP-A1 structure. Then, the fatigue damage matrix is assembled as follows:

$$FD = \begin{bmatrix} 3.81e-11 & 1.25e-11 & 4.03e-11 & 2.16e-12 & 9.24e-13 & 6.44e-13 & 5.34e-13 & 5.01e-13 & 5.54e-13 \\ 4.53e-12 & 1.38e-11 & 9.16e-12 & 5.6e-12 & 1.96e-12 & 1.15e-12 & 8.63e-13 & 7.45e-13 & 7.30e-13 \\ 1.13e-12 & 6.68e-12 & 9.13e-12 & 7.89e-12 & 3.48e-12 & 1.68e-12 & 1.04e-12 & 7.95e-13 & 7.06e-13 \\ 4.15e-13 & 2.25e-12 & 5.80e-12 & 7.10e-12 & 5.76e-12 & 3.02e-12 & 1.54e-12 & 9.70e-13 & 7.59e-13 \\ 2.01e-13 & 7.78e-13 & 2.40e-12 & 3.99e-12 & 6.52e-12 & 5.17e-12 & 2.83e-12 & 1.46e-12 & 9.33e-13 \\ 1.29e-13 & 3.91e-13 & 9.91e-13 & 1.82e-12 & 5.76e-12 & 5.93e-12 & 4.59e-12 & 2.43e-12 & 1.29e-12 \\ 8.03e-14 & 2.07e-13 & 4.17e-13 & 6.73e-13 & 3.48e-12 & 4.42e-12 & 5.63e-12 & 4.37e-12 & 2.36e-12 \\ 5.42e-14 & 1.22e-13 & 2.13e-13 & 3.03e-13 & 1.96e-12 & 2.08e-12 & 4.22e-12 & 5.39e-12 & 4.28e-12 \\ 3.29e-14 & 4.81e-14 & 7.61e-14 & 1.02e-13 & 9.24e-13 & 4.72e-13 & 1.23e-12 & 2.49e-12 & 3.25e-12 \end{bmatrix}$$

Further, the accumulated fatigue damage matrix can be found by multiplying normal distribution matrix and fatigue damage matrix as follows:

$$DI = \begin{bmatrix} 9.04e-6 & 2.36e-6 & 3.59e-6 & 4.09e-6 & 4.93e-6 & 3.94e-6 & 2.98e-6 & 1.99e-6 & 1.29e-6 \end{bmatrix}$$

Each value of the DI matrix represents the accumulated fatigue damage in each response point. It is found that when the 1,000,000 passes of traffic with wheel wander (σ=10 in.) yields maximum accumulated fatigue damage of 4.93e-6 at 35 inches from the edge of the slab.

To find the effect of different distributions of the traffic on accumulated fatigue damage, wheel wanders with different standard deviations of 0, 2, 4, 6, 8, 10 inches were considered for the calculation, and the results were plotted in Figure 4-42. As shown in this figure, channelized traffic (wander with a standard deviation of zero) produces the highest damage under the wheel path. Also, it is observed that as the standard deviation increases, the maximum fatigue damage index in the pavement structure decreases. An increase in standard deviation from 0 to 6 inches results in a 12% reduction in fatigue damage under the wheel path. This reduction increases to 25% when the standard deviation of the wheel wander is 10 inches. This shows that truck platooning traffic in this pavement structure causes 25% more fatigue damage compared to normal traffic which is associated with 10 inches wheel wander. Moreover, it is observed that the fatigue damage at the edge of pavement increases as the standard deviation increases.

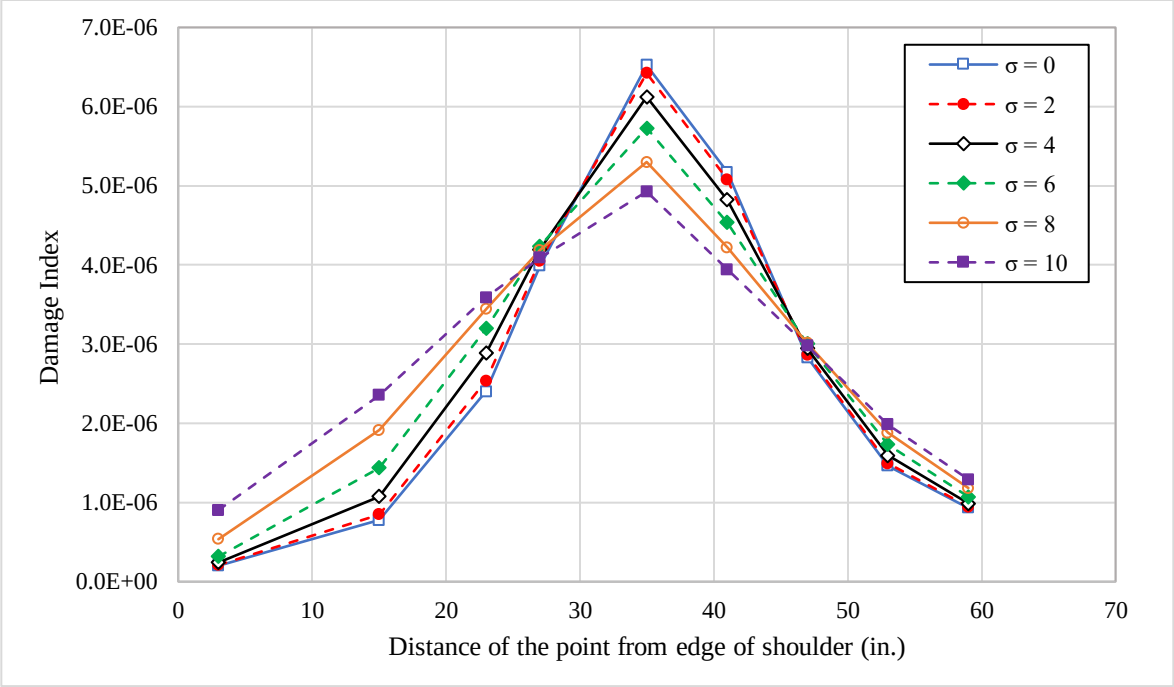

Figure 4-42. Impact of standard deviation on the fatigue damage for JPCP-A1.

The results obtained for JPCP-A2, JPCP-A3, and JPCP-A4 are plotted in Figures 4-43 to 4-45. As can be observed, in all of these pavement structures, increasing the standard deviation of wheel wander lowers the fatigue damage accumulation in the pavement structures. Increasing the standard deviation of wheel wander from 0 to 10 inches reduces the accumulated fatigue damage at 35 inches from the edge by 16.7%, 3.3%, and 2.9% for JPCP-A2, JPCP-A3, and JPCP-A4, respectively. It reveals that as the thickness increases the fatigue damages created by different levels of wander get closer to each other. Therefore, it can be concluded that the impact of wheel wander on the development of fatigue damage can be reduced by increasing the thickness of the slab. Furthermore, it was found that when the thickness increases to 12 inches and higher, the accumulated damage created by channelized traffic is lower than those created by traffic with a standard deviation of 4 inches However, still, the channelized traffic creates higher accumulated fatigue damage compared to traffic with a standard deviation of 10 inches.

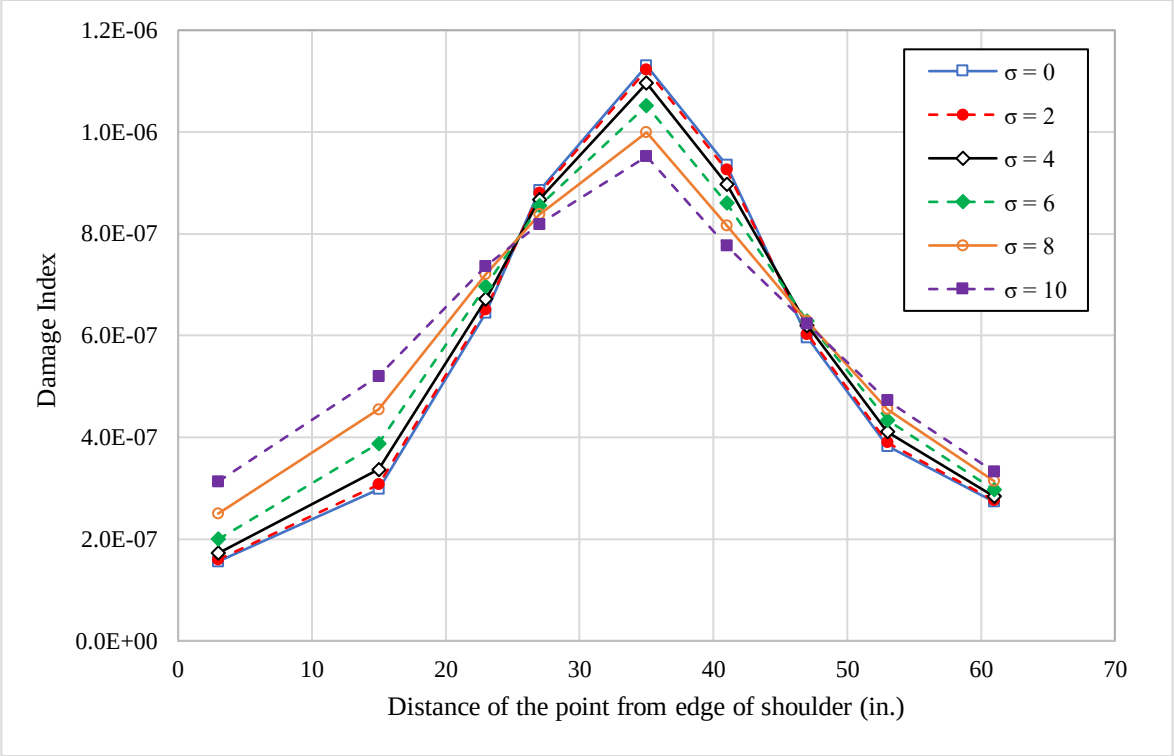

Figure 4-43. Impact of standard deviation on the fatigue damage for JPCP-A2.

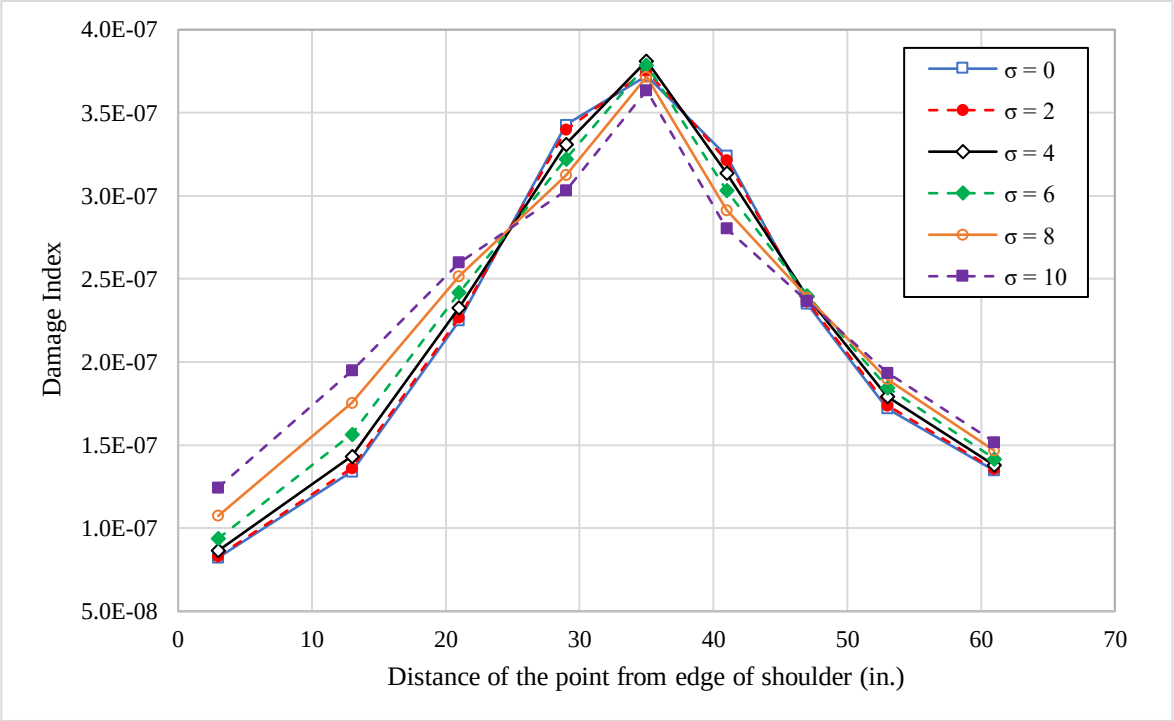

Figure 4-44. Impact of standard deviation on the fatigue damage for JPCP-A3.

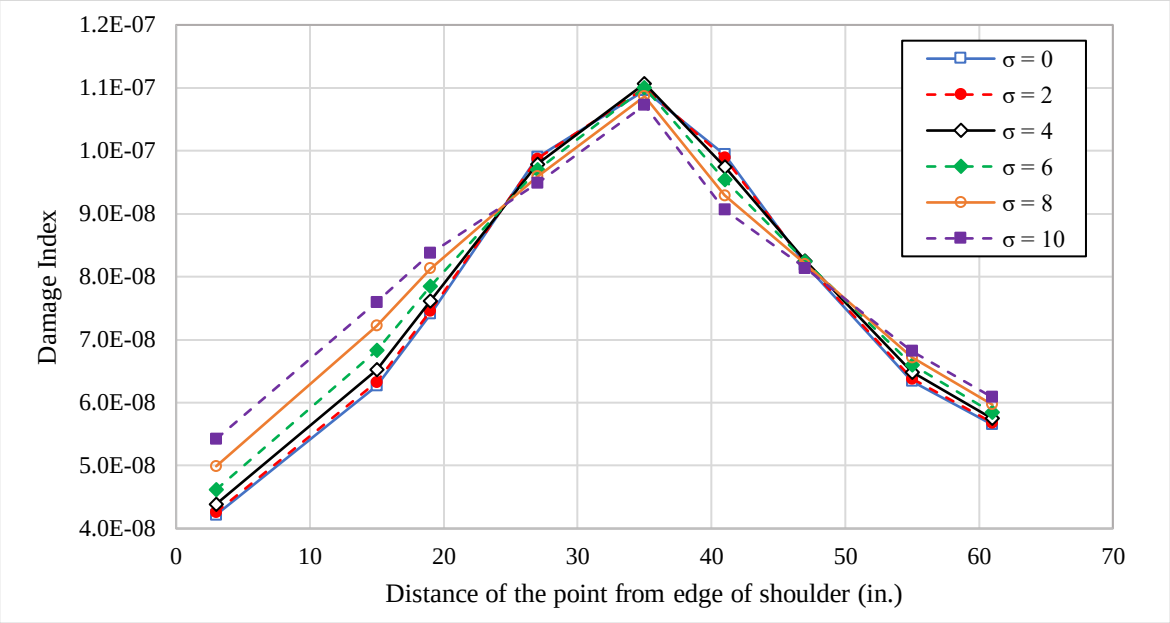

Figure 4-45. Impact of standard deviation on the fatigue damage for JPCP-A4.

A similar principle was applied to JPCP structures with trench under the wheel path. Figures 4-46 and 4-47 illustrate the accumulated fatigue damages in JPCP-B1 and JPCP-B2 structures. As can be seen in these figures, wheel wander has a similar impact on the accumulated fatigue damage at the bottom of thickened part of the slab and it decreases by the higher level of wheel wander. However, it was found that when the standard deviation of the wheel wander increases to 8 inches and higher, the maximum accumulated fatigue damage does not occur at the location where the trench was provided, instead, it occurs at the top edge of the trench. As it can be observed in Figures 4-46 and 4-47, for JPCP-B1 with a bottom trench width of 26 inches, the maximum accumulated fatigue damage occurs 21 inches away from the edge of the pavement, while for JPCP-B2 with a bottom trench width of 32 inches, it occurs in 13 inches away from the edge. Therefore, it can be concluded that even though providing the trench decrease the accumulated fatigue damage for channelized traffic, the maximum accumulated fatigue damage occurs at the top edge of the trench under the normal traffic with wheel wander (σ=10 in.).

Table 4-4. The induced stresses from different lateral wander of the load in JPCP-A1.

Wheel wander (in.)	Stress (psi) at response points (distance from the edge of the slab)								
	-4 (3 in.)	-3 (15 in.)	-2 (23 in.)	-1 (27 in.)	0 (35 in.)	1 (41 in.)	2 (47 in.)	3 (53 in.)	4 (59 in.)
-24	200.40	177.23	153.61	140.64	122.94	115.43	111.52	110.19	112.32
-18	156.08	179.32	170.72	160.48	138.58	127.56	121.54	118.46	118.03
-12	127.13	164.15	170.66	167.61	150.54	135.42	125.47	119.83	117.34
-6	106.27	141.46	161.21	165.42	161.08	147.64	133.65	123.97	118.85
0	91.15	119.36	142.86	153.41	163.65	158.83	146.28	132.52	123.16
6	129.93	143.11	156.34	161.67	161.08	137.06	124.42	105.07	82.01
12	142.52	155.32	160.57	155.53	150.54	116.34	106.39	91.82	72.09
18	154.87	159.67	154.56	139.82	138.58	99.75	92.37	80.81	63.91
24	149.17	143.61	128.91	108.99	122.94	77.02	70.98	61.41	53.51

Table 4-5. The calculated fatigue damage from different lateral wander of the load in JPCP-A1.

Wheel wander (in.)	Fatigue damage at response points (distance from the edge of the slab)								
	-4 (3 in.)	-3 (15 in.)	-2 (23 in.)	-1 (27 in.)	0 (35 in.)	1 (41 in.)	2 (47 in.)	3 (53 in.)	4 (59 in.)
-24	3.81E-11	1.25E-11	4.03E-12	2.16E-12	9.24E-13	6.44E-13	5.34E-13	5.01E-13	5.54E-13
-18	4.53E-12	1.38E-11	9.16E-12	5.60E-12	1.96E-12	1.15E-12	8.63E-13	7.45E-13	7.30E-13
-12	1.13E-12	6.68E-12	9.13E-12	7.89E-12	3.48E-12	1.68E-12	1.04E-12	7.95E-13	7.06E-13
-6	4.15E-13	2.25E-12	5.80E-12	7.10E-12	5.76E-12	3.02E-12	1.54E-12	9.70E-13	7.59E-13
0	2.01E-13	7.78E-13	2.40E-12	3.99E-12	6.52E-12	5.17E-12	2.83E-12	1.46E-12	9.33E-13
6	1.29E-13	3.91E-13	9.91E-13	1.82E-12	5.76E-12	5.93E-12	4.59E-12	2.43E-12	1.29E-12
12	8.03E-14	2.07E-13	4.17E-13	6.73E-13	3.48E-12	4.42E-12	5.63E-12	4.37E-12	2.36E-12
18	5.42E-14	1.22E-13	2.13E-13	3.03E-13	1.96E-12	2.08E-12	4.22E-12	5.39E-12	4.28E-12
24	3.29E-14	4.81E-14	7.61E-14	1.02E-13	9.24E-13	4.72E-13	1.23E-12	2.49E-12	3.25E-12

A similar analysis was performed on JPCP-C1, JPCP-C2, JPCP-D1, and JPCP-D2. The results are presented in Figures 4-48 to 4-51. It can be observed that in all of these structures regardless of the level of lateral wander, the maximum fatigue damage is accumulated in the same location when the vehicle runs from the center of the lane. However, the maximum accumulated fatigue damage decreases by increasing the standard deviation of wheel wander.

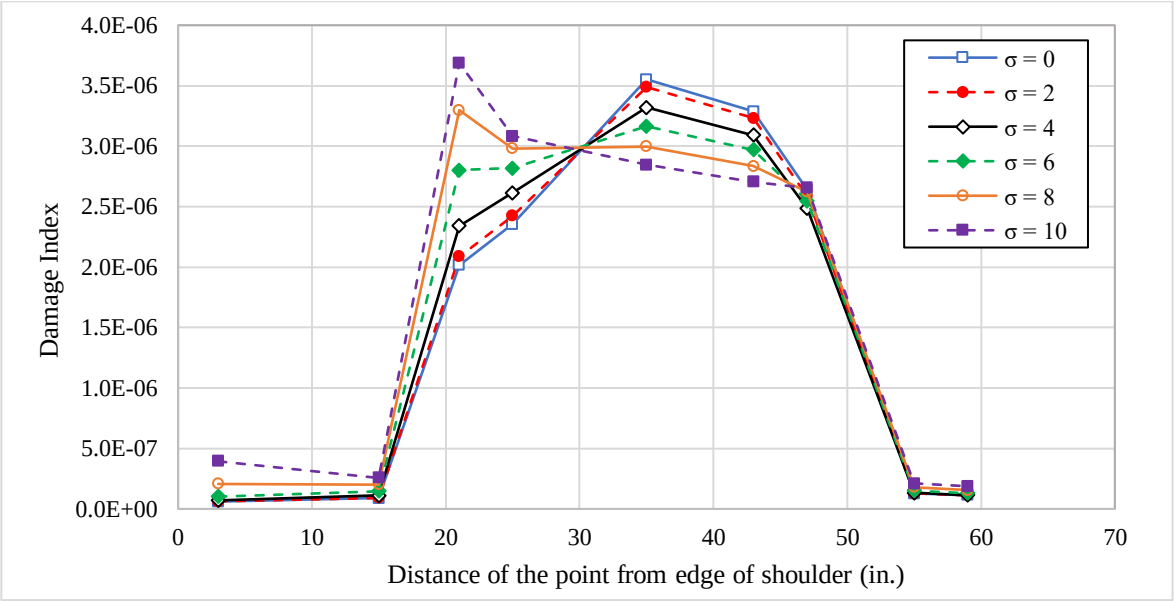

Figure 4-46. Impact of standard deviation on the fatigue damage for JPCP-B1.

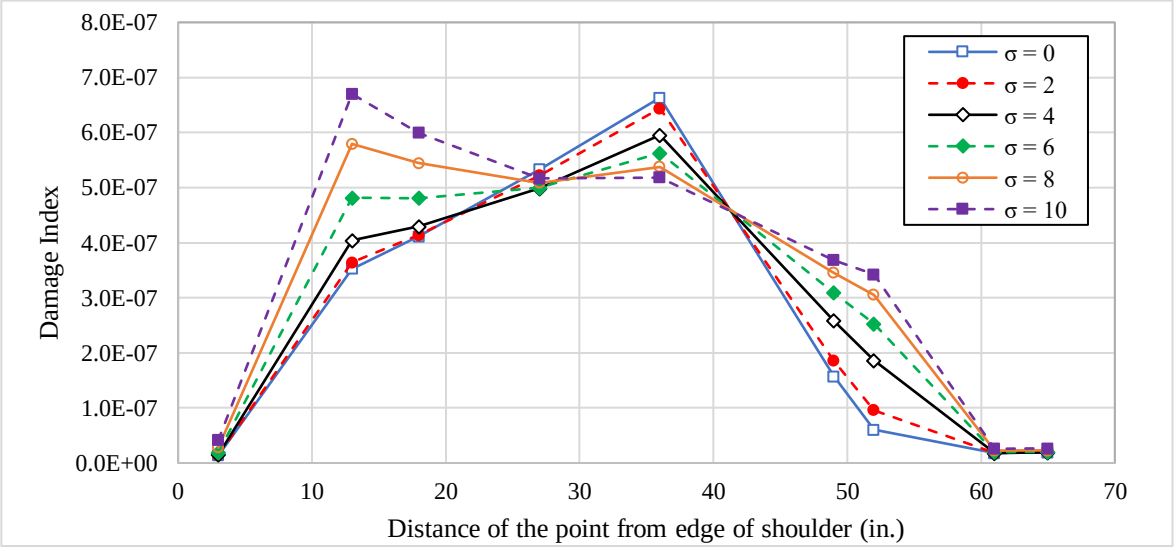

Figure 4-47. Impact of standard deviation on the fatigue damage for JPCP-B2.

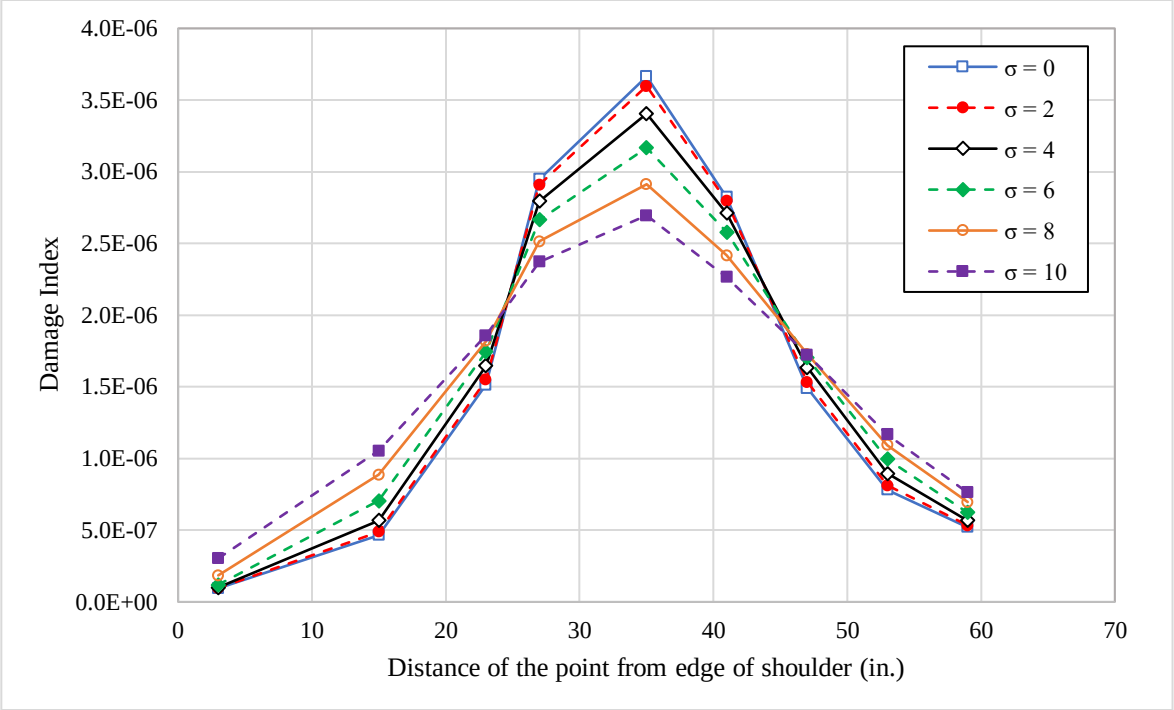

Figure 4-48. Impact of standard deviation on the fatigue damage for JPCP-C1.

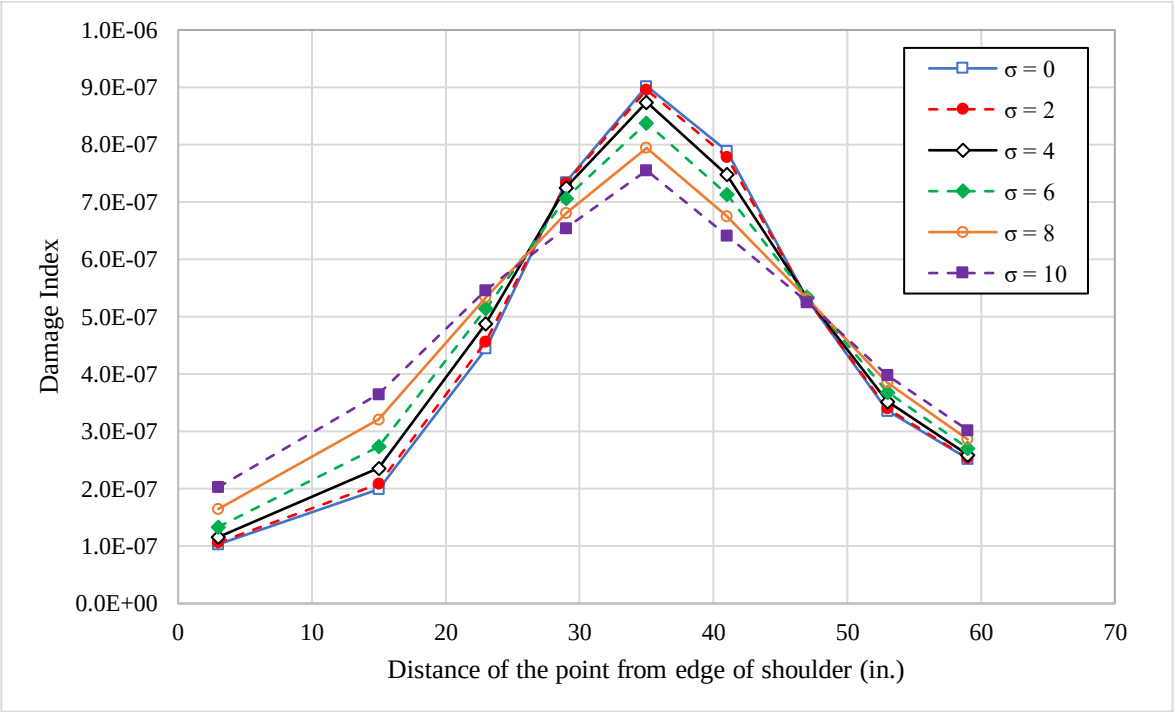

Figure 4-49. Impact of standard deviation on the fatigue damage for JPCP-C2.

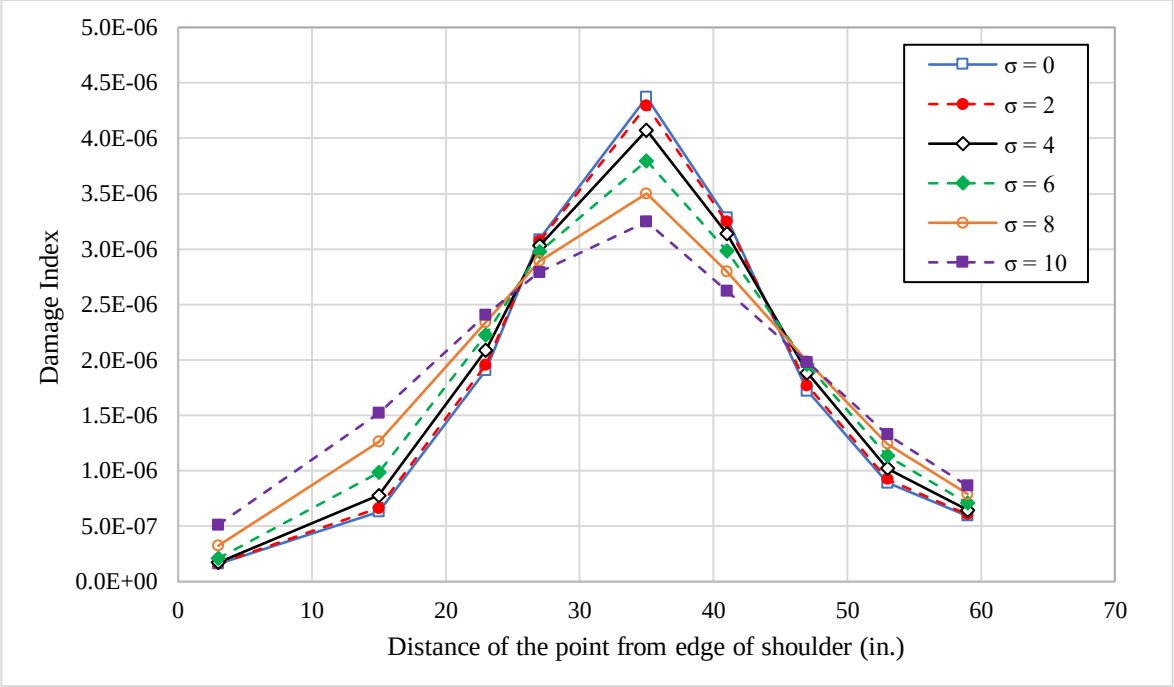

Figure 4-50. Impact of standard deviation on the fatigue damage for JPCP-D1.

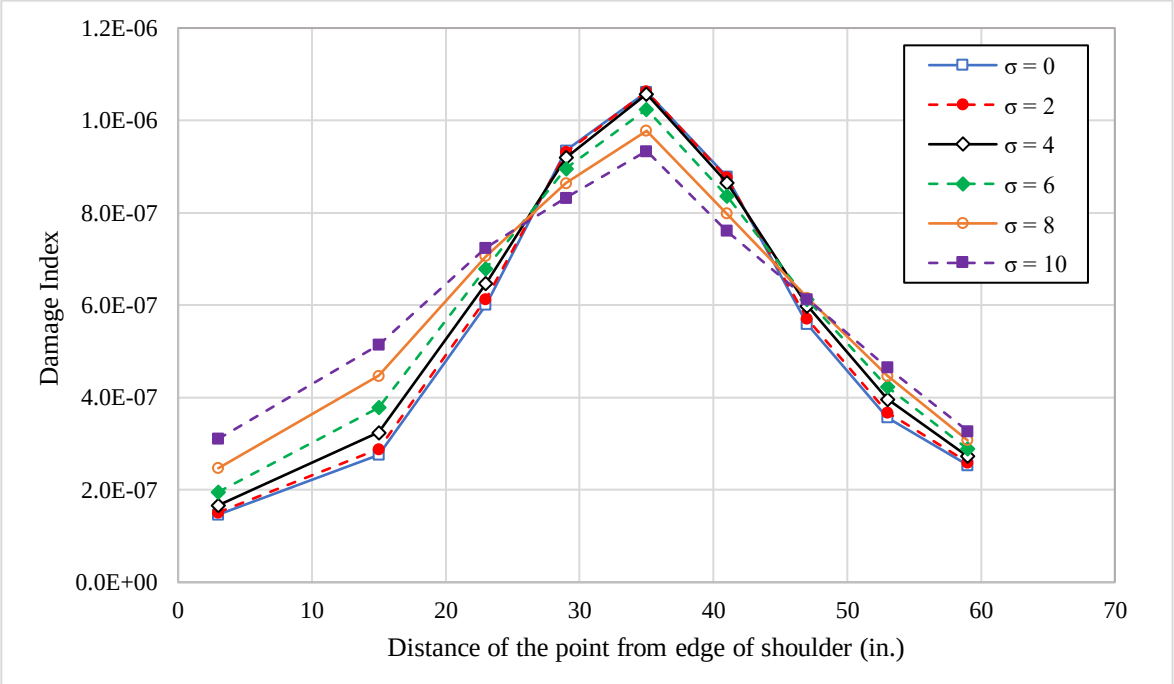

Figure 4-51. Impact of standard deviation on the fatigue damage for JPCP-D2.

In order to compare the fatigue performance of the discussed pavement structures under truck platooning traffic and normal traffic with wheel wander, the maximum accumulated fatigue damages calculated for wheel wanders with standard deviations of 0 and 10 inches are summarized in Figure 4-52. As illustrated, all of the design considerations have a positive impact on improving fatigue performance of JPCP structures under both channelized traffic and traffic with normal wheel wander. As can be seen, increasing the thickness of PCC slabs significantly improves the fatigue performance of the pavement. Increasing the thickness from 8 inches to 10 inches reduces the damage index created by channelized traffic and normal traffic with wheel wander of 10 inches by 82.67% and 80.60%, respectively. Increasing the thickness of the slab to 12 inches further improves these reductions to 94.30% and 92.43%, respectively. Therefore, it can be concluded that increasing the thickness of the slab causes similar improvement on fatigue performance of the discussed structure under channelized traffic and normal traffic. Furthermore, it can be seen that in JPCP-A1, channelized traffic creates a damage index of 6.52e-6, while normal traffic produces a damage index of 4.92e-6. However, these numbers for JPCP-A4 are 1.09e-7 and 1.07e-7, respectively. It shows that the thicker the slab, the lower the impact of channelized traffic on accumulated fatigue damage. Therefore, it can be concluded that if the slab is designed to be thick enough its fatigue performance under channelized traffic and traffic with normal wander will be the same. As discussed earlier, in JPCP-B1 and JPCP-B2 structures, the accumulated fatigue damage at the top edge of the trench is higher than those created at the bottom of the trench. However, as can be seen in Figure 4-52, this design consideration provides better fatigue damage performance compared to JPCP-A1 and JPCP-A2. Comparing the result for JPCP-A1 and JPCP-B1 shows that thickening the slab under the wheel path of channelized traffic (vehicle runs from the center of the lane) by 2 inches improves the fatigue performance by 45% under the channelized

traffic. However, its performance under normal traffic with standard deviation of wheel wander of 10 inches improves by 24%. These values for JPCP-B2 were obtained to be 41% and 28%, respectively. Also, comparing damage indices for JPCP-A1 and JPCP-C1 shows that replacing dowel bars with a larger size causes a reduction of 43.87% in damage index for channelized traffic and 45.15% for normal traffic with a standard deviation of 10 inches wheel wander. However, replacing only dowel bars in the wheel path (JPCP-D1) shows a 32.98% and 34.02% decrease in damage index, respectively. It proves that dowel bars in the wheel path have a high contribution in the reduction of damage index in this pavement structure and replacing dowel bars located away from the wheel path improves the fatigue performance of this pavement structure by 10%. In addition, the relative life of each design alternative was computed and presented in Figure 4-53. It can be seen that increasing the thickness of the slab significantly increases the life of pavement while replacing dowel bars in the wheel path has the lowest impact on the fatigue life of JPCP.

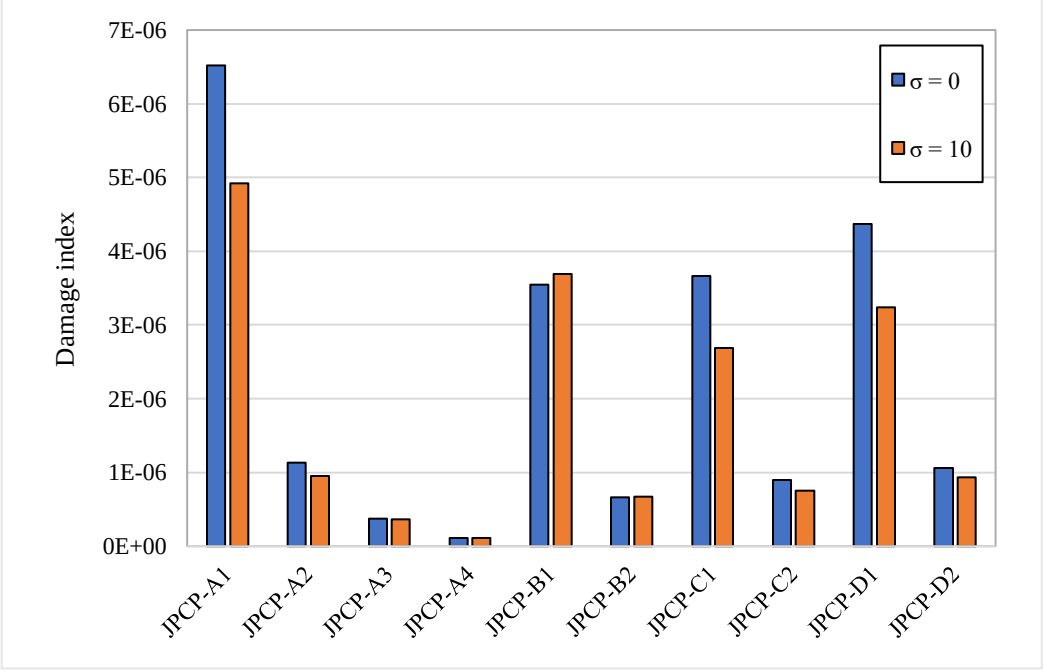

Figure 4-52. Comparing the maximum fatigue damage created by channelized traffic and normal traffic in JPCP structures with granular base.

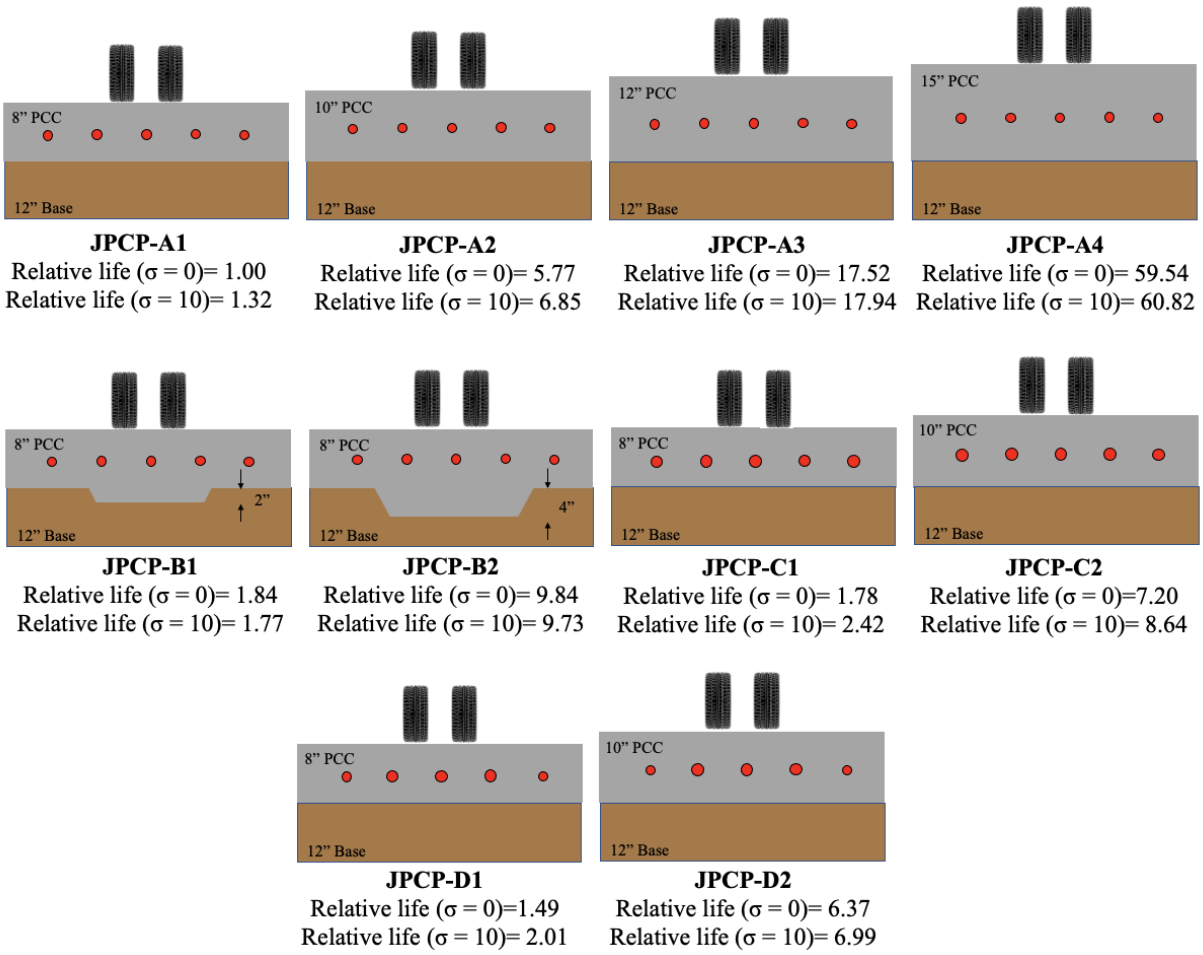

Figure 4-53. Comparing the life of different JPCP design alternatives under channelized and normal traffic.

A similar analysis was performed on JPCP structures with asphalt base. Figure 4-54 shows the damage index calculated for JPCP-A1-AB under different levels of lateral wander. As can be seen, the damage profile is similar to that induced in JPCP with granular base with this difference that the values of the damage indices are lower because of higher stiffness of asphalt base. For the sake of brevity, the figures for other design considerations are presented in the appendix. The maximum accumulated fatigue damages for all design considerations are summarized in Figure 4-55. It can be seen that placing an asphalt base does not change the effectiveness of the design considerations and it only reduce the values of damage index proportionally due to the stiffness of

the asphalt base. Therefore, similar results as JPCP with granular base can be drawn for JPCP with asphalt base. In addition, comparing the results obtained for JPCP-A1 with JPCP-A1-AB indicates that the asphalt base decreases the accumulated fatigue damage by 44.3% for channelized traffic and 45.3% for normal traffic. These values for 10 inches slabs are 22.7% and 24.2%. This reveals that as the thickness of the PCC slab increases, the impact of asphalt base in fatigue damage reduction decreases. However, the main benefits of using asphalt base are its great impact in eliminating erosion of underlying layers, pumping, and consequently reduction of faulting damage. The improvement in the performance of this pavement by each design alternative under channelized and normal traffic in terms of fatigue life is illustrated in Figure 4-56. This figure compares the life of JPCP structures with an asphalt base with JPCP with a granular base. As shown, the presence of the asphalt layer increases the fatigue life of pavement compared to equivalent structure with a granular base, but the impact of this layer in life improvement in thinner slabs are higher than those with thick slabs.

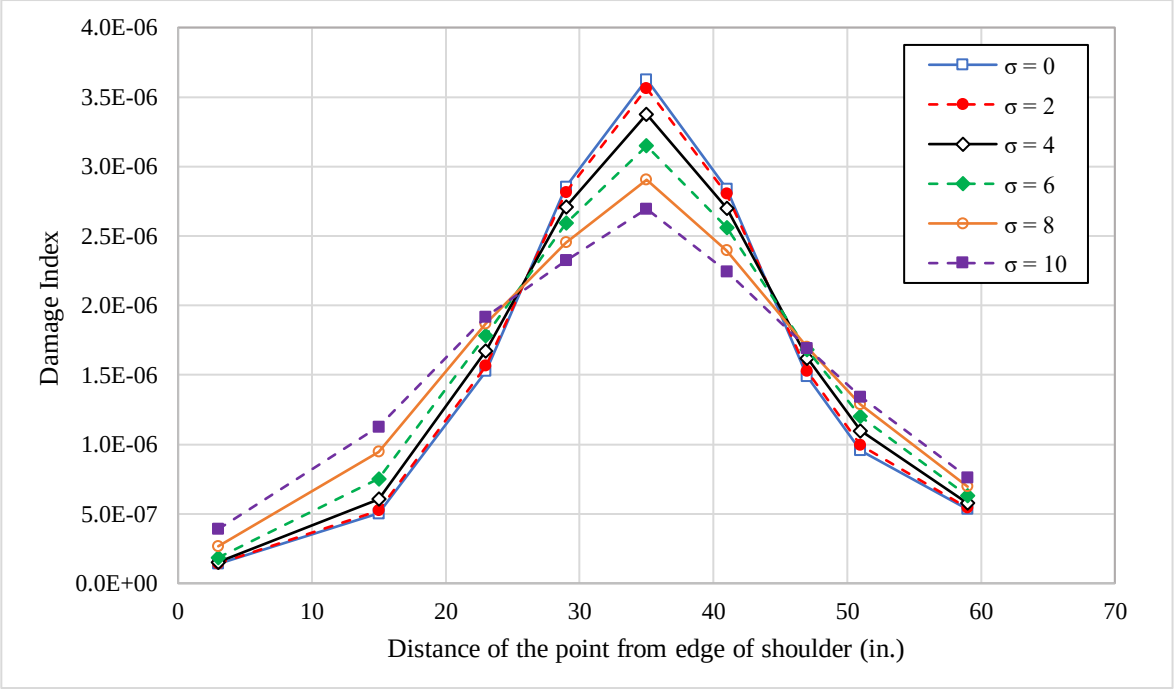

Figure 4-54. Impact of standard deviation on the fatigue damage for JPCP-A1-AB.

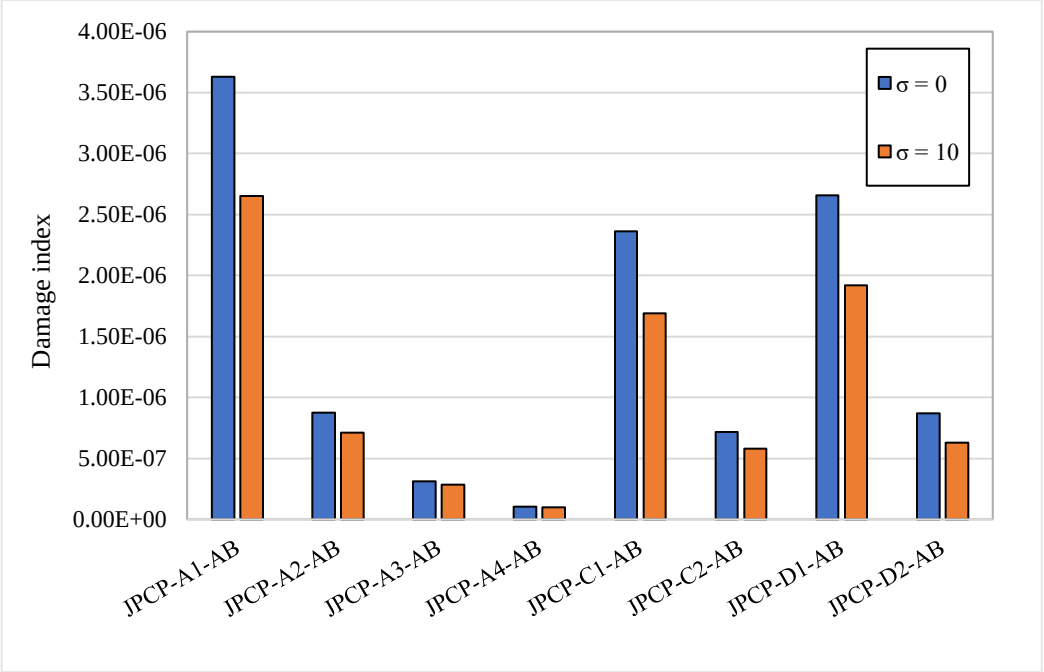

Figure 4-55. Comparing the maximum fatigue damage created by channelized traffic and normal traffic in JPCP structures with asphalt base.

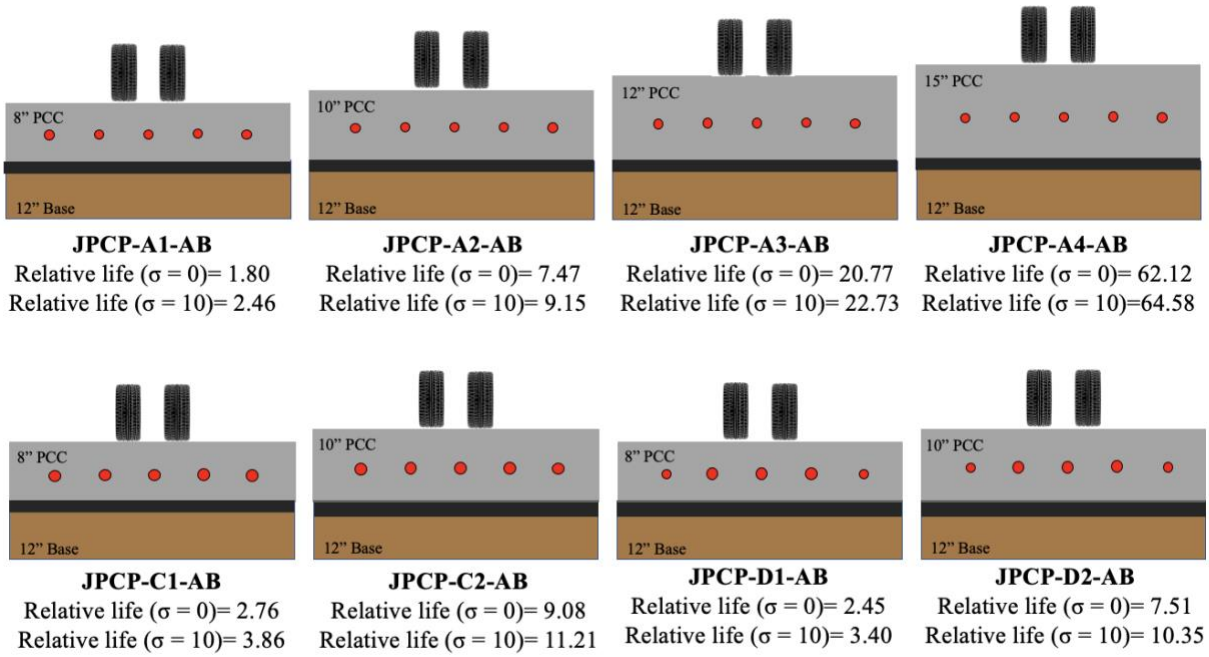

Figure 4-56. Comparing the relative life of various JPCP structures with asphalt base under channelized traffic and normal traffic with JPCP-A1 structure (relative life=1.00).

Likewise, the fatigue performance of different structure alternatives of CRCP under truck platooning and traffic with wheel wanders was compared. Figure 4-57 represents the accumulated fatigue damage in CRCP-A1 structure. As indicated, the highest fatigue damage in this structure is developed by truck platooning traffic, and this damage is decreased by increasing the standard deviation of wheel wander. In this structure, channelized traffic causes a 28% increase in the maximum accumulated fatigue damage compared to traffic with normal wheel wander (σ=10 in.). Figures 4-58 and 4-59 illustrate the accumulated fatigue damages in CRCP-A2 and CRCP-A3, respectively. As shown, the higher the standard deviation of wheel wander, the lower the maximum accumulated damage. It is observed that truck platooning increases the maximum accumulated fatigue damage by 21% and 13% compared to normal traffic with wheel wander for CRCP-A2 and CRCP-A3, respectively. Therefore, as the thickness of the PCC slab increases the impact of truck platooning on the fatigue performance of CRCP structures decreases.

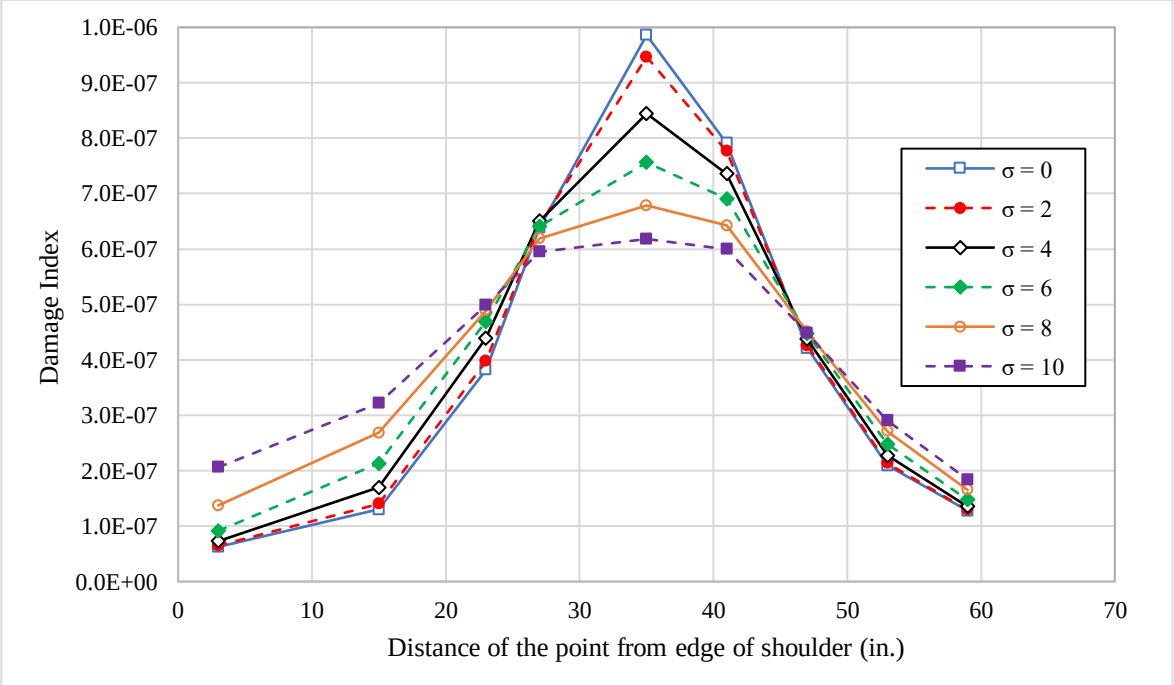

Figure 4-57. Impact of standard deviation on the fatigue damage for CRCP-A1.

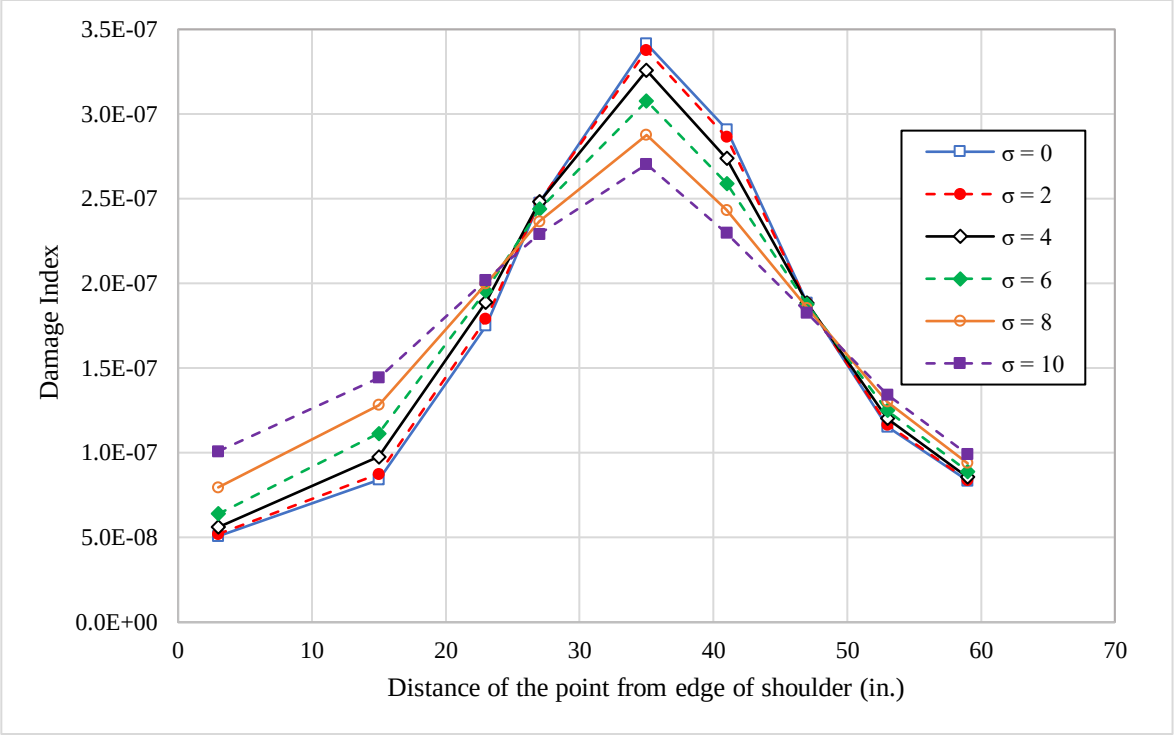

Figure 4-58. Impact of standard deviation on the fatigue damage for CRCP-A2.

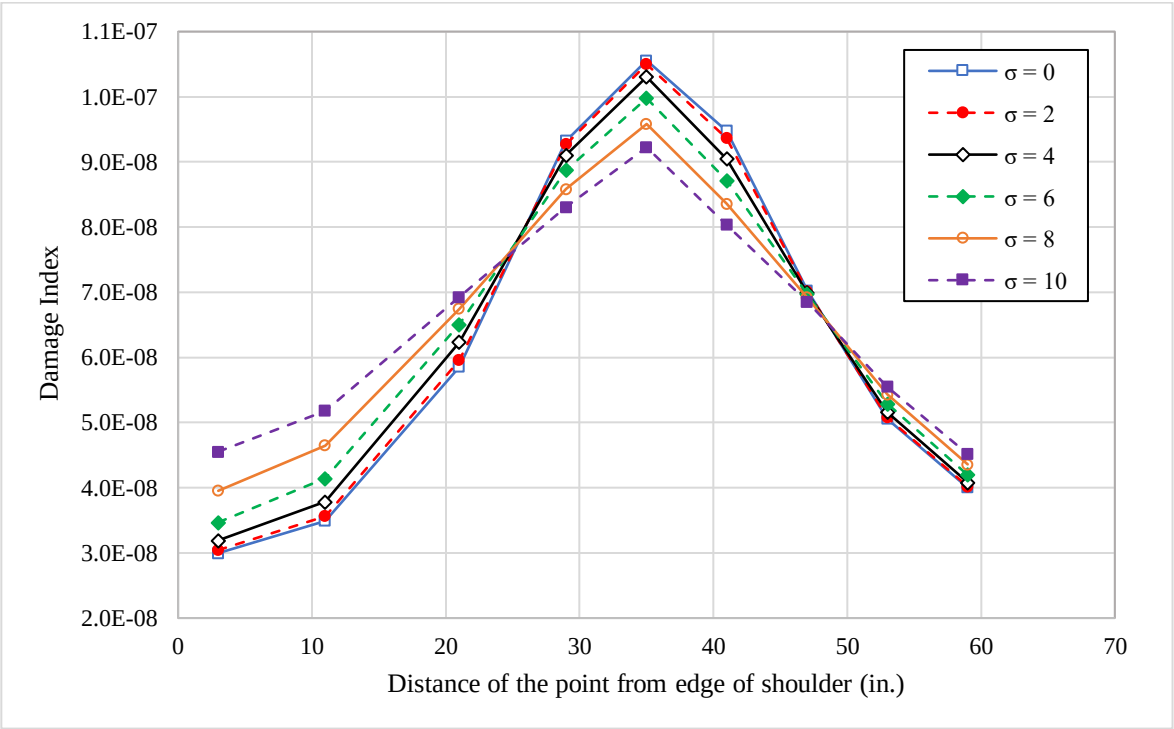

Figure 4-59. Impact of standard deviation on the fatigue damage for CRCP-A3.

The results are shown in Figures 4-60 and 4-61 for CRCP with thickened slabs under the wheel path of channelized traffic show that although increasing the standard deviation reduces the fatigue damage in the thickened part of the slab, once the standard deviation increases to 8 inches. the accumulated damage at the edge of the trench will be higher than those under the wheel path of channelized traffic. Therefore, in this structure, the bottom-up cracking initiates from the edge of the trench when it is subjected to traffic with 10 inches standard deviation for a lateral wander.

The results obtained for CRCP-C1 and CRCP-C2 which contain larger size rebars in the wheel path are presented in Figures 4-62 and 4-63. As can be seen, the performance of these pavements is similar to CRCP-A1 and CRCP-A2, and no significant change in accumulated fatigue damage is observed.

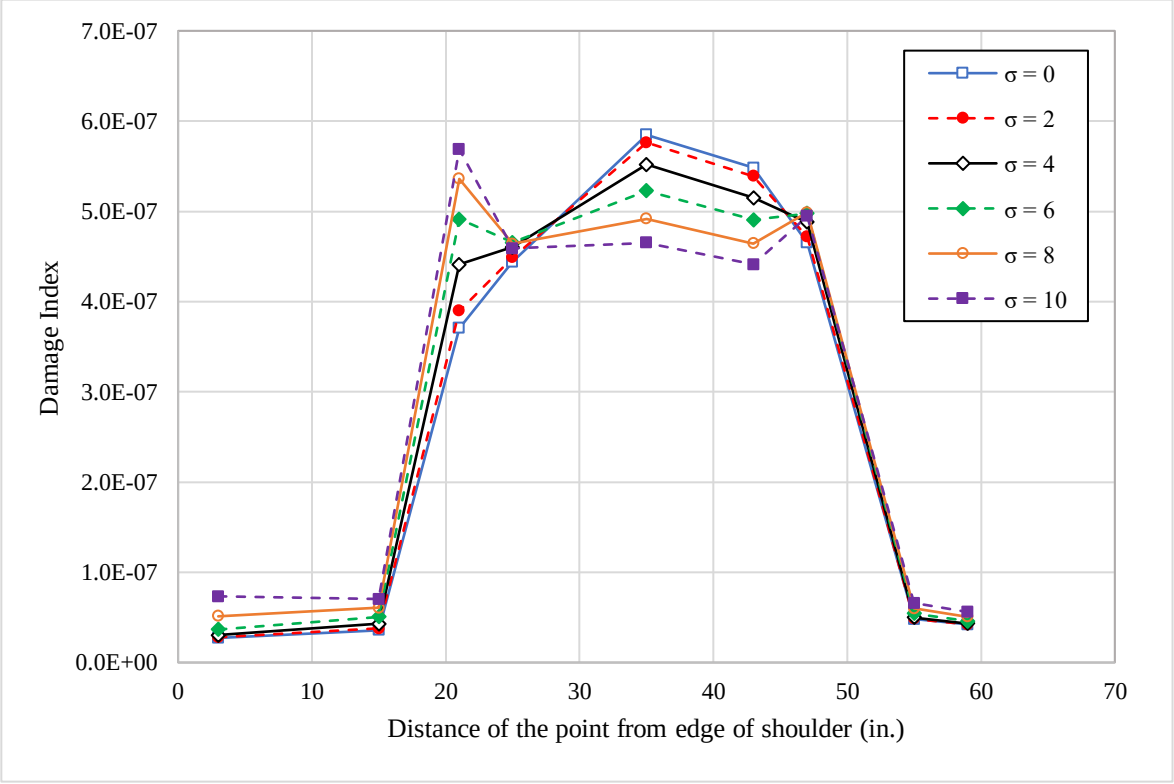

Figure 4-60. Impact of standard deviation on the fatigue damage for CRCP-B1.

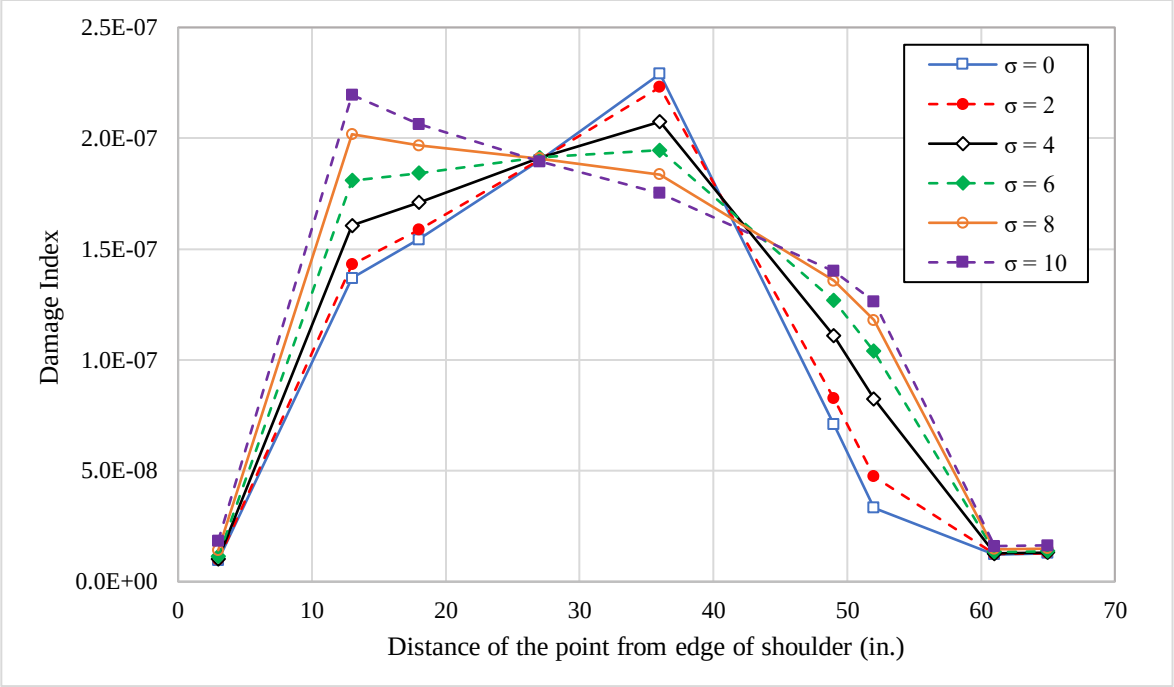

Figure 4-61. Impact of standard deviation on the fatigue damage for CRCP-B2.

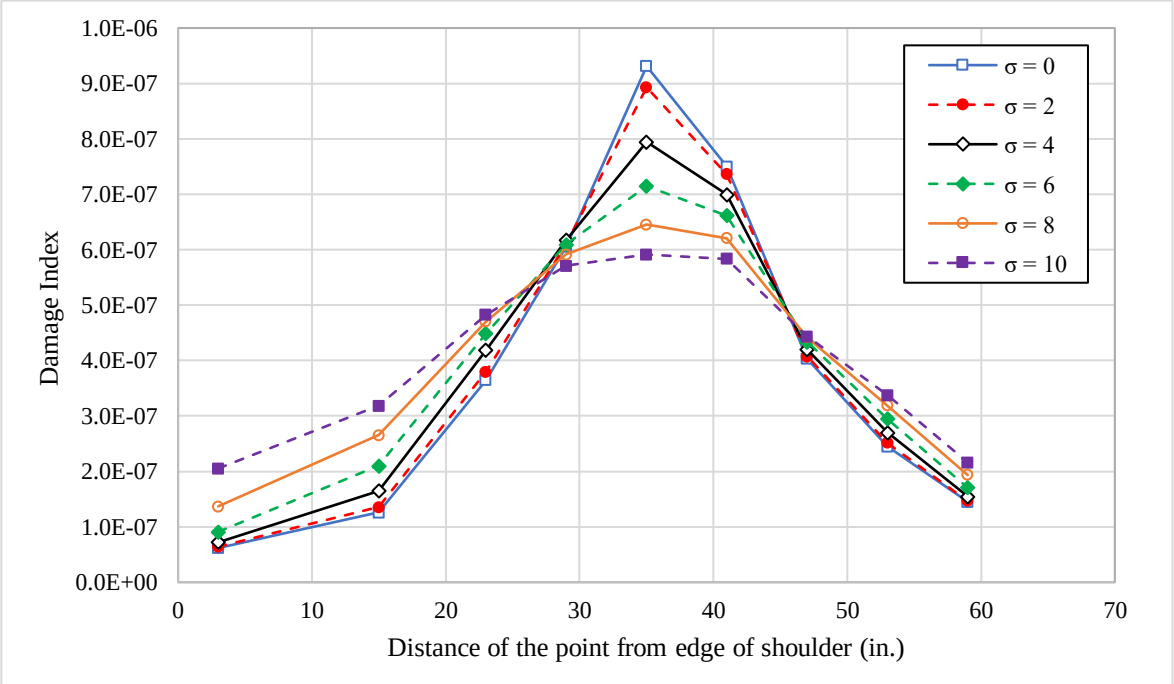

Figure 4-62. Impact of standard deviation on the fatigue damage for CRCP-C1.

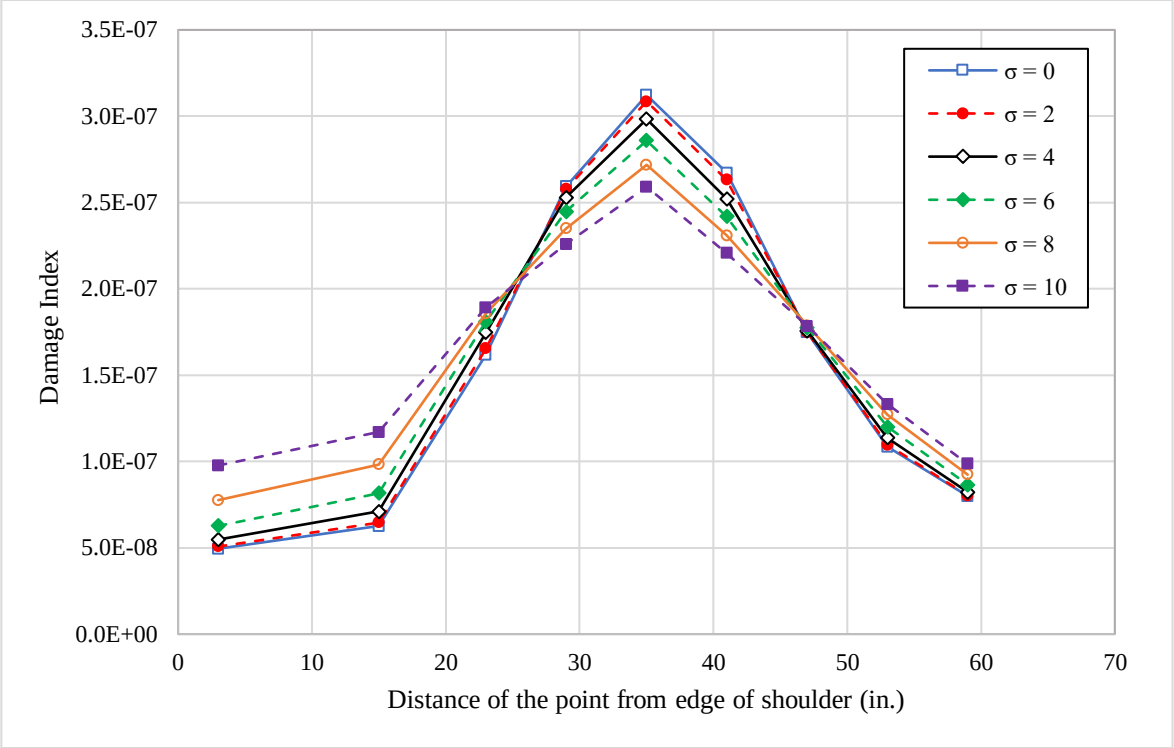

Figure 4-63. Impact of standard deviation on the fatigue damage for CRCP-C2.

The maximum accumulated fatigue damages for 1,000,000 passes of channelized and normal traffic with a standard deviation of 10 inches for wheel wander created in each of CRCP structures are plotted in Figure 4-64. As can be seen, increasing the thickness of the PCC slab has a considerable impact on decreasing the maximum fatigue damage in CRCP structures for both truck platooning and normal traffic. It is observed that increasing the thickness of the slab by 2 inches and 4 inches decrease the maximum accumulated fatigue damage caused by truck platooning by 65% and 89%, respectively. These changes in the thickness reduce the induced fatigue damage developed by normal traffic by 56% and 85%, respectively. In addition, it is observed that as the thickness increases the difference between the damages created by truck platooning and normal traffic with wheel wander (σ=10 in.) decreases. Comparing the damage indices obtained for CRCP-A1 and CRCP-B1 shows that thickening the slab under the wheel path results in a 40% improvement in fatigue performance under channelized traffic, while its

performance under normal traffic improves by only 7%. Furthermore, it is observed that replacing rebars embedded in the wheel path reduces the fatigue damage created by 5% and 8% for 8 inches and 10 inches thick slabs, respectively, when they are subjected to channelized traffic. However, this measure reduces the induced fatigue damage by 4% for both 8 inches and 10 inches thick slabs when subjected to traffic with normal wander. Therefore, it can be concluded that even though larger rebars in the wheel path show better fatigue performance under channelized traffic, it causes no significant improvement in fatigue performance of the CRCP structures. Also, these findings were shown in terms of the relative life of these design alternatives in Figure 4-65. As can be seen, increasing the thickness has the highest impact in improving the fatigue life. However, comparing the results from CRCP with JPCP reveals that since the induced stress in CRCP is smaller than those in equivalent JPCP, the impact of thickness in life improvement is less in CRCP structures. In addition, it can be seen increasing the size of rebars located in the wheel path has a negligible effect on the improvement of fatigue life.

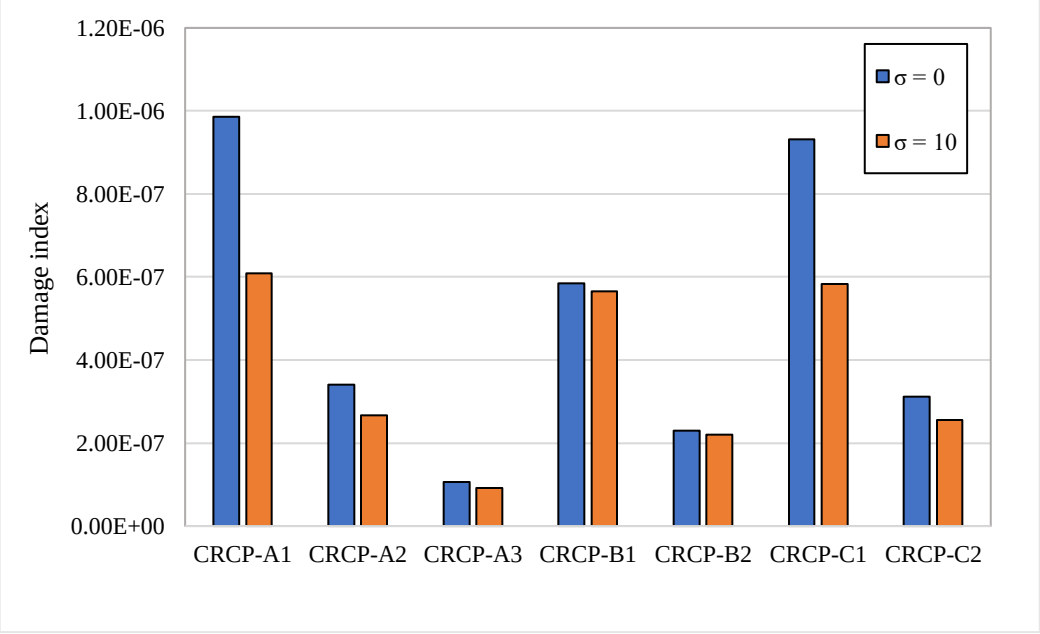

Figure 4-64. Comparing the maximum fatigue damage created by channelized traffic and normal traffic in CRCP structures.

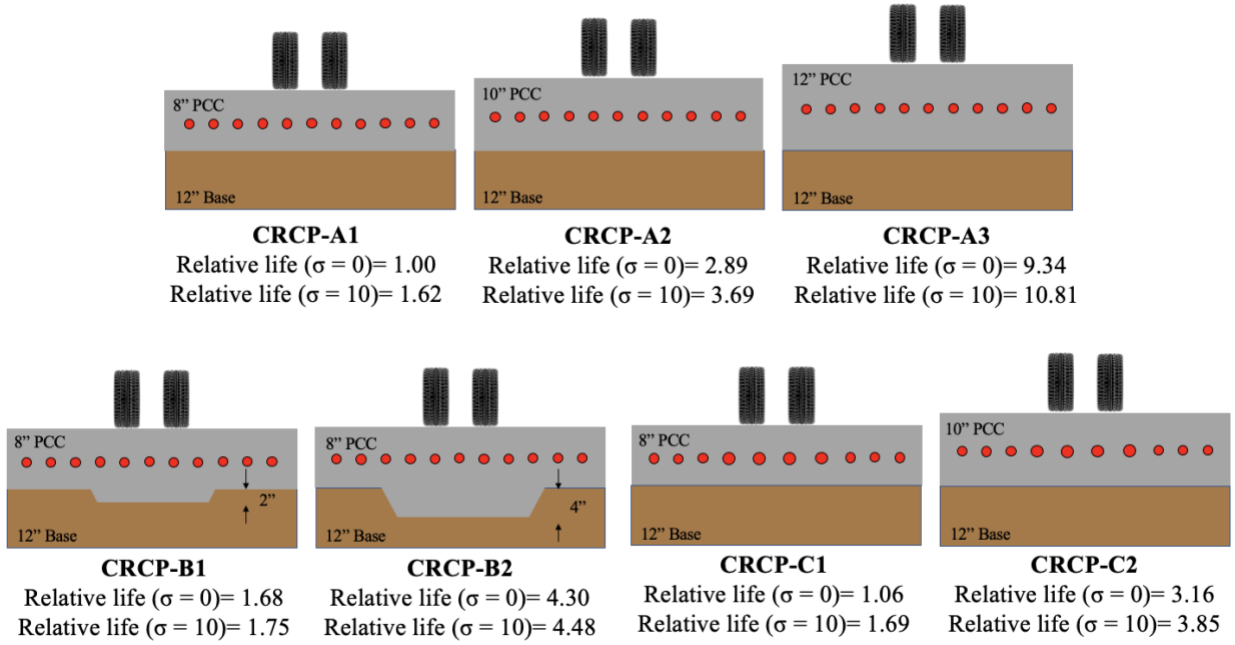

Figure 4-65. Comparing the life of different CRCP design alternatives under channelized traffic and normal traffic.

CHAPTER 5: COST ANALYSIS

5.1. Introduction

As observed in Chapter four, each of the design considerations provides a different level of improvement on fatigue performance. Also, it has been shown that increasing the thickness of the slab has a superior impact on predicted service life and fatigue performance. However, it is clear that constructing pavements with thicker slabs results in a significantly higher cost of construction. Therefore, it is required to conduct a cost analysis to recognize the design consideration which performs in the most cost-effective manner under the truck platooning traffic. To do so, the cost analysis is performed based on TxDOT (Texas Department of Transportation) average low bid unit price and cost of materials.

5.2. Estimating cost of construction based on TxDOT average low bid unit price

The average unit bid price of actual pavement construction projects can provide a basic understanding of the probable construction cost of pavements. The average low bid unit prices for highway construction bid items are available on TxDOT website in form of spreadsheets. The provided unit prices are derived from average low bid prices based on statewide projects during 3 and 12 consecutive months. Table 5-1 summarizes the 12 months average unit price for applicable items for the discussed pavement structures in this study. As can be seen in this table, the unit prices are provided based on the unit area of pavements and include the cost of all materials, labor, placement, etc. Also, no details on the size of reinforcements or dowel bars are provided. Therefore, the cost estimation based on the average low bid unit price cannot consider the cost of implementing larger rebars or dowel bars. Moreover, the unit price for some items, such as the unit price for 12-inch JPCP, are is available. This is because there were no highway construction projects with 12-inch JPCP during the last 12 consecutive months. To perform the cost analysis,

the following assumptions are made based on available bid items. Since the unit price for 11-inch and 13-inch JPCP are available, the average of their unit prices was used for 12-inch JPCP. In addition, the unit price of 14-inch JPCP was considered to be 30% more than 10-inch JPCP. The unit prices implemented for cost analysis are summarized in Table 5-2.

Table 5-1. Selected TxDOT average low bid unit prices.

Item Description	Unit	Unit Price ($)
8" Jointed plain concrete pavement	SY	50.00
10" Jointed plain concrete pavement	SY	82.45
11" Jointed plain concrete pavement	SY	98.00
12” Jointed plain concrete pavement	SY	Not available
13" Jointed plain concrete pavement	SY	70.00
15" Jointed plain concrete pavement	SY	Not available
8" Continuous reinforced concrete pavement	SY	46.17
10" Continuous reinforced concrete pavement	SY	55.37
12" Continuous reinforced concrete pavement	SY	59.31
2" Hot mix asphalt pavement	SY	2.07

Table 5-2. Average low bid unit price for various design alternatives used in this study.

Item Description	Unit	Unit Price ($)
8" Jointed plain concrete pavement	SY	50.00
10" Jointed plain concrete pavement	SY	82.45
12" Jointed plain concrete pavement	SY	84.00
15" Jointed plain concrete pavement	SY	107.19
8" Continuous reinforced concrete pavement	SY	46.17
10" Continuous reinforced concrete pavement	SY	55.37
12" Continuous reinforced concrete pavement	SY	59.31
2" Hot mix asphalt pavement	SY	2.07

To determine the optimal pavement structures, the cost of construction for the discussed design alternatives is computed per lane-mile. Since the lane width was considered to be 12 ft., the surface area of one-mile pavement will be 7040 square-yard. Table 5-3 presents the calculated cost of construction for different design alternatives along with their damage index under truck platooning and traffic with normal wander using Tepfers model.

Table 5-3. Construction cost per lane-mile for various design alternatives.

Pavement structure	Slab thickness (in.)	Unit Price ($/SY)	Unit Price ($/lane-mile)	Damage index (Channelized traffic)
JPCP-A1	8	50.00	352,000.00	6.52E-06
JPCP-A2	10	82.45	580,448.00	1.13E-06
JPCP-A3	12	84.00	591,360.00	3.72E-07
JPCP-A4	15	107.19	754,582.40	1.10E-07
JPCP-A1-AB	8	52.07	366,572.80	3.63E-06
JPCP-A2-AB	10	84.52	595,020.80	8.73E-07
JPCP-A3-AB	12	86.07	605,932.80	3.14E-07
JPCP-A4-AB	15	109.26	769,155.20	1.05E-07
CRCP-A1	8	46.17	325,036.80	9.86E-07
CRCP-A2	10	55.37	389,804.80	3.41E-07
CRCP-A3	12	59.31	417,542.40	1.06E-07

Cost estimate of structures per lane-mile shows that although JPCP-A2 structure costs 65% more than JPCP-A1 structure, it provides 83% better fatigue performance under truck platooning. Increasing the slab thickness from 8 inches (JPCP-A1) to 12 inches (JPCP-A3) will be a 68% more expensive alternative, but it improves the fatigue performance by 94%. However, JPCP-A4 costs 2.14 times more than JPCP-A1 and it improves the fatigue performance by 98%. Comparing the fatigue performance improvements offered by these structures, it can be concluded that JPCP-A3 is a more cost-effective alternative compared to JPCP-A4 structure. Evaluating the construction cost of a 2 inches asphalt layer under the JPCP slabs shows that it increases the cost of construction by 2% to 4%, while it offers up to 44% in fatigue performance. JPCP-A1-AB structure costs 4% more than JPCP-A1 structure, while it shows 44% better fatigue performance. However, the impact of the asphalt layer in fatigue performance improvement decreases as the thickness of the slab increases. Even though placing a 2 inches asphalt layer increase the cost by less than 4%, JPCP-A2-AB, JPCP-A3-AB, and JPCP-A4-AB improve the fatigue performance by 23%, 16%, and 5%, respectively, compared to equivalent structures with granular base. Therefore, it can be concluded that placing a 2 inches asphalt layer under the JPCP slabs thinner than 12 inches is the

most cost-effective design alternative to resist truck platooning traffic. It should be noted that to select the cost-effective alternative, the life cycle cost analysis (LCCA) must be performed considering fatigue life and the cost of rehabilitation and maintenance measures.

Increasing the thickness of concrete slab in CRCP structures from 8 inches to 10 inches and 12 inches increase the cost of construction by 20% and 28% respectively, while they improve the fatigue performance by 66% and 89%. Comparing the cost of construction of CRCP with JPCP structures with similar slab thickness indicate that the CRCP structures provide over 70% better fatigue performance against truck platooning, and they cost less than JPCP structures. However, this cannot be true since CRCP structures are known as the most expensive pavement type. The reason for higher unit prices of JPCP structures in TxDOT average low unit price is the quantity of this pavement structure is significantly less than projects with CRCP structures. Regardless of the size of projects, contractors incur fixed costs in addition to the costs related to quantities. These fixed costs in smaller projects are divided into small quantities which increases the unit costs in small projects. Also, the location of the project and the availability of materials in that area are other factors that are taken into considerations during bidding. All of these factors affect the average unit bid prices which will be reflected in the cost estimate based on these values.

5.3. Estimating cost of construction based on cost of materials

Since the cost estimate based on average unit bid price highly depends on the total quantity of construction, it may not be a suitable approach for a cost analysis for this study. Therefore, to determine the optimal pavement design, the cost of materials was used to perform the cost analysis. Since all design alternatives have a similar base and subgrade layer, only the cost of materials on the surface layer was used for the sake of comparison. In addition, although the structures with trenches under the wheel path (JPCP-B and CRCP-B) require less base material, the deduction was

not performed to account for the extra effort and cost for cutting the trenches. The cost of materials used to perform cost analysis is tabulated in Table 5-4. The cost of concrete mix, granular base, and asphalt concrete mix was obtained by a query from local suppliers. Also, the cost of dowel baskets, tie bars, and rebars was provided by BoMetals inc., a concrete accessories manufacturer. It should be noted that the intent of this study is not to report the actual cost of materials but to use the cost of materials accurately enough to be able to select the cost-effective structure between the discussed design alternatives.

Table 5-4. Unit cost of concrete pavement materials.

Material	Unit	Unit cost ($)
Concrete mix class C	CY	125.00
Asphalt concrete mix type C	Ton	65.00
Dowel baskets consist of 11x1.25" dowels	LF	8.13
Dowel baskets consist of 11x1.5" dowels	LF	10.90
Customized dowel baskets consist of 5x1.25" dowels and 6x1.5” dowels*	LF	9.52
#5 tie bar - 30" long	EA	2.00
#5 tie bar - 40" long	EA	2.80
#5 rebar (20ft.)	EA	12.51
#6 rebar (20 ft.)	EA	29.89

** Price was calculated based on average cost of 1.25” and 1.5” dowel baskets.*

Based on the inputs provided in Table 5-4, the cost of material per lane-mile was computed for each design alternative and is shown in Table 5-5. Also, the fatigue performance of each alternative under truck platooning traffic was included in this table. As can be seen, the cost of concrete constitutes a large portion of the total cost, and the cost of dowel bars/tie bars has less influence on the overall cost. In addition, it is observed that, as expected, the cost of construction of CRCP structures is higher than that of JPCP structures.

Table 5-5. Total cost (per lane-mile) and fatigue performance of various design alternatives.

Pavement structure	Concrete cost ($/lane-mile)	Dowel basket /Rebar cost ($/lane-mile)	Tie bars cost ($/lane-mile)	Asphalt mix cost ($/lane-mile)	Total cost ($/lane-mile)	Damage index (Channelized traffic)
JPCP-A1	195,555.56	36,780.12	8,870.40	–	241,206.08	6.52E-06
JPCP-A2	244,444.44	36,780.12	8,870.40	–	290,094.96	1.13E-06
JPCP-A3	293,333.33	36,780.12	8,870.40	–	338,983.85	3.72E-07
JPCP-A4	366,666.67	36,780.12	8,870.40	–	412,317.19	1.10E-07
JPCP-B1	214,567.90	36,780.12	8,870.40	–	260,218.42	3.55E-06
JPCP-B2	244,444.44	36,780.12	8,870.40	–	290,094.96	6.63E-07
JPCP-C1	195,555.56	49,311.60	8,870.40	–	253,737.56	3.66E-06
JPCP-C2	244,444.44	49,311.60	8,870.40	–	302,626.44	9.02E-07
JPCP-D1	195,555.56	43,045.86	8,870.40	–	247,471.82	4.37E-06
JPCP-D2	244,444.44	43,045.86	8,870.40	–	296,360.70	1.06E-06
JPCP-A1-AB	195,555.56	36,780.12	8,870.40	52,408.89	293,614.96	3.63E-06
JPCP-A2-AB	244,444.44	36,780.12	8,870.40	52,408.89	342,503.85	8.73E-07
JPCP-A3-AB	293,333.33	36,780.12	8,870.40	52,408.89	391,392.74	3.14E-07
JPCP-A4-AB	366,666.67	36,780.12	8,870.40	52,408.89	464,726.08	1.05E-07
JPCP-C1-AB	195,555.56	49,311.60	8,870.40	52,408.89	306,146.44	2.36E-06
JPCP-C2-AB	244,444.44	49,311.60	8,870.40	52,408.89	355,035.33	7.18E-07
JPCP-D1-AB	195,555.56	43,045.86	8,870.40	52,408.89	299,880.70	2.66E-06
JPCP-D2-AB	244,444.44	43,045.86	8,870.40	52,408.89	348,769.59	8.69E-07
CRCP-A1	195,555.56	95,776.56	9,292.80	–	300,624.92	9.86E-07
CRCP-A2	244,444.44	95,776.56	9,292.80	–	349,513.80	3.41E-07
CRCP-A3	293,333.33	95,776.56	9,292.80	–	398,402.69	1.06E-07
CRCP-B1	214,567.90	95,776.56	9,292.80	–	319,637.26	5.85E-07
CRCP-B2	244,444.44	95,776.56	9,292.80	–	349,513.80	2.29E-07
CRCP-D1	195,555.56	150,836.40	9,292.80	–	355,684.76	9.31E-07
CRCP-D2	244,444.44	150,836.40	9,292.80	–	404,573.64	3.12E-07

Considering JPCP-A1 as a base design alternative, it is observed that increasing the thickness of JPCP slab from 8 inches to 10 inches, and 12 inches increase the cost of construction by 20% and 41%, while the fatigue performance improves by 83% and 94%. Even though the less costly alternative is more sensitive to changes in the cost of materials, it is observed that JPCP-A2 is the more efficient design of these two alternatives. JPCP-A4 improves the fatigue performance by 98%, but it is 71% costlier than JPCP-A1 structure. This structure is found to be the costliest design to improve the fatigue performance of the JPCP. In addition, JPCP-B1 and JPCP-B2 cost 8% and 20% more than JPCP-A1 and they improve the performance of pavement by 46% and 90%, respectively. Even though the cost of materials for JPCP-B2 and JPCP-A2 are the same, due to the better performance of slabs with uniform thickness under normal traffic with wander, JPCP-A2 is a better alternative. Increasing the size of dowel bars (JPCP-C1) increases the total cost by 5%, while it offers a 44% improvement in fatigue performance. The cost comparison between JPCP-C and JPCP-D slabs shows that using larger dowel bars only in the wheel path does not significantly reduce the cost of construction per lane-mile of pavement (2.5%), but it still improves the performance of JPCP by 33% against truck platooning. These findings are also can be expressed in terms of the fatigue life of these structures. Figure 5-1 represents the relative fatigue life of each design alternatives subjected to channelized traffic and their cost of construction. As can be seen, increasing the size of dowel bars located in the wheel path can improve the fatigue life by 50% with a 3% increase in the cost of construction.

Placing a 2-inch asphalt layer under the JPCP slab alone increases the cost of construction by 22%, while it improves the fatigue performance by 44%. In addition, it can be seen that instead of using asphalt layer under JPCP slabs, the slab thickness can be increased with a lower cost which is found to be 2 times more effective in improvement of fatigue performance than JPCP-

A1-AB. This result is in contrast with what is observed by the cost estimate performed using average unit bid prices. Comparison between JPCP structures with those with asphalt base does not show a significant change in fatigue performance.

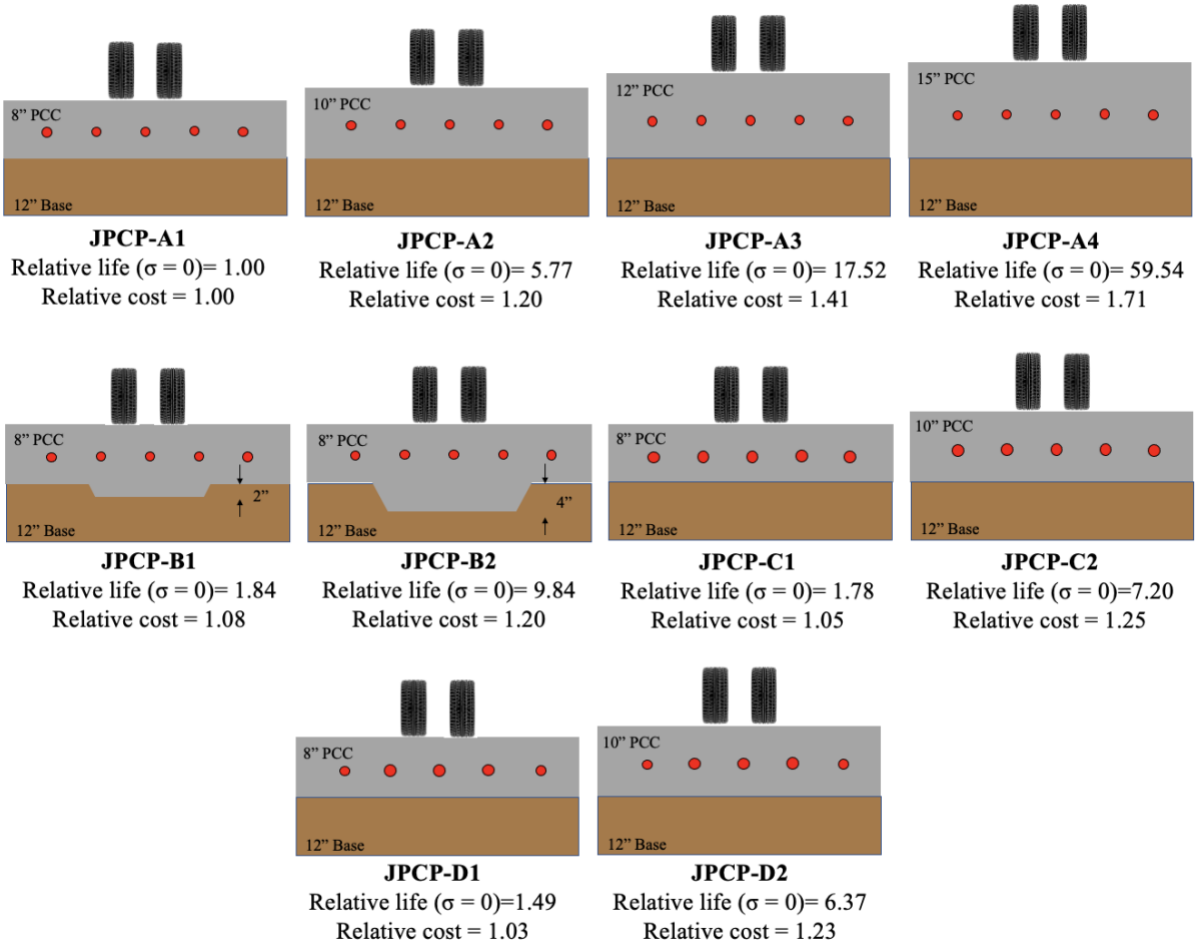

Figure 5-1. Comparing the relative cost of construction and fatigue life of JPCP structures with granular base under channelized traffic.

CRCP structures cost more than JPCP structures, but they show significantly better fatigue performance. Comparing CRCP-A1 and JPCP-A1 shows that CRCP-A1 costs 25% more, while it improves the fatigue performance by 85%. Increasing the thickness of the CRCP structure from 8 inches to 10 inches and 12 inches increases the cost of construction by 16% and 33%, while their fatigue performance is improved by 66% and 89%. CRCP-B1 costs 6% more than CRCP-A1, but

it yields a 41% improvement in fatigue performance which makes it an efficient design. However, since CRCP-B2 and CRCP-A2 require the same quantity of concrete mix, due to the better performance of CRCP-B2, it can be considered as a preferable design over CRCP-A2. Increasing the size of rebars in the wheel path in CRCP-C1 and CRCP-C2 increases the cost of construction by over 18%, while they offer less than 8% improvement in fatigue performance. Therefore, this alternative cannot be considered as a cost-effective measure to achieve higher fatigue performance under truck platooning. In addition, for better comparing these design alternatives, their cost of construction and relative life is presented in Figure 5-2. It can be seen that the cost of construction of CRCP-A3 and CRCP-C2 are almost the same, but CRCP-A3 provides 3 times longer fatigue life. In order to select the cost-effective alternative for improving the fatigue performance of concrete pavements, a life cycle cost analysis is required to consider the extended life offered by each alternative as well as rehabilitation and maintenance costs.

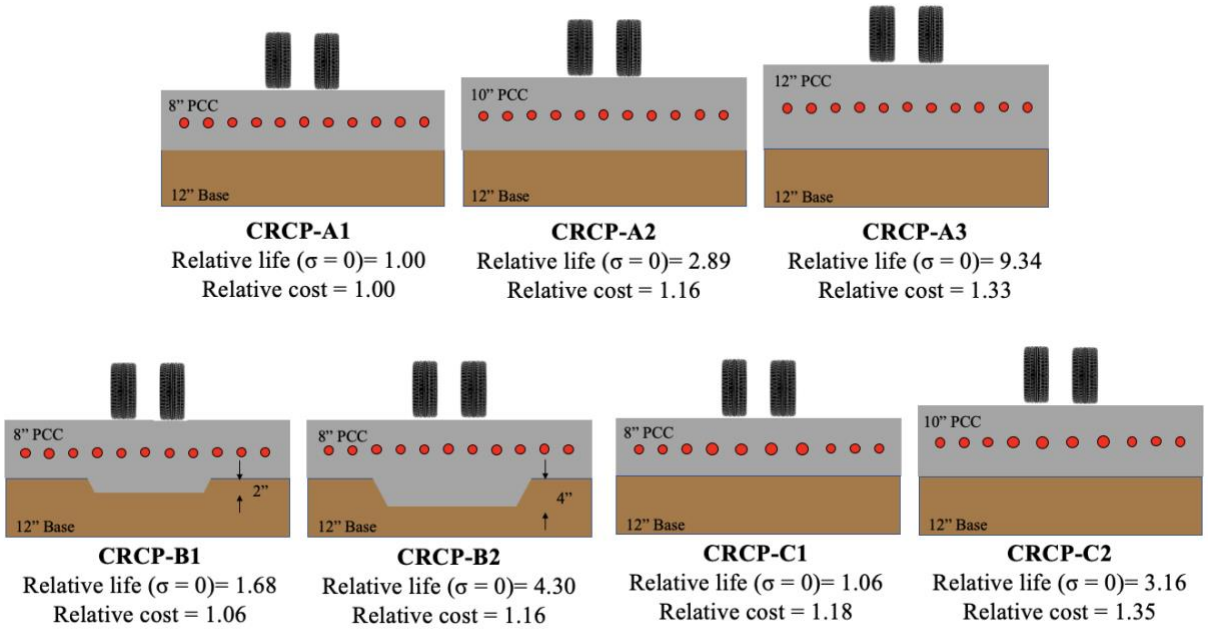

Figure 5-2. Comparing the relative cost of construction and fatigue life of CRCP structures under channelized traffic.

CHAPTER 6: CONCLUSIONS AND RECOMMENDATIONS

6.1. Summary and conclusions

In this study, the impacts of truck platooning on structural responses and performance of concrete pavements including JPCP and CRCP were studied. Three-dimensional finite element models were developed to examine various design alternatives in order to improve the fatigue performance of the concrete pavements. The critical stresses induced in each design alternative under different lateral positions of the load were recorded and evaluated. Based on the obtained results, the following conclusions can be drawn:

- Increasing the thickness of the slab has a significant impact on reducing the induced tensile stresses at the bottom of PCC slabs in JPCP and CRCP structures subjected to channelized traffic from truck platooning.
- The longitudinal stress induced at the bottom of the PCC slab in JPCP and CRCP structures can be reduced by thickening the slab under the wheel path of truck platooning. However, because of stress concentration at the top edge of the trench, to increase the thickness by 2 inches and 4 inches, respectively, a minimum bottom width of 26 inches and 32 inches for trenches are required to avoid bottom-up cracking from the edge of the thickened part of the slab.
- In JPCP structures, increasing the size of dowel bars slightly decreases the induced stresses. However, the impact of the size of dowel bars in longitudinal stress reduction decreases with thicker slabs. This is because thicker slabs are more resistant against bending, so fewer loads need to be transferred through dowel bars into the adjacent slabs.
- Replacing all dowel bars with one size larger showed a 2% reduction in maximum longitudinal stress in JPCP structures compared to replacing dowels only located in the

wheel path of the channelized traffic. Therefore, increasing the size of dowel bars located outside the wheel path of channelized traffic has a minor effect on stress reduction at the bottom of the slab.

- Replacing #5 rebars embedded under wheel path with #6 rebars has a minimal effect (less than 2%) on the reduction of longitudinal stresses in the CRCP pavement structure subjected to truck platooning.
- The lateral position of the load significantly changes the induced stresses at the bottom of the slab in JPCP and CRCP structures. The longitudinal stress increases by wheel wander of the vehicle, and the maximum longitudinal stress at the bottom of the slab is created when the axle wheels run over the edge of the slab.
- In structures with partially thickened slabs, a significant increase in longitudinal stress was observed when wheel loads are located outside the thickened part of the slab. However, both JPCP and CRCP structures experience an increase followed by a decrease in transverse stress when the load is shifted toward the edge of the slab. This is due to the presence of tie bars at the longitudinal joints of the slabs. Also, in structures with partially thickened slabs, the maximum transverse stress occurs when the load is located at the edge of the thickened portion of the slab which intensifies the stress concentration at this point.

Fatigue damage calculations were carried out to determine the effectiveness of each design consideration on improving the service life of concrete pavements under truck platooning. The results showed that:

- The Tepfers fatigue model computes the lowest allowable load repetitions in comparison to Darter and MEPDG fatigue models and reflects less changes in the life of pavements by

changing the pavement structure. In addition, it was found that MEPDG fatigue model provides an unrealistic result for the studied pavement structures.

- The fatigue analysis performed with the Tepfers model shows that increasing the thickness of PCC slabs is the most effective method in improving the performance of pavement under truck platooning; a 2.0 inch increase in the thickness of the concrete layer enhances the life of JPCP and CRCP by 5.77 and 2.89 times, respectively. However, thickening the dowel bars in JPCP and the rebars in CRCP located in the wheel paths have the lowest impact on the improvement of fatigue performance among all design alternatives leading to only 49% and 6% life improvement respectively. These relative improvements are considerably dependent on the fatigue model used, so different levels of improvements will be achieved if other fatigue models are used.
- Placing an asphalt layer under the JPCP increases the life of the pavement by up to 80%. However, as the thickness of the PCC slab increases the impact of this measure decreases as such an improvement for 15.0 inch thick slab is only 4%.

To compute the accumulated fatigue damage under traffics with different levels of wheel wander, a matrix multiplication method was developed. The comparison of fatigue performance of different design considerations under truck platooning and under normal traffic with wheel wander revealed that:

- In all design alternatives except structures with partially thickened slabs, the maximum accumulated fatigue damage occurs under the wheels of the vehicle running at the center of the lane regardless of the level of wheel wander.
- Increasing the standard deviation of wheel wander from 0.0 to 10.0 inches decreases the maximum accumulated fatigue damage in the pavement structures up to 25% and increases

the fatigue damage at the edge of the slab by 4.3 times. Therefore, the lack of wheel wander in truck platooning traffic reduces the fatigue life of the pavement structures.

- In pavement structures with partially thickened slabs, the accumulated fatigue damage at the bottom of thickened part of the slab decreases by increasing the standard deviation of wheel wander. However, when the standard deviation of the wheel wander increases to 8.0 inches or more, the maximum accumulated fatigue damage occurs at the top edge of the trench. Therefore, even though providing the trench decrease the accumulated fatigue damage for channelized traffic, the maximum accumulated fatigue damage occurs at the top edge of the trench under the normal traffic with wheel wander, which has a standard deviation of 10.0 inches.
- Increasing the thickness of the PCC slab reduces the difference between the maximum accumulated fatigue damage created by truck platooning and traffic with normal wander. Thus, the negative impact of channelized traffic on fatigue performance of concrete pavements reduces as the thickness of the slab increases.
- In partially thickened slabs the maximum accumulated fatigue damage under normal traffic occurs at the top edge of the trench. However, it still shows improvement in fatigue performance under both truck platooning and normal traffic.
- The thickening of dowel bars in JPCP structures has a similar impact on the reduction of the maximum accumulated fatigue damage induced by channelized traffic and normal traffic. However, it was observed that the thickening of dowel bars outside of the wheel path of truck platooning improves the fatigue performance of JPCP structures under truck platooning by only 10% compared to the fatigue performance of the structures with thickened dowel bars placed only in the wheel path.

- Placing an asphalt base in JPCP structure improves the fatigue performance by decreasing the magnitudes of stresses, but it does not provide a considerable change in the effectiveness of design considerations under truck platooning and normal traffic.
- The cost analysis performed using the cost of materials indicated that increasing the thickness of the slab is the most expensive measure. However, increasing the thickness of the JPCP slab by 2.0 inches is a cost-effective measure as it improves the performance under truck platooning by 83% while the cost of construction increases only by 20%.
- Thickening the dowel bars was found to be the optimal measure to improve the fatigue performance of JPCP structures. This measure improves the performance of JPCP by 44%, while it increases the cost of construction by only 5%. Thickening only the dowel bars located in the wheel path reduces the cost of construction by only 2.5% in comparison to the cost of replacing all dowel bars at the joint. However, a life cycle cost analysis is required for selecting the optimum alternative.
- Providing 2.0 inches asphalt layer under the JPCP slabs costs as much as increasing the thickness of the PCC slab, while increasing the slab thickness is twice more effective in improvement of fatigue performance. However, using an asphalt layer reduces the potential of faulting.
- The cost of construction of CRCP is 25% higher than that of JPCP structures, while it shows 85% better fatigue performance against truck platooning. Thickening the rebars under the wheel path showed an 8% improvement in fatigue performance and an 18% increase in the cost of construction. Increasing the thickness of the slab under the wheel path by 2.0 inches can be selected as an efficient measure since a 41% improvement in the fatigue performance can be achieved only by a 6% increase in the cost of construction.

6.2. Recommendations

The following recommendations are derived from this research:

- The study presented in this dissertation is based on the results of analyses performed through finite element models. However, this study should be complemented by field data obtained from instrumented concrete pavements under real tuck traffic or Accelerated Pavement Testing (APT) loading.
- An additional study is required to investigate the impact of truck platooning and wheel wander on the performance of concrete pavements subjected to the combined effects of moving loads, temperature gradient, and moisture variations.
- The results of this study showed that the fatigue models have a big impact on the predicted performance of concrete pavement structures. Thus, further studies are required to validate the model used or to develop new ones for a wide variety of concrete pavement structures.
- The life cycle cost analysis (LCCA) should include in addition to the evaluation of construction costs, the estimation of maintenance and rehabilitation costs for all design alternatives.

REFERENCES

ABAQUS Standard User's Manual (2014). version 6.14-3. Hibbit, Karlsson and Sorenson Inc., Providence, RI.

Aguirre, N. (2020). RPAS: An Enhanced Finite Element Code for the Mechanistic Analysis of Rigid Pavements (Doctoral dissertation, The University of Texas at El Paso).

Al Alam, A., Gattami, A., & Johansson, K. H. (2010, September). An experimental study on the fuel reduction potential of heavy duty vehicle platooning. In 13th International IEEE Conference on Intelligent Transportation Systems (pp. 306-311). IEEE.

Al-Qadi, I. L., & Elseifi, M. A. (2006). Mechanism and modeling of transverse cracking development in continuously reinforced concrete pavement. International Journal of Pavement Engineering, 7(4), 341-349.

Al-Qadi, I. L., Okte, E., Ramakrishnan, A., Zhou, Q., & Sayeh, W. (2021). Truck Platooning on Flexible Pavements in Illinois. Illinois Center for Transportation/Illinois Department of Transportation.

Alam, A., Besselink, B., Turri, V., Mårtensson, J., & Johansson, K. H. (2015). Heavy-duty vehicle platooning for sustainable freight transportation: A cooperative method to enhance safety and efficiency. IEEE Control Systems Magazine, 35(6), 34-56.

Aljhayyish, A. K. (2019). Optimizing Slab Thickness and Joint Spacing for Long-Life Concrete Pavement in Ohio (Doctoral dissertation, Ohio University).

American Association of State Highway and Transportation Officials. (2008). Mechanistic-Empirical Pavement Design Guide, Interim Edition: A Manual of Practice, AASHTO, Washington, D.C.

American Association of State Highway and Transportation Officials (AASHTO). (1993). AASHTO Guide for Design of Pavement Structures, 1993 (Vol. 1). AASHTO, Washington, DC.

American Concrete Pavement Association (ACPA). (2009, June). Concrete Pavement Fundamentals. Retrieved from: http://www.pavement.com/Concrete_Pavement/Technical/Fundamentals/index.asp.

American Transportation Research Institute (ATRI). (2020). Critical Issues in The Trucking Industry. Retrieved from: https://truckingresearch.org/2020/10/27/critical-issues-in-the-trucking-industry-2020/

American Trucking Association (ATA). (2019). Truck Driver Shortage Analysis 2019. Retrieved from: https://www.trucking.org/news-insights/ata-releases-updated-driver-shortage-report-and-forecast

Ashley, S. (2013). Truck platoon demo reveals 15% bump in fuel economy. SAE International.

Blab, R., & Litzka, J. (1995). Measurements of the lateral distribution of heavy vehicles and its effects on the design of road pavements. In Proceedings of the International Symposium on Heavy Vehicle Weights and Dimensions, Road Transport Technology, University of Michigan (pp. 389-395).

Buiter, R., Cortenraad, W. M. H., Van Eck, A. C., & Van Rij, H. (1989). Effects of transverse distribution of heavy vehicles on thickness design of full-depth asphalt pavements. Transportation Research Record, (1227).

Cambridge Systematics Inc. (2017). San Joaquin Valley I-5/SR 99 Goods Movement Study-Demonstration Project: Truck Platooning. Technical Memorandum for Strategic Programs and Their Feasibility Assessment.

Channakeshava, C., Barzegar, F., & Voyiadjis, G. Z. (1993). Nonlinear FE analysis of plain concrete pavements with doweled joints. Journal of Transportation Engineering, 119(5), 763-781.

Chatti, K., Lysmer, J., & Monismith, C. L. (1994). Dynamic finite-element analysis of jointed concrete pavements. Transportation Research Record, (1449). 79-90.

Chatti, K., Manik, A., Salama, H., Haider, S. W., Brake, N., Mohtar, C. E. (2009). Effect of Michigan multi-axle trucks on pavement distress: Volume I–Rigid pavements (No. RC-1504).

Chou, Y. T. (1984). Stress analysis of small concrete slabs on grade. Journal of transportation engineering, 110(5), 481-492.

Darter, M. I., and Barenberg, E.J. (1977). Design of a Zero-maintenance Plain Jointed Concrete Pavement, Volume One-Development of Design Procedures, Report No. FHWA-RD-77-111, Report for the Federal Highway Administration, University of Illinois, Urbana, IL, June 1977.

Davids, W. G., Turkiyyah, G. M., & Mahoney, J. P. (1998). EverFE: Rigid pavement three-dimensional finite element analysis tool. Transportation Research Record, 1629(1), 41-49.

Dávila, A., & Nombela, M. (2011). Sartre-safe road trains for the environment reducing fuel consumption through lower aerodynamic drag coefficient (No. 2011-36-0060). SAE Technical Paper.

Delatte, N. J. (2014). Concrete pavement design, construction, and performance. CRC Press.

Dere, Y., Asgari, A., Sotelino, E. D., & Archer, G. C. (2006). Failure prediction of skewed jointed plain concrete pavements using 3D FE analysis. Engineering Failure Analysis, 13(6), 898-913.

El Bouchihati, M. (2020). The impact of Truck Platooning on the pavement structure of Dutch Motorways.: The link between truck platooning and road surface wear. (Master thesis, Delft University of Technology).

Erlingsson, S., Said, S., & McGarvey, T. (2012, September). Influence of heavy traffic lateral wander on pavement deterioration. In Proceedings of the 4th European Pavement Asset Management Conference, Malmö, Sweden.

European Automobile Manufacturers' Association (ACEA). (2016, March 10). What is truck platooning?, Retrieved from: https://www.acea.be/news/article/what-is-truck-platooning.

Federal Motor Carrier Safety Administration (FMCSA). (2018). Large Truck and Bus Crash Facts 2018. Retrieved from: https://www.fmcsa.dot.gov/safety/data-and-statistics/large-truck-and-bus-crash-facts-2018

Federal Motor Carrier Safety Administration. (2002). Second Draft for Crash Event Assessment Form. (pg. 32).

Friberg, B. F. (1940). Design of dowels in transverse joints of concrete pavements. Transactions of the American Society of Civil Engineers, 105(1), 1076-1095.

Gillespie, T.D., Karamihas, S.M., Cebon, D., Sayers, M.W., Nasim, M.A., Hansen, W, and N. Ehsan. (1993). Effects of Heavy Vehicle Characteristics on Pavement Response and Performance, National Cooperative Highway Research Program Report 353, Transportation Research Board, National Research Council, Washington, DC.

Greer, L., Fraser, J. L., Hicks, D., Mercer, M., & Thompson, K. (2018). Intelligent transportation systems benefits, costs, and lessons learned: 2018 update report (No. FHWA-JPO-18-641). United States. Dept. of Transportation. ITS Joint Program Office.

Gungor, O. E., & Al-Qadi, I. L. (2020). All for one: Centralized optimization of truck platoons to improve roadway infrastructure sustainability. Transportation Research Part C: Emerging Technologies, 114, 84-98.

Ha, S., Yeon, J., Choi, B., Jung, Y., Zollinger, D. G., Wimsatt, A., & Won, M. C. (2011). Develop mechanistic-empirical design for CRCP (No. FHWA/TX-11-0-5832-1).

Hammons, M. I., (1997). Development of an Analysis System for Discontinuities in Rigid Airfield Pavements, Final Report No.GL-97-3, U.S. Army Corps of Engineers, Waterways Experiment Station, Vicksburgh, MS 39180-6199.

Hiller, J. E. (2007). Development of Mechanistic-Empirical Principles for Jointed Plain Concrete Pavement Fatigue Design, University of Illinois - Urbana Champaign.

Hiller, J.E., and Roesler J.R. (2002). Transverse Joint Analysis for Use in Mechanistic-Empirical Design of Rigid Pavements", Transportation Research Record 1809, TRB, National Research Council, Washington, D.C., pp. 42-51.

Huang, Y. H. (2003). Pavement Analysis and Design, 2nd edition, Prentice Hall, Upper Saddle River, New Jersey.

Huang, Y. H., & Wang, S. T. (1973). Finite-element analysis of concrete slabs and its implications for rigid pavement design. Highway Research Record, (466).

Ioannides, A. M., & Donnelly, J. P. (1988). Three-dimensional analysis of slab on stress-dependent foundation. Transportation Research Board (No. 1196).

Ioannides, A.M. (1984). Analysis of Slabs on Grade for a Variety of Loading and Support Conditions. Ph.D. Thesis. University of Illinois at Urbana-Champaign, Urbana, Illinois.

Janssen R., H. Z. (2015). Truck Platooning Driving the Future of Transportation - TNO whitepaper.

Kelleher, K., & Larson, R. M. (1989). The design of plain doweled jointed concrete pavement. In International Conference on Concrete Pavement Design and Rehabilitation, 4th, 1989, West Lafayette, USA.

Kennedy, J. C., R. D. Everhart, T. P. Forte, and J. A. Hadden, 1994. Development of a Governing Primary Response Model (GPRM) for Airport Pavement Design and Analysis: Volume I, Battelle and Resource International Institute, Columbus, Ohio 43201-2693, Final Report, Contract No. VA 2043, DTRS-57-89-D-00006.

Khazanovich, L., & Ioannides, A. M. (1993, December). Finite element analysis of slabs-on-grade using higher order subgrade soil models. In Proceedings of the Conference on Airport Pavement Innovations (pp. 16-30). Publ by ASCE.

Khazanovich, L., Buch, N., & Gotlif, A. (2001). Evaluation of alignment tolerances for dowel bars and their effects on joint performance (No. RC-1395). Michigan State University, Pavement Research Center of Excellence.

Khazanovich, L., Hoegh, K., & Snyder, M. B. (2009). Guidelines for dowel alignment in concrete pavements (Vol. 637). Washington, DC, USA: Transportation Research Board.

Khazanovich, L., Yu, H. T., Rao, S., Galasova, K., Shats, E., & Jones, R. (2000). ISLAB2000-Finite element analysis program for rigid and composite pavements. User's Guide. Champaign, IL: ERES Consultants.

Kim, K., Chun, S., Han, S., & Tia, M. (2018). Effect of dowel bar arrangements on performance of jointed plain concrete pavement (JPCP). International Journal of Concrete Structures and Materials, 12(1), 1-11.

Kim, K., Han, S., Tia, M., & Greene, J. (2018). Optimization of Parameters to Minimize Horizontal Cracking in Continuously Reinforced Concrete Pavement (CRCP) Using Finite Element Analysis (No. 18-00263).

Kim, S. M., Cho, Y. K., & Lee, J. H. (2020). Advanced reinforced concrete pavement: Concept and design. Construction and Building Materials, 231, 117130.

Kim, S. M., Won, M. C., & McCullough, B. F. (1997). Development of a finite element program for continuously reinforced concrete pavements (No. FHWA/TX-98/1758-S,).

Kim, S. M., Won, M., & Frank McCullough, B. (1998). Numerical modeling of continuously reinforced concrete pavement subjected to environmental loads. Transportation Research Record, 1629(1), 76-89.

Kim, S. M., Won, M. C., & Frank McCullough, B. (2000). Three-dimensional analysis of continuously reinforced concrete pavements. Transportation Research Record, 1730(1), 43-52.

Kim, S. M., Won, M., McCullough, B. F., & River, R. (2001). CRCP-10 computer program user's guide (No. FHWA/TX-0-1831-4,). Center for Transportation Research, Bureau of Engineering Research, The University of Texas at Austin.

Kong, D., Guo, X., Yang, B., & Wu, D. (2016). Analyzing the impact of trucks on traffic flow based on an improved cellular automaton model. Discrete dynamics in nature and society.

Korovesis, G. T. (1990). Analysis of slab-on-grade pavement systems subjected to wheel and temperature loadings (Doctoral dissertation, University of Illinois at Urbana-Champaign).

Kuhn, B., Lukuc, M., Poorsartep, M., Wagner, J., Balke, K. N., Middleton, D., ... & Moran, M. (2017). Commercial truck platooning demonstration in Texas–level 2 automation (No. FHWA/TX-17/0-6836-1). Texas. Dept. of Transportation. Research and Technology Implementation Office.

Lammert, M. P., Duran, A., Diez, J., Burton, K., & Nicholson, A. (2014). Effect of platooning on fuel consumption of class 8 vehicles over a range of speeds, following distances, and mass. SAE International Journal of Commercial Vehicles, 7(2014-01-2438), 626-639.

Lee, X., Brill D. R., and Guo. E. H. (1998). “Advances in Finite Element Models for Airport Pavement Design,” Proceedings of the First National Symposium on 3D Finite Element Modeling for Pavement Analysis and Design, Charleston, West Virginia, pp. 112-127.

Lennie, S. C., & Bunker, J. M. (2003). Evaluation of lateral position for multi-combination vehicles, Proceedings of the Queensland Main Roads Road System and Engineering Technology Forum, Bardon, Brisbane.

Luo, W., & Wang, K. C. (2013). Wheel path wandering based on field data. In Airfield and Highway Pavement 2013: Sustainable and Efficient Pavements (pp. 506-515).

Mackiewicz, P. (2015). Finite-element analysis of stress concentration around dowel bars in jointed plain concrete pavement. Journal of Transportation Engineering, 141(6), 06015001.

Maitra, S. R., Reddy, K. S., & Ramachandra, L. S. (2009). Load transfer characteristics of dowel bar system in jointed concrete pavement. Journal of Transportation Engineering, 135(11), 813-821.

Mallick, R. B., & El-Korchi, T. (2013). Pavement engineering: principles and practice. CRC Press.

Masad, E., Taha, R., & Muhunthan, B. (1996). Finite-element analysis of temperature effects on plain-jointed concrete pavements. Journal of Transportation Engineering, 122(5), 388-398.

McAuliffe, B., Croken, M., Ahmadi-Baloutaki, M., & Raeesi, A. (2017). Fuel-economy testing of a three-vehicle truck platooning system.

McCracken, J. K. (2008). Seasonal analysis of the response of jointed plain concrete pavements to FWD and truck loads (Doctoral dissertation, University of Pittsburgh).

McCullough, B. F., Adou-Ayyash, A., Hudson, W. R., & Randall, J. P. (1976). Design of continuously reinforced concrete pavements for highways. NCHRP Research Results Digest, (82).

MEPDG. (2004). Guide for Mechanistic-Empirical Design of New and Rehabilitated Pavement Structures.” National Cooperative Highway Research Program (NCHRP).

Monismith, C. L., Deacon, J. A., & Harvey, J. T. W. (2000). Performance Models for Permanent Deformation and Fatigue [R]. Berkeley: Pavement Research Center, University of California.

NCHRP. (2003). National Cooperative Highway Research Program. Guide for Mechanistic-Empirical Design of New and Rehabilitated Pavement Structures. Final Report, Champaign, Illinois.

Neubauer, M., Schauer, O., & Schildorfer, W. (2019, July). A Scenario-Based Investigation of Truck Platooning Acceptance. In International Conference on Applied Human Factors and Ergonomics (pp. 453-461). Springer, Cham.

Noorvand, H., Karnati, G., & Underwood, B. S. (2017). Autonomous vehicles: assessment of the implications of truck positioning on flexible pavement performance and design. Transportation Research Record, 2640(1), 21-28.

Nowakowski, C., Shladover, S. E., Lu, X. Y., Thompson, D., & Kailas, A. (2015). Cooperative adaptive cruise control (CACC) for truck platooning: Operational concept alternatives.

Packard, R. G., & Tayabji, S. D. (1983). Mechanistic design of concrete pavements to control joint faulting and subbase erosion. Portland Cement Association.

Pandazis, J. C., & Winder, A. (2015). Study of Intelligent Transport Systems for reducing CO2 emissions for passenger cars. Eur. Road Transp. Telemat. Implement. Coord. Organ, 1, 49.

Patten, J., McAuliffe, B. R., Mayda, W. & Tanguay, B. (2012). Review of Aerodynamic Drag Reduction Devices for Heavy Trucks and Buses. Report No. CSTT-HVC-TR-205, National Research Council Canada.

Peloton. (2019). PlatoonPro Truck Platooning. Connected - Grounded in Safety - Properly Tested.

Pickett, G. and G. Ray, “Influence Charts for Rigid Pavements”, Transactions, American Society of Civil Engineers (ASCE), Vol. 116, pp. 49-73, 1951.

Roesler, J. R. (1998). Fatigue of concrete beams and slabs. Ph. D. Dissertation, University of Illinois, Urbana, IL.

Roesler, J. R., Hiller, J. E., & Brand, A. S. (2016). Continuously Reinforced Concrete Pavement Manual, Guidelines for Design, Construction, Maintenance, and Rehabilitation (No. FHWA-HIF-16-026). United States. Federal Highway Administration.

Sadeghi, V., & Hesami, S. (2018). Investigation of load transfer efficiency in jointed plain concrete pavements (JPCP) using FEM. International Journal of Pavement Research and Technology, 11(3), 245-252.

Salsilli, R. A., Barenberg E. J. and Darter M. I. (1993). Calibrated Mechanistic Design Procedure to Prevent Transverse Cracking of Jointed Plain Concrete Pavements. Proceedings of the fifth International Conference on Concrete Pavement Design and Rehabilitation, Purdue University. West LaFayette, IN, pp. 71-90.

Sargand, S. M. and Beegle D. I. (1998). Three-Dimensional Finite-Element Software Development and Verification Case Study. Proceedings of the First National Symposium on 3D Finite Element Modeling for Pavement Analysis and Design, Charleston, West Virginia.

Sargand, S. M., & Abdalla, B. (2006). Truck/pavement/economic modeling and in-situ field test data analysis applications: Verification and validation of finite element models for rigid

pavement using in-situ data – Selection of joint spacing. Ohio Research Institute for Transportation and the Environment.

Shladover, S. E., Lu, X. Y., Yang, S., Ramezani, H., Spring, J., Nowakowski, C., David Nelson, Deborah Thompson, Aravind Kailas, Brian McAuliffe & Glover, K. D. (2019). Partial Automation for Truck Platooning (No. FHWA-HRT-19-028). Federal Highway Administration. Office of Research, Development, and Technology.

Shladover, S., Lu, X. Y., Yang, S., Ramezani, H., Spring, J., Nowakowski, C., & Nelson, D. (2018). Cooperative adaptive cruise control (CACC) for partially automated truck platooning (No. CA18-2623). California. Dept. of Transportation. Division of Research and Innovation.

Shoukry, S. N., & William, G. W. (1999). Performance evaluation of backcalculation algorithms through three-dimensional finite-element modeling of pavement structures. Transportation Research Record, 1655(1), 152-160.

Shoukry, S. N., Fahmy, M., Prucz, J., & William, G. (2007). Validation of 3DFE analysis of rigid pavement dynamic response to moving traffic and nonlinear temperature gradient effects. International Journal of Geomechanics, 7(1), 16-24.

Stempihar, J. J., Williams, R. C., & Drummer, T. D. (2005). Quantifying the lateral displacement of trucks for use in pavement design. Transportation Research Board Preprint, Washington, DC.

Suh, Y. C., Hankins, K., & McCullough, B. F. (1992). Early-age behavior of continuously reinforced concrete pavement and calibration of the failure prediction model in the CRCP-7 program (No. FHWA/TX-92+ 1244-3).

Tabatabaie, A. M., & Barenberg, E. J. (1978). Finite-element analysis of jointed or cracked concrete pavements. Transportation Research Record, (671).

Tadakuma, K., Doi, T., Shida, M., & Maeda, K. (2016). Prediction formula of aerodynamic drag reduction in multiple-vehicle platooning based on wake analysis and on-road experiments. SAE International Journal of Passenger Cars-Mechanical Systems, 9(2016-01-1596), 645-656.

Tawari, A., Sivaraman, S., Trivedi, M. M., Shannon, T., & Tippelhofer, M. (2014, June). Looking-in and looking-out vision for urban intelligent assistance: Estimation of driver attentive state and dynamic surround for safe merging and braking. In 2014 IEEE Intelligent Vehicles Symposium Proceedings (pp. 115-120). IEEE.

Tayabji, S. D., & Colley, B. E. (1986). Analysis of jointed concrete pavements. FHWA/RD-86-041.

Tepfers, R., & Kutti, T. (1979, May). Fatigue strength of plain, ordinary, and lightweight concrete. In Journal Proceedings (Vol. 76, No. 5, pp. 635-652).

Tia, M., Armaghani, J. M., Wu, C. L., Lei, S., & Toye, K. L. (1987). FEACONS III computer program for analysis of jointed concrete pavements. Transportation Research Record, (1136).

Timm, D. H., & Barrett, W. (2005). Analysis of the 2002 design guide for rigid pavement (No. ALDOT Project 930-554). Auburn University. Highway Research Center.

Timm, D. H., & Priest, A. L. (2005). Wheel wander at the NCAT test track (No. 05-02, p. 28). Report.

Tsugawa, S., Jeschke, S., & Shladover, S. E. (2016). A review of truck platooning projects for energy savings. IEEE Transactions on Intelligent Vehicles, 1(1), 68-77.

U.S. Department of Transportation (U.S. DOT). (2020). National Freight Strategic Plan. Retrieved from: https://www.transportation.gov/freight/NFSP

Uddin, W., Hackett, R. M., Joseph, A., Pan, Z., & Crawley, A. B. (1995). Three-dimensional finite-element analysis of jointed concrete pavement with discontinuities. Transportation Research Record, 1482, 26-32.

Vesic, A. S., & Saxena, S. K. (1968). Analysis of structural behavior of road test rigid pavements. Duke University, School of Engineering.

Vissers, J., Banspach, J., Liga, V., Tang, T., Nordin, H., Julien, S., Martinez, S. & Villette, C. (2018). V1 Platooning use-cases, scenario definition and Platooning Levels. D2.2 of H2020 project ENSEMBLE (platooningensemble.eu).

Vohra, V., Wahba, M., Akarslan, G., Ni, R., & Brennan, S. (2018, August). An examination of vehicle spacing to reduce aerodynamic drag in truck platoons. In 2018 IEEE Vehicle Power and Propulsion Conference (VPPC) (pp. 1-6). IEEE.

Westergaard, H. M. (1926). Stresses in concrete pavements computed by theoretical analysis. Public roads.

William, G. W. (2003). Effect of temperature variations on premature cracking of dowel jointed concrete pavements.

William, G. W., & Shoukry, S. N. (2001). 3D finite element analysis of temperature-induced stresses in dowel jointed concrete pavements. International Journal of Geomechanics, 1(3), 291-307.

Won, M. C. (1989). Mechanistic analysis of continuously reinforced concrete pavement considering material characteristics, variability, and fatigue (Doctoral dissertation, The University of Texas at Austin).

Won, M., Hankins, K., & McCullough, B. F. (1991). Mechanistic analysis of continuously reinforced concrete pavements considering material characteristics, variability, and fatigue.

Wu, R., & Harvey, J. T. (2008, February). Evaluation of the effect of wander on rutting performance in HVS tests. In Proceedings of the 3rd international conference on accelerated pavement testing.

Zaghloul, S. M., & White, T. D. (1994). Guidelines for Permitting Overloads; Part 1: Effect of Overloaded Vehicles on the Indiana Highway Network.

Zaghloul, S. M., White, T. D., & Kuczek, T. (1994). Evaluation of heavy load damage effect on concrete pavements using three-dimensional, nonlinear dynamic analysis. Transportation Research Record, (1449).

Zhou, F., Hu, S., Chrysler, S. T., Kim, Y., Damnjanovic, I., Talebpour, A., & Espejo, A. (2019). Optimization of lateral wandering of automated vehicles to reduce hydroplaning potential and to improve pavement life. Transportation research record, 2673(11), 81-89.

Zhou, F., Hu, S., Xue, W., & Flintsch, G. (2019). Optimizing the lateral wandering of automated vehicles to improve roadway safety and pavement life.

APPENDIX A: IMPACT OF WHEEL WANDER ON JPCP STRUCTURES WITH ASPHALT BASE

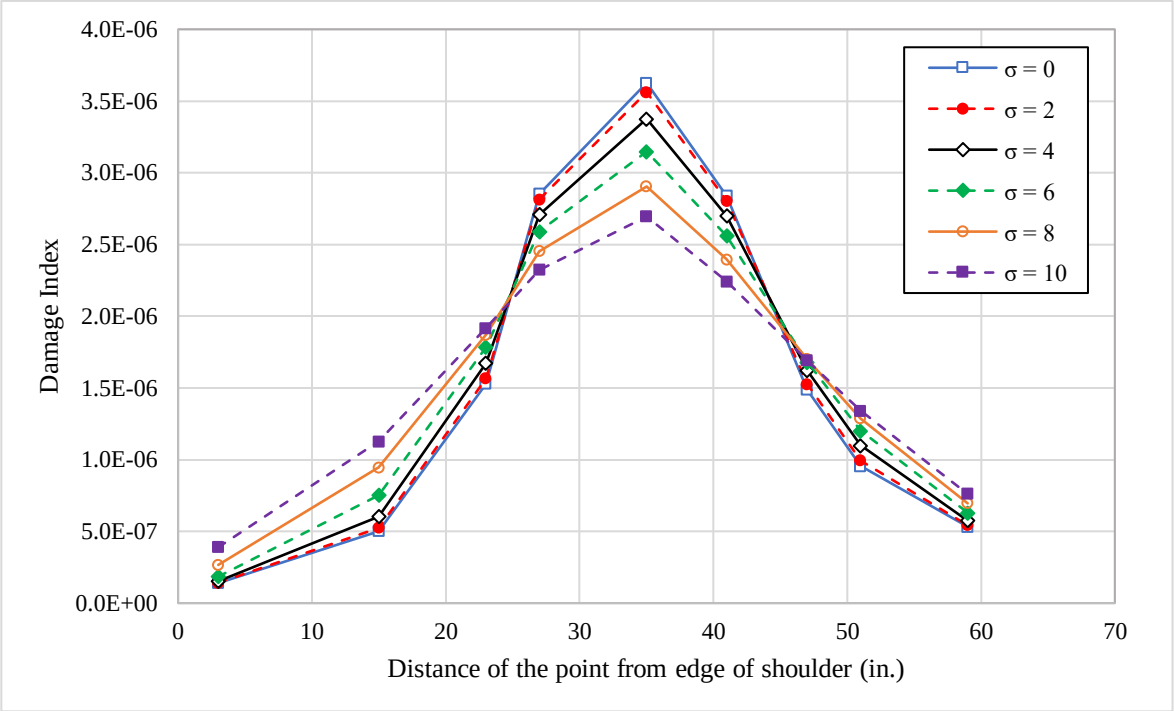

Figure A1. Impact of standard deviation on the fatigue damage for JPCP-A1-AB.

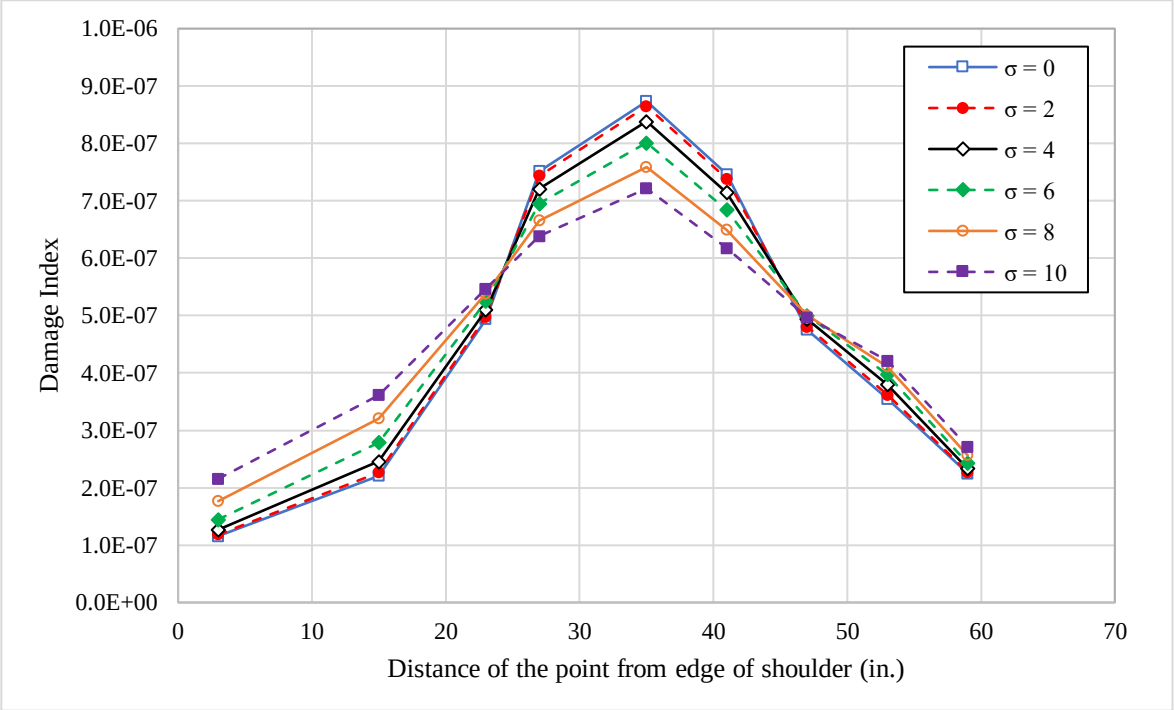

Figure A2. Impact of standard deviation on the fatigue damage for JPCP-A2-AB.

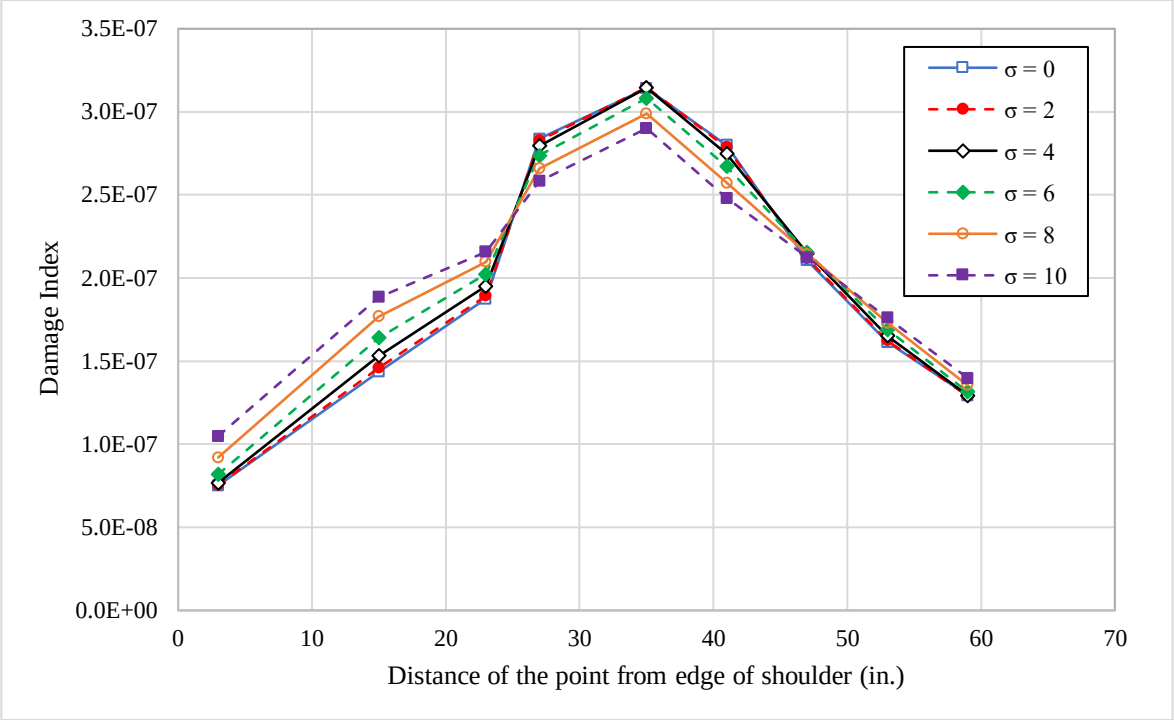

Figure A3. Impact of standard deviation on the fatigue damage for JPCP-A3-AB.

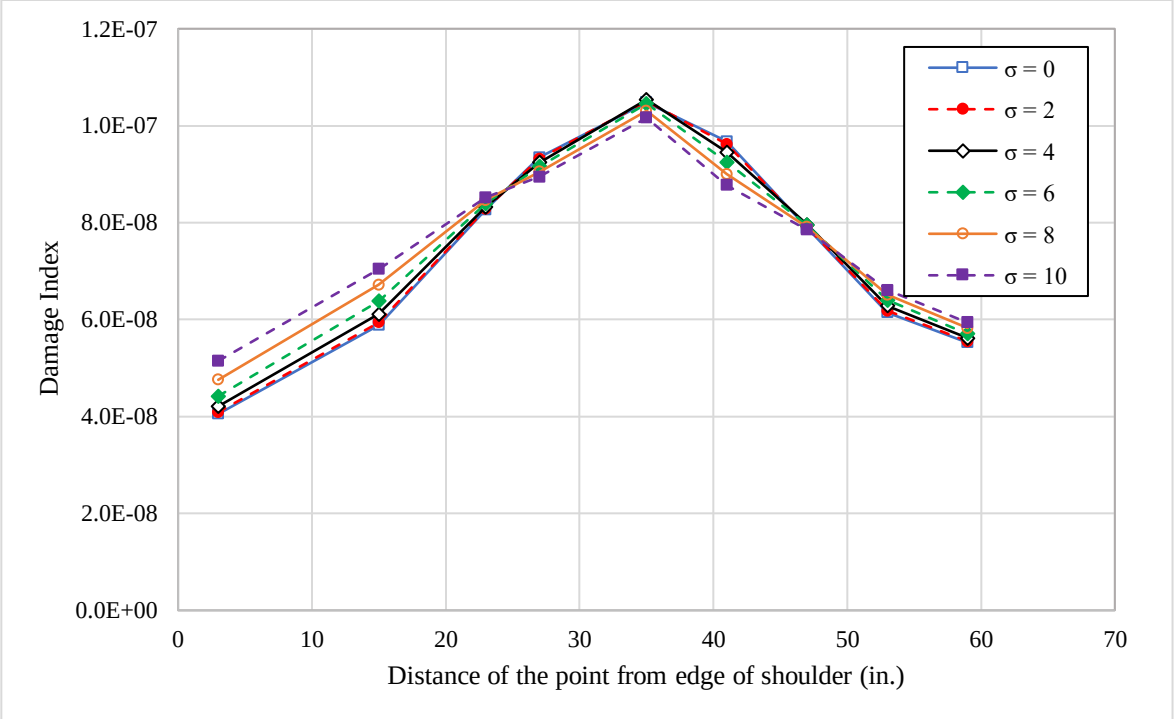

Figure A4. Impact of standard deviation on the fatigue damage for JPCP-A4-AB.

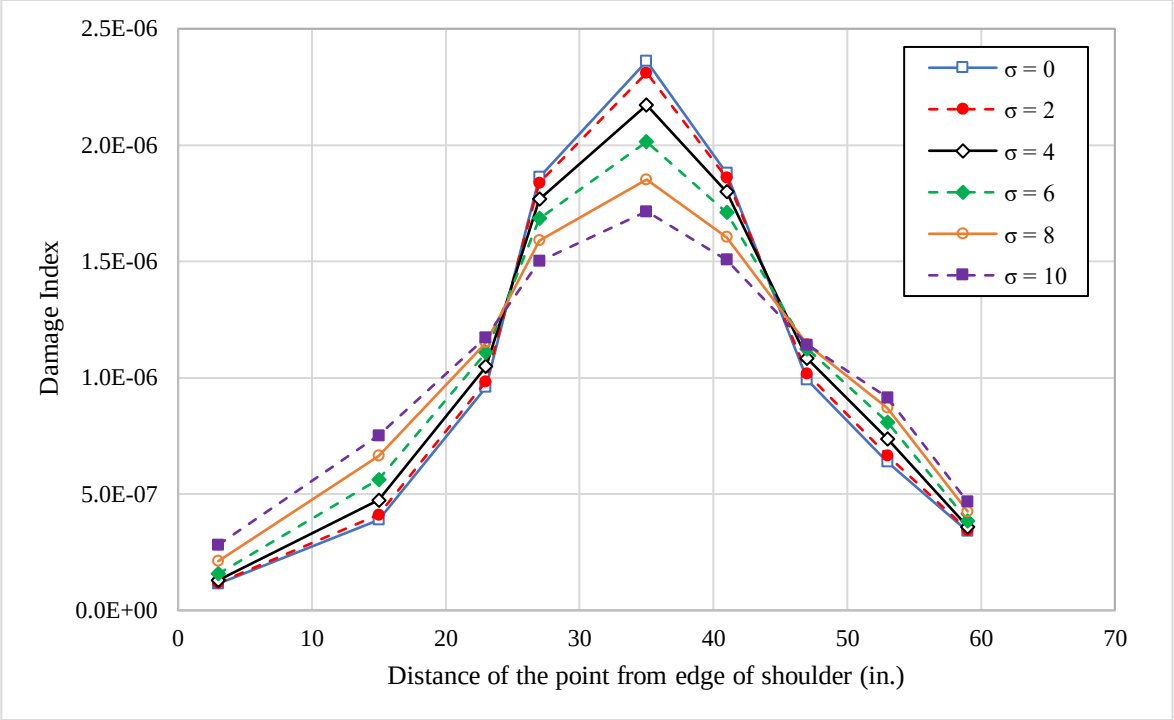

Figure A5. Impact of standard deviation on the fatigue damage for JPCP-C1-AB.

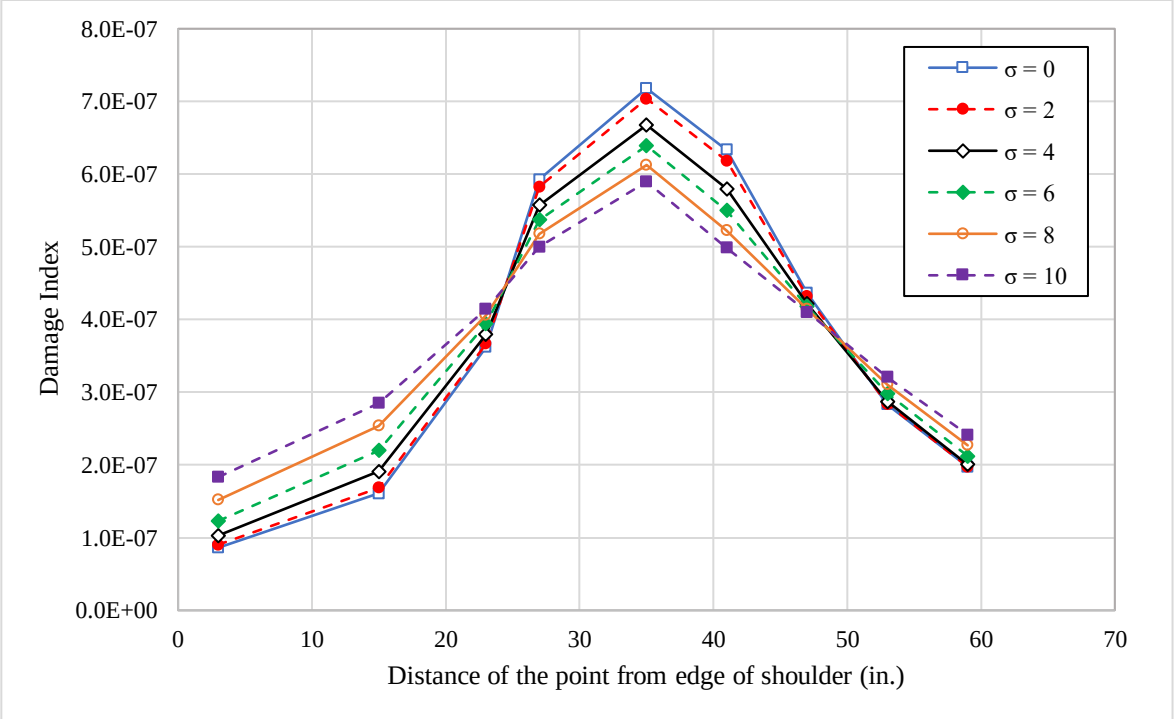

Figure A6. Impact of standard deviation on the fatigue damage for JPCP-C2-AB.

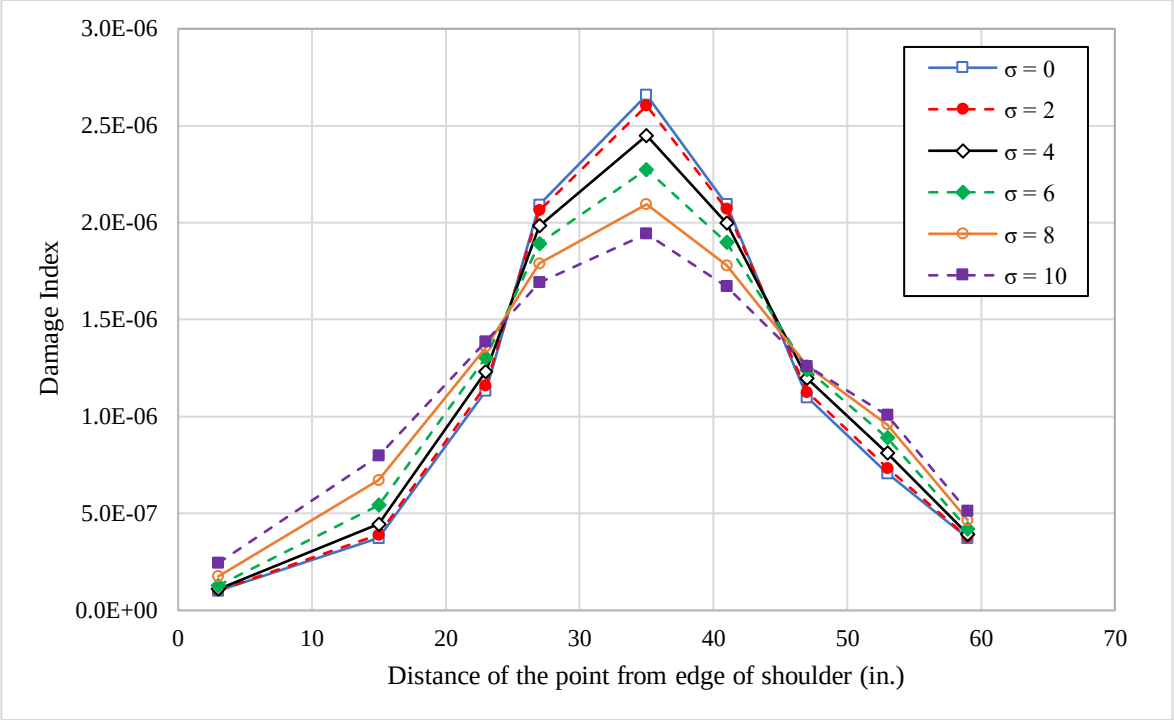

Figure A7. Impact of standard deviation on the fatigue damage for JPCP-D1-AB.

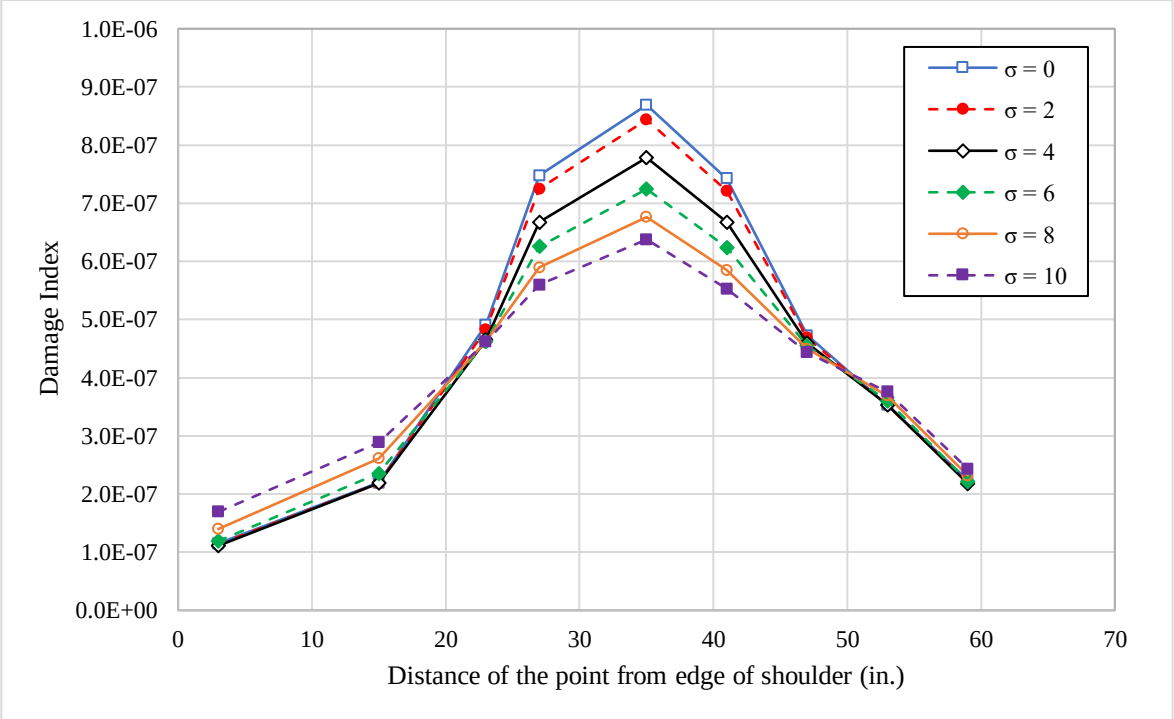

Figure A8. Impact of standard deviation on the fatigue damage for JPCP-D2-AB.